Alma Mater Studiorum – Università di Bologna

DOTTORATO DI RICERCA

Scienze della Terra, della Vita e dell'Ambiente

Ciclo XXXI

Settore Concorsuale di afferenza: 05/B1 - ZOOLOGIA E ANTROPOLOGIA

Settore Scientifico disciplinare: BIO/08 - ANTROPOLOGIA

TITOLO TESI

EXPLORING MORPHOLOGICAL VARIATION IN HOMINID TALAR BONES USING GEOMETRIC MORPHOMETRIC APPROACHES

Presentata da: Rita Sorrentino

Coordinatore Dottorato

Prof. Giulio Viola

Relatore

Prof.ssa Maria Giovanna Belcastro

Correlatore

Prof. Stefano Benazzi

Esame finale anno 2019

TABLE OF CONTENTS

ABSTRACT

The linkage between shape and function in hominid talus makes it a pivotal element for understanding the evolution of bipedalism as well as for evaluating the role of biological and behavioral factors which determine morphological variability.

This thesis focused on the exploration of morphological variation in extinct and extant hominid talar bones through (semi)landmark-based geometric morphometric methods.

The first section of this project analyzes sexual dimorphism in three modern human groups for which the sex is known from cemetery and municipal records. Shape, form and size variables have been investigated. Results shown that changes in size have the higher power in driving sexual differences in modern humans.

The second section aims to evaluate both external and internal (trabecular bone) architecture of modern human tali related to populations with different lifestyle (nomadic vs. sedentary) and subsistence strategy. The goal is to determine changes related to different loadings during bipedal locomotion using both geometric morphometric and biomechanical methods. Overall, the results show differences between hunter-gatherers and sedentary groups, indicating that different locomotor behaviors of modern humans affect both internal and the external talar morphology.

The third section investigate the morphological variability of extinct and extant hominid tali. Beside the whole talus, individual and combined talar facets are analyzed to determine the evolutionary timing of human-like features and their contribution to characterize bipedal locomotion. Our results corroborate that extinct hominins acquired bipedal locomotion even if there may variation between species. Navicular and lateral malleolar facets evolve earlier towards the human-like condition, while other talar facets show broader variability which cause overlap among hominid taxa. The combined trochlea, navicular and posterior calcaneal facets separates australopiths from *Homo*, suggesting that in the former the medial longitudinal arch was not properly developed yet. Overall, our results offer an evolutionary model for the insurgence of bipedalism and the transition from habitual to obligate bipedalism.

In conclusion, this research points out that the talar morphology could be informative of intra- and inter specific anatomical variability in hominid taxa.

Chapter 1

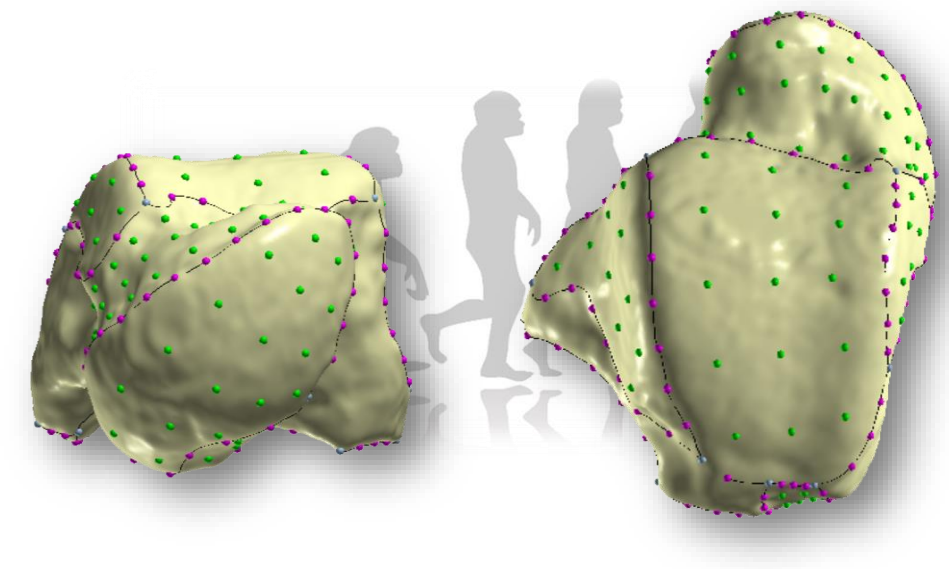

"If it be an advantage to man to stand firmly on his feet […] then I can see no reason why it should not have been advantageous to the progenitors of man to have become more and more erect or bipedal."

Charles Darwin
(The Descent of Man, 1871)

1.1 Background

Several differences exist between the anatomy of modern humans and their closely related living African apes. The most cited distinctive feature of the human species are the increase of brain size, the production of tools and walking on two limbs instead of four (Lovejoy, 1988; Wood and Richmond, 2000). However, earlier species in the hominin fossil record show primitive characteristics in the brain size expressing in a neurocranium of similar size to those of the modern chimpanzee (Haile-Selassie, 2001; White et al., 2009). Moreover, even though the earliest stone tools were predated to 3.3 Ma (Lomekwian technology), indicating that this technological development is older than Oldowan assemblages attributed to *Homo* (Harmand et al., 2015), there is no proof that earliest hominins of late Miocene produce stone tools. Then, the terrestrial bipedalism is the primary evolutionary hallmark used to separate extinct and extant hominins from apes (Kivell and Schmitt, 2009; Harcourt-Smith, 2010).

How and when terrestrial bipedalism emerged is one of the longest-standing questions in paleoanthropology. While the capacity for upright walking (Haile-Selassie, 2001; Zollikofer et al., 2005; Richmond and Jungers, 2008; Lovejoy et al., 2009; White et al., 2009) in the earliest hominins living between 7 Ma and 4 Ma (i.e., *Sahelanthropus tchadensis, Orrorin tugenensis, Ardipithecus kadabba, Ardipithecus ramidus)* is still debated (Brunet, 2002; Wolpoff et al., 2002; Zollikofer et al., 2005; Crompton, 2016), it is broadly accepted that *Australopithecus* and *Paranthropus* engaged in habitual terrestrial bipedalism, which is characterized by a "waddling" gait and upright body posture intermediate between those of chimpanzees and those of humans (Ward, 2002; Harcourt-Smith and Aiello, 2004; Preuschoft, 2004; Drapeau and Harmon, 2013). The bipedal locomotion in australopiths is confirmed by the 3.6 Ma footprints from Laetoli, generally attributed to *A. afarensis* (Stern and Susman, 1983; Raichlen et al., 2010). However, australopiths also maintain skeletal characteristics linked to arboreality (Harcourt-Smith and Aiello, 2004; Preuschoft, 2004; Desilva, 2009; Prang, 2016), suggesting that multiple locomotor repertories evolved in Africa between 4 and 2 Ma (Harcourt-Smith and Aiello, 2004; Haile-Selassie et al., 2012). It is accepted that within the genus *Homo* bipedalism becomes the obligate form of locomotion and some derived post-cranial morphology in early *Homo* (e.g., increased relative hind-limb length, plantar arch) indicate increase capability for long distance walking and running (Bramble and Lieberman,

2004; Haeusler and McHenry, 2004; Pontzer, 2012; Antón et al., 2014). However, primitive retentions present in Late Pleistocene *H. naledi* and *H. floresiensis* suggest that modern human gait and posture may even be unique to *H. sapiens* (Jungers et al., 2009; Harcourt-Smith et al., 2015; Harcourt-Smith, 2016). Despite this uncertainty, it is clear that over a time-span of around 5 million years hominins evolved a suite of specialized anatomical features (e.g., anteriorly placed foramen magnum, S-shape spine, broad and flattened ribcage, wide and short pelvis, long lower limb, stable knee, relatively long and robust ankle region, arched foot), which together facilitated an efficient bipedal gait and upright stance (Aiello and Dean, 1990; Harcourt-Smith, 2010).

Among all adaptations that have evolved in the hominin locomotor system, the foot is highly specialized and unique among primates since it represents the only structure that directly interfaces with the ground during locomotion (Aiello and Dean, 1990; Kidd, 1999; Harcourt-Smith and Aiello, 2004). During a single step of the gait cycle, the human foot transits from a compliant shock absorber at heel strike, to a rigid lever at toe-off (i.e., windlass mechanism) (Griffin et al., 2015) (Fig.1). Structurally, the human foot is defined as a twisted plate forming transverse and longitudinal arches (Sarrafian, 1987). When standing up, the human foot is an elastic, arched structure that actively maintains the body's stability, adjusting itself with small sideward displacements of the talus (Huson, 1991).

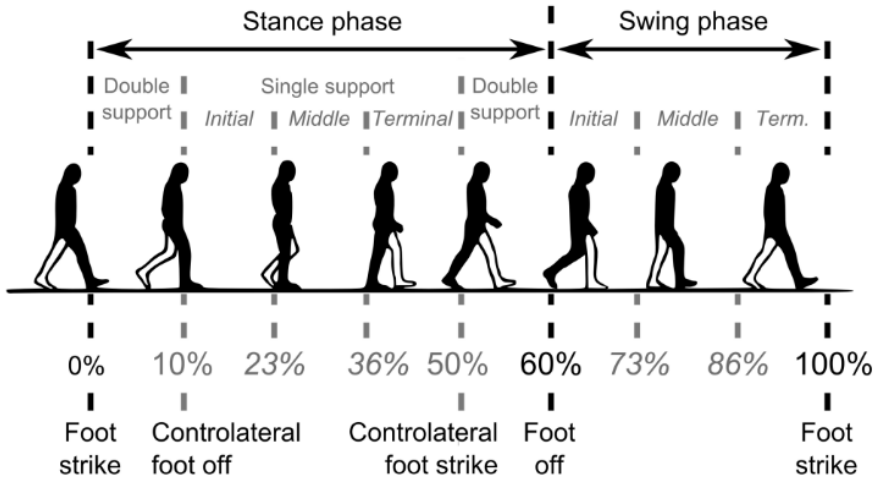

Figure 1. The gait cycle (in Bonnefoy-Mazure and Armand, 2015).

Particularly, the human talus occupies a key position between the leg and foot, as 1) it is defined as the tenon of the ankle mortise, 2) it sustains the entire body weight while distributing the load anteriorly to the navicular

and inferiorly to the calcaneus 3) it allows plantar and dorsal flexion of the foot, and 4) it is part of the medial longitudinal arch (Aiello and Dean, 1990; Huson, 1991; Griffin et al., 2015).

The talus is an articular unit isolated by a fibrous capsule that is part of two distinct synovial joints, such as the ankle (talocrural) joint and the talo-calcaneo-navicular joint. It consists of three main parts (the body, the neck, and the head) and seven articular facets. The upper surface of the body (trochlea facet) articulates with the inferior surface of the tibia and bears most of the weight sustained by ankles. Medial malleolar facet articulates with the tibial malleolus, while lateral facet accommodates the fibular malleolus, and both tibia and fibula blind the talus in the ankle mortise. Posteriorly, the talar body has two processes (medial and lateral tubercles) separated by the flexor hallucis longus (FHL) groove. The talar head possesses a convex expanded surface for the articulation with the navicular bone. Inferiorly, three articular facets (posterior, medial and anterior) create the joint with the calcaneus. The large concave posterior calcaneal facet allows complex motion and prevents excessive inversion and eversion. Anterior and medial calcaneal surfaces are often joined in a single surface (Steele and Bramblett, 1988) (Fig. 2).

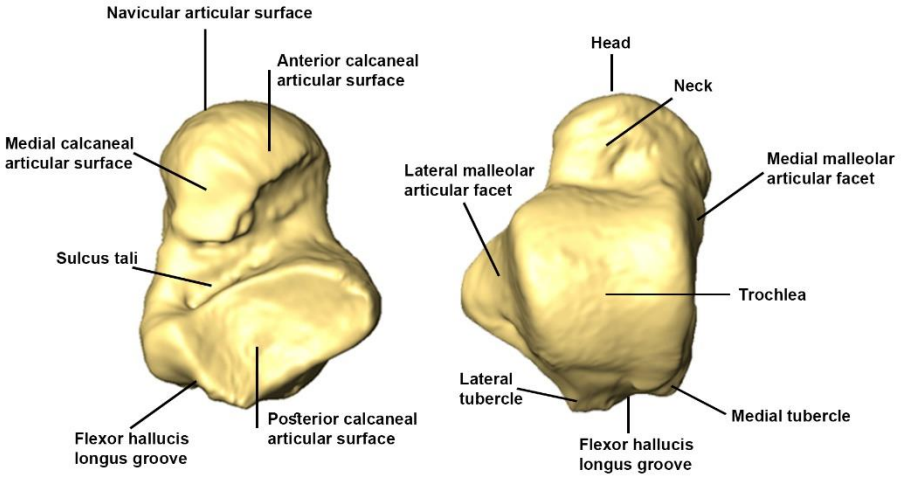

Figure 2. Structure of talus.

Since the talus is one of the most represented findings in the fossil record and its morphology is linked to locomotor strategies (Harcourt-Smith, 2002; Parr et al., 2011a; Turley and Frost, 2013, 2014), there is a vast literature evaluating derived bipedal features in extinct hominins referring to talar morphology (Day andWood, 1968; Rhoads and Trinkaus, 1977;

Latimer et al., 1987; Christie and Ridley, 1989; Kidd, 1996; Harcourt-Smith and Aiello, 2004; Gebo and Schwartz, 2006; White et al., 2009; Jungers et al., 2009; DeSilva and Throckmorton, 2010; Pontzer et al., 2010; Zipfel et al., 2011; Su et al., 2013; Prang, 2016; Harcourt-Smith et al., 2015; Prang, 2015).

Although the morphology of the talus is tightly correlated to locomotor strategies, other factors could influence intra-specific talar variation (e.g., body mass, environmental loading, sexual dimorphism) (Harcourt-Smith, 2002; Kidd and Oxnard, 2002; Parr et al., 2011a, 2014; Turley and Frost, 2013). It is known that intra-specific diversity of tarsal bones in *Gorilla* and *Pan* is influenced by variation in locomotion, substrate use and body mass dimorphism (Harcourt-Smith, 2002; Shaw and Ryan, 2012; Turley and Frost, 2014; Knigge et al., 2015; Turley c, 2015). However, less is known about variability in talar morphology within modern humans (Harcourt-Smith, 2002; Kidd and Oxnard, 2002; Turley et al., 2015).

Modern humans have the capability to use their feet for other activities such as climbing, running, striding, bring things up (Ingold, 2004). Differences in modern human pedal bones could result from different levels of mobility (e.g., sedentary vs. nomadic), technological factors (e.g., shod vs. unshod), substrate use (e.g., asphalt vs. rough terrain) and likely size dimorphism. Therefore, due to the key role covered by the talus in the foot, we assume that its intraspecific variation is strictly related to different human behaviors, physiology and cultural variables.

1.2 Objectives

This thesis aims to investigate shape and form of extinct and extant hominid tali using geometric morphometric methods.
The goals of this thesis are three-folds:

1) to explore sexual dimorphism in modern human tali assessing what variables (shape, form, size) could determine the major differences between sexes.
2) to assess both external and internal talar morphological variation among groups of modern humans differing in footwear use, as well as in subsistence economy and levels of mobility.
3) to quantify hominid talar variation using (semi)landmarks and compare the results with previous works, determine a timeline for the evolution of derived talar facet morphology, and formally assess the contribution of individual and combined facets in identifying bipedal features.

1.3 Materials

The talar bones collected in this study belong to extant and extinct hominids. Collection records or anthropological analysis have been used to select only adult individuals. When present, left tali were preferred in the selection, otherwise right tali were mirrored to be included in the work. Each talus has been checked for avoiding the presence of pathological condition such as osteoarthritic growth, bone anomalies and fractures. Finally, different subsets of the sample were used to rich the three goals of this thesis.

The extant sample consists of two species of great apes, *Pan troglodytes* and *Gorilla gorilla*, and 13 modern human groups (Table 1).

Modern human groups are characterized by different subsistence and mobility strategies. We collected information related to geographical location, chronology, economies, level of mobility and, when possible, information related to footwear.

The oldest sample includes Late Stone Age (Clark Howell, Omo) from Ethiopia (Parr et al., 2011a) and Late Upper Paleolithic specimens from Italy (Romito, Veneri and Villabruna). Since they lived before the neolithic revolution, it is assumed that their economy was based on hunting and gathering and they were habitually barefoot (Trinkaus, 2005).

Other hunter-gatherer populations in the sample are Black Earth (3000 B.C.) from Illinois and Native Americans (Shell Midden Cultures, ~1500 B.C. - 500 A.D.) from San Francisco Bay (California). While Black Earth had nomadic lifestyle likely stopping in forager base camp (Jefferies, 2013), Shell Midden people lived close to the mud flats and estuaries collecting mollusks and fishing in the region (Turley et al., 2015). Belonging to the Prehistoric American period it is also the Norris Farm group. The latter comes from the Norris Farms #36 site (Illinois) dated to approximately 1300 A.D.. Archaeological records suggest that the people from Norris Farms #36 had a mixed economy based on both agriculture and foraging (Santure et al., 1990; Saers et al., 2016). Finding traces on footwear in such ancient times is very difficult. However, the archaeological record attests the use of sandals in North American Southwest around ca. 9000 B.P. (Geib, 2000), whereas post-contact reports inform that native people were unshod (Turley et al., 2015). In any case, the footwear used in Prehistoric period were highly unlikely hard soled and rigid like modern shoes. Probably they could consist in soft sandals and

skin boots which guarantee freedom of ankle motion, allowing adaptability of the foot to the substrate (Trinkaus, 2005).

The Point Hope sample (~1600 - 500 B.C.) are Paleo-Eskimo individuals (Alaska) with a maritime subsistence (Dumond, 2011). They protect their foot from the cold environment using sealskin boots with stiff sealskin soles (Trinkaus, 2005; Turley et al., 2015).

Also Egyptian (~600 - 350 B.C.) from El Hesa had a maritime existence around the Nile River, but they also practiced agriculture and commerce. They could wear sandals or soft leather boots or be unshod (Turley et al., 2015).

Medieval sample includes three individuals date back to VI-VII century B.C.. They are from archaeological site of Guidizzolo (Italy) and as documented by the archaeological and historical findings these individuals were mainly involved in farmer activities.

Two mountain dweller groups are present in the sample. The first one consists in Paleo Pueblo specimens (New Mexico) lived around 1000 BC in stone dwelling constructed in the Canyon de Chelly. They wore double layer woven yucca sandals (Kankainen and Casjens, 1995; Turley et al., 2015). The second one is represented by individuals from Roccapelago (Italy, 17th-18th century). Antropological and historical evidence suggests gender division of the occupational activities. Men were mainly involved in husbandry of cattle, materials handling and transport, while female occupations were related to domestic tasks (Lugli et al., 2017; Traversari, 2017). Generally, the activities were carried out barefoot, with socks reinforced on the plant and on the heels. Shoes with rigid soles were worn only when going to the city or during holiday days (Anselmi, 1995).

The six Nguni individuals (five Zulu and one Basuto of Southern Bantu) in the sample were originally collected by Raymond A. Dart (Dart Collection, Department of Anatomical Sciences, University of the Witwatersrand, South Africa) and then, in the 1926, they were included in the Anthropological Collection of the University of Bologna managed by Prof. Fabio Frassetto. Nguni are South African people of pre- European colonization (20th century). They were herders and farmers living in tribes and clans based on male ancestry. Despite the importance of cattle breeding in their economy, they were tendentially sedentary. Their clothes were made with animal skins and their traditional sandals are called “imbadada”(Gentili, 1995).

The identified skeletal collections (by age, sex, cause of death, occupation) of Sassari and Bologna are part of the Frassetto collection (Museum of Anthropology, University of Bologna, Italy). The Bologna sample consists of individuals from the Certosa Cemetery (Bologna, Italy) died between 1898 and 1944 (Belcastro et al., 2017).

The Sassari Collection (Sardinia, Italy) consists of individuals who died in the first half of the twentieth century that were exhumed from municipal cemeteries (Hens et al., 2008).

New York sample consists of early 20th century post-industrial individuals from New York (USA) (Turley et al., 2015).

Sassari, Bologna and New York represent modern urban societies of the end of the 19th and the beginning of 20th century in which the cities are surmounted by steel infrastructures and crossed by asphalt roads. The economy is based on different labours and specializations (agrarian, maritime, agricultural, urban). Contemporary humans wear heavy leather shoes and boots (Turley et al., 2015; Belcastro et al., 2017).

The fossil hominin sample includes *Australopithecus afarensis* (A.L. 288-1), *Australopithecus africanus* (StW 88, StW 363, StW 486), *Australopithecus sediba* (U.W. 88-98), *Paranthropus robustus* (TM 1517), *Homo habilis/ Paranthropus boisei* (OH8), *Homo* spp. / *Paranthropus boisei* (KNM-ER 1464, KNM-ER 1476), *Homo* spp. (KNM-ER 813), *Homo erectus* (KNM-ER 5428), *Homo ergaster georgicus* from Dmanisi (D4110), *Homo naledi* (U.W. 101-1417, U.W. 101-1417), *Homo neanderthalensis* (EM 3519, Krapina 235, Krapina 237, SP4B, Ferrassie 1, Ferrasie 2), *Homo floresiensis* (LB1-15) (Table 2).

Table 1. The extant sample examined in the present study.

Sample	Number	Collections[1]
H. sapiens		
UP/LSA[2]	6	DBP/ NHMP
Black Earths	15	SIU
Native American	9	PAHM
Norris Farms	10	ISM
Point Hope	8	AMNH
Egyptian	7	AMNH
Paleo Pueblo	6	AMNH
Medieval	3	DBC
Roccapelago	15	SAPAB
Nguni	6	BiGeA
Bologna	39	BiGeA
Sassari	36	BiGeA
New York	21	NMNH
Gorilla		
Gorilla gorilla	31	NHM, PCM, UCL, NMNH, CMNH
Pan		
Pan troglodytes	29	NHM, PCM, UCL, NMNH, CMNH

[1]DBP, Department of Biology, University of Pisa, Pisa; NHMP, The Natural History Museum, Department of Earth Sciences, London; SIU, Southern Illinois University, Carbondale; PAHM, P. A. Hearst Museum Collections, University of California, Berkeley; ISM, Illinois State Museum, Springfield; AMNH, American Museum of Natural History, New York; DBC, Department of Cultural Heritage, University of Bologna, Ravenna; SAPAB, Soprintendenza Archeologia, Belle Arti e Paesaggio per la città metropolitana di Bologna e le province di Modena, Ferrara e Reggio Emilia; BiGeA, Department of Biological, Geological and Environmental Sciences, University of Bologna, Bologna; NMNH, National Museum of Natural History, Smithsonian, Washington; NHM, Natural History Museum London, Mammals collection, London; PCM, Powell Cotton Museum, Birchington, Kent; UCL, Anthropology Department Napier Collection, University College London; CMNH, Cleveland Museum of Natural History, Cleveland.

[2]UP, Upper Paleolithic (Romito 7, Romito 8, Romito 9, Veneri 2 and Villabruna); LSA, Late Stone Age (Clark Howell Omo, Ethiopia).

Table 2. Extinct hominin sample.

Specimens	Taxon designation	Date
A.L. 288-1	*A. afarensis*	3.18 Ma
StW 363	*A. africanus*	2.0-2.6 Ma
StW 486	*A. africanus*	2.0-2.6 Ma
StW 88	*A. africanus*	2.0-2.6 Ma
U.W. 88-98	*A. sediba*	1.97 Ma
TM 1517	*P. robustus*	1.9 - 2.0 Ma
OH 8	*H. habilis/*	1.8 Ma
	P. boisei?	
KNM-ER 1464	*Homo* spp./	1.7 Ma
	P. boisei?	
KNM-ER 1476	*Homo* spp./	1.88 Ma
	P. boisei?	
KNM-ER 813	*Homo* spp.	1.85 Ma
KNM-ER 5428	*H. erectus*	1.6 Ma
D4110 (Dmanisi)	*H. erectus*	1.77 Ma
U.W. 101-148/149	*H. naledi*	236 - 335 Ka
U.W. 101-1417	*H. naledi*	236 - 335 Ka
LB1-15	*H. floresiensis*	18 Ka
Ferrassie 1	*H. neanderthalensis*	43 - 45 Ka
Ferrassie 2	*H. neanderthalensis*	43 - 45 Ka
SP4B (Spy 2)	*H. neanderthalensis*	ca. 36 Ka
EM 3519 (Tabun C1)	*H. neanderthalensis*	122±16 Ka
Krapina 235	*H. neanderthalensis*	130 Ka

1.4 Methods

1.4.1 Data acquisition

Original bones or high-quality casts (e.g., fossils) were subjected to computed tomography (CT), microCT or 3D surface scan to generate 3D surface models.

The human samples of Medieval period and Roccapelago (voxel size: 0.470 x 0.470 x 0.6 mm), Bologna (voxel size: 0.960 x 0.960 x 0.7 mm), Sassari and Nguni (voxel size: 0.976 x 0.976 x 0.5 mm) were scanned with medical CT at the Department of Diagnostic Imaging of Santa Maria delle Croci Hospital in Ravenna (Italy).

The tali from the Norris Farms #36 collection were scanned on the OMNI-X HD600 industrial microCT system at the Penn State Center for Quantitative Imaging. Norris Farm data were collected with energy settings of 180kV and 0.11 mA, inline pixel sizes of 0.048 mm, and slice thickness and spacing of 0.051 mm. The tali from the Carrier Mills Black Earth collection were scanned on a GE v|tome|x L300 microCT system at the Penn State Center for Quantitative Imaging. Data were collected with energy settings of 85kV and 0.33 mA and voxel dimensions of 0.032 mm. Three-dimensional surface reconstructions of Norris Farms and Black Earths were made from the microCT data using Avizo 9.0.

Casts of the Late Stone Age talus of Clark Howell Omo (Omo deposits, Ethiopia), as well as Native American, Point Hope, Egyptian, Paleo Pueblo, New York, Gorilla and Pan sample, and hominin fossil casts of EM3519 and SPB4 (*H. neanderthalensis*), A.L.-288-1 (*A. afarensis*), OH8 talus (*H. habilis / P. boisei*?), Koobi Fora specimens KNM-ER 1464 and KNM-ER 1476 (*Homo spp. / P. boisei?*) from the Natural History Museum, London, Palaeontology Department collection were scanned with a Konica Minolta Vivid 910 surface laser scanner (X: ± 0.22 mm, Y: ± 0.16 mm, Z: ± 0.10 mm). Surface scan data were processed using the scanner's associated software (Polygon Editing Tool, Konica Minolta, 2006) and Geomagic Studio 8.

Fossils casts of KNM-ER 813 (*Homo spp.*) and KNM-ER 5428 (*H. erectus*) were scanned with an Artec Spider.

Scan parameters and protocols for StW 88, StW 363, StW 486, and TM 1517 are given by Su and Carlson (Su and Carlson, 2017).

The Malapa talus was generated from high resolution CT data with energy settings of 130kV and 390uA, 4000 projections, isotropic voxel

dimensions of 57.1 um and 1.2 mm of copper was used to prefilter the beam hardening setting.

LB1-15 (*H. floresiensis*) was scanned using a NextEngine 3D Scanner (macro setting, 16 scans per orientation, minimum two orientations per bone). Triangular meshes of the bone were created in ScanStudio HD PRO software and then aligned and merged in Geomagic Studio software.

CT data of Dmanisi talus (D4110) was acquired in Department of Computed Tomography, Research Institute of Clinical Medicine (Todua Clinic) using Siemens Somatom Sensation 64 medical CT scanner. The Spine Routine protocol was used for image acquisition. Relevant scan parameters for this fossil include: 120kVp, a tube exposure time 750, a slice thickness of 1.00mm, and a reconstruction increment of 0.4mm. Subsequent to the acquisition of these raw data, image data were reconstructed as 16-bit singed DICOM images using a bone reconstruction algorithm (i.e. a "B60s" Convolution kernel). 3D model was reconstructed using -200 threshold value.

Virtual models of H. naledi tali (U.W. 101-148/149 and U.W. 101-1417) are from www.morphosource.org

CT data of Krapina 235 was obtained from the NESPOS (Neanderthal Studies Professional Online Service) Database (voxel size: 0.154 x 0.154 x 0.4 mm). CT data of Ferrassie 1 (voxel size: 0.219 x 0.219 x 0.4 mm) and Ferrassie 2 (voxel size: 0.251 x 0.251 x 0.5 mm) were kindly provided by Museum National d'Histoire Naturelle, Departement Hommes, Natures, Societes. Digital three- dimensional (3D) models were virtually obtained generating isosurface reconstruction in Avizo 7.1 (Visualization Science Group Inc.).

1.4.2 Geometric Morphometrics

Modern research aiming at exploring morphological bone variability takes advantage from new methods developed in geometric morphometrics (GM) (Rohlf and Slice, 1990). Traditional morphometric analysis using linear dimensions lose the information of the full geometry of a configuration which is, instead, preserved with landmark data (O'Higgins, 2000).

Landmarks are anatomical homologous points that correspond in all specimens of a data set. Sets of landmarks can be recorded in 2 (x- and y-coordinates) or 3 dimensions (x-,y-, z-coordinates) (O'Higgins, 2000; Adams et al., 2004; Slice, 2005; Baab et al., 2012). However, because some complex structures cannot be captured using traditional landmarks, semilandmarks might overcome this issue. Semiladnamrks are not

anatomical landmarks, but thanks to sliding procedures based on thin plate spline interpolation function, they became geometrical homologous between individuals, and they can be analyzed along with traditional landmarks (Gunz et al., 2005; Gunz and Mitteroecker, 2013).

In this thesis, a 3D-template of 251 (semi) landmarks (15 anatomical landmarks, 105 curve semilandmarks and 131 surface semilandmarks) was created in Viewbox 4 software on a specimen of Roccapelago group to capture the full talar geometry (Fig.3 and Table 3).

The template configuration was applied to the targets, allowing the semilandmarks to slide on the curves (curves semilandmarks) and on the surface (surface semilandmarks) to minimize the thin-plate spline (TPS) bending energy (Slice, 2005) between the target and the template. As a result, semilandmarks can be considered geometrical homologous (Gunz and Mitteroecker, 2013).

The (semi)landmarks coordinates were converted into shape coordinates standardizing size, position and orientation by means of Generalized Procrustes analysis (GPA) (Slice, 2006). Procrustes coordinates were subjected to Principal Component (PC) analysis using the function in R package "Morpho" (Schlager, 2017) in order to explore shape differences in talar morphology. Following GPA, a Procrustes form analysis was performed adding the logatithm of centroid size (CS) as another variables (Klingenberg, 2016). Further analyses were carried out to investigate specific issues in each section of this work (see Chapter 2). Data analysis were written in R software (Team, 2017).

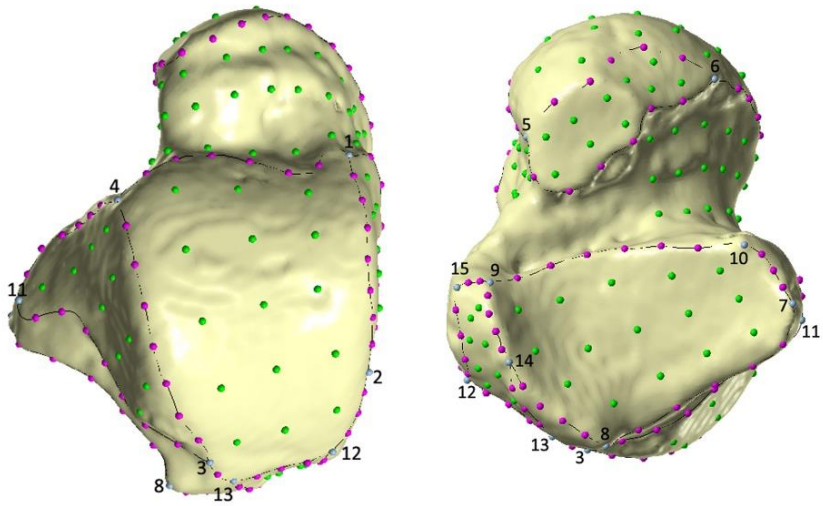

Figure 3. Talar configuration of landmarks and semilandmarks: 15 fixed landmarks (blue), 105 curve semilandmarks (pink) and 131 surface semilandmarks (green).

Table 3. Landmarks of talar configuration. Type of landmarks according to Bookstein, 1991.

Landmarks	Type	Labels
Most distal lateral point of contact between the medial malleolar facet and the trochlear surface	II	1
Most proximal point of contact between the medial malleolar facet and the trochlear surface	II	2
Most proximal point of contact between the lateral malleolar facet and the trochlear surface	II	3
Most distal point of contact between the lateral malleolar facet and the trochlear surface	II	4
Most medial point of contact between the head/navicular facet	III	5
Most lateral point on the head/navicular facet	III	6
Most lateral point on the proximal calcaneal facet	III	7
Deepest (most dorsal) point on the proximal calcaneal facet	III	8
Most proximo-medial point on the proximal calcaneal facet	III	9
Most disto-lateral point on the proximal calcaneal facet	II	10
Most plantar point on the lateral malleolar facet	III	11
Flexor hallucis longus: most distal point on the medial margin	III	12
Flexor hallucis longus: most distal point on the lateral margin	III	13
Flexor hallucis longus: intersection with calcaneus curve	II	14
Flexor hallucis longus: most postero-inferior prominent point	III	15

1.5 Structure of thesis

The core of this thesis consists in three papers focusing on the hominid talar variability at intra and inter specific level. In the following pages it is reported a brief presentation of these works, whereas the papers are presented in Chapter 2.

Paper I: Exploring sexual dimorphism of modern human talus through geometric morphometric methods.
Resubmitted after review to Forensic Science International.

In this paper we address the first goal of the thesis about sex determination from modern human tali. Here, we assess which variables (shape, form, size) could determine the major differences between sexes in

three early 20th century populations by means of GM methods. The identified skeletal collections of Sassari and Bologna (Italy), and New York (USA) were analyzed at intra and inter-specific population level.

Furthermore, a talus from the Bologna sample with known sex (not included in the previous analysis) was selected to run a virtual resection, followed by two digital reconstructions based on the mean shape of both the pooled sample and the Bologna sample. The sex of the reconstructed talus was predicted using the discriminant functions obtained for both the pooled and Bologna samples.

Overall, this study aims to assess the most accurate approach for sex discrimination of modern human tali (complete or damaged), ultimately providing useful tools for forensic and archaeological investigations.

Paper II: The influence of mobility strategy on the modern human talus.

The manuscript is under review in Scientific Reports.

In the Paper II, we evaluate the influence of cultural and environmental factors on talar morphology within modern humans.

External and internal (trabecular structure) talar morphology of 11 modern human populations which reflect variation in mobility strategy (active vs. sedentary), substrate (flat vs. uneven) and footwear use (shod vs. unshod) was analyzed using two methods.

Morphological data were collected by means of a 3D configuration consisting of 251 (semi)landmarks covering the entire talus. The functional significance of the relevant morphological differences was assessed by quantifying the trabecular structure (i.e., bone volume fraction (BV/TV), degree of anisotropy (DA), and elastic modulus (E), which are known to vary in relation to habitual mechanical loading.

This work aims to determine anatomical pedal changes related to different human behaviors during bipedal walking that may be useful in inferring the ranges of joint movements (arthrokinematics), mobility patterns, and the behavior of extinct hominin taxa.

Paper III: The evolutionary history of the hominid talus.

The manuscript is under review in PNAS.

In this paper, we investigate the whole talus, as well as individual and

combined talar facets, of extinct and extant hominids using a 3D geometric morphometrics approach. The aim is to determine a timeline for the evolution of derived talar facets and the contribution of individual and combined facets in identifying bipedal features.

A template of 251 (semi)landmarks was used to analyze 81 *H. sapiens*, 31 *Gorilla gorilla*, 29 *Pan troglodytes*, and 20 fossil hominins. The hominin fossil sample includes *Australopithecus afarensis* (A.L. 288-1), *Australopithecus africanus* (StW 88, StW 363, StW 486), *Australopithecus sediba* (U.W. 88-98), *Paranthropus robustus* (TM 1517), *Homo habilis*/ *Paranthropus boise*i (OH8), *Homo spp. / Paranthropus boisei* (KNM-ER 1464, KNM-ER 1476), *Homo spp.* (KNM-ER 813), *Homo erectus* (KNM-ER 5428), *Homo ergaster georgicus* from Dmanisi (D4110), *Homo naledi* (U.W. 101-1417, U.W. 101-1417), *Homo neanderthalensis* (EM 3519, Krapina 235, Krapina 237, SP4B, Ferrassie 1, Ferrasie 2), *Homo floresiensis* (LB1-15).

The advantage to use semi-landmarks together with traditional landmarks is that semi-landmarks allow more robust estimation of missing data in incomplete specimens that are frequently left out from analyses due to their fragmentary conditions. Here, the estimation of missing (semi)landmarks was carried out using Thin Plate Spline (TPS) interpolation in Viewbox. The reconstruction was performed for the whole talus, or for singular/combined facets in order to include as many fossils as possible in each analysis (i.e., analyses for the whole talus and for individual and combined facets).

Cartesian coordinates were converted to shape coordinates by GPA and PCAs were performed in order to explore shape and form variability of the whole talus and of individual and combined talar facets among hominids.

This study contributes to increase our knowledge on the evolution of terrestrial bipedalism.

Chapter 2

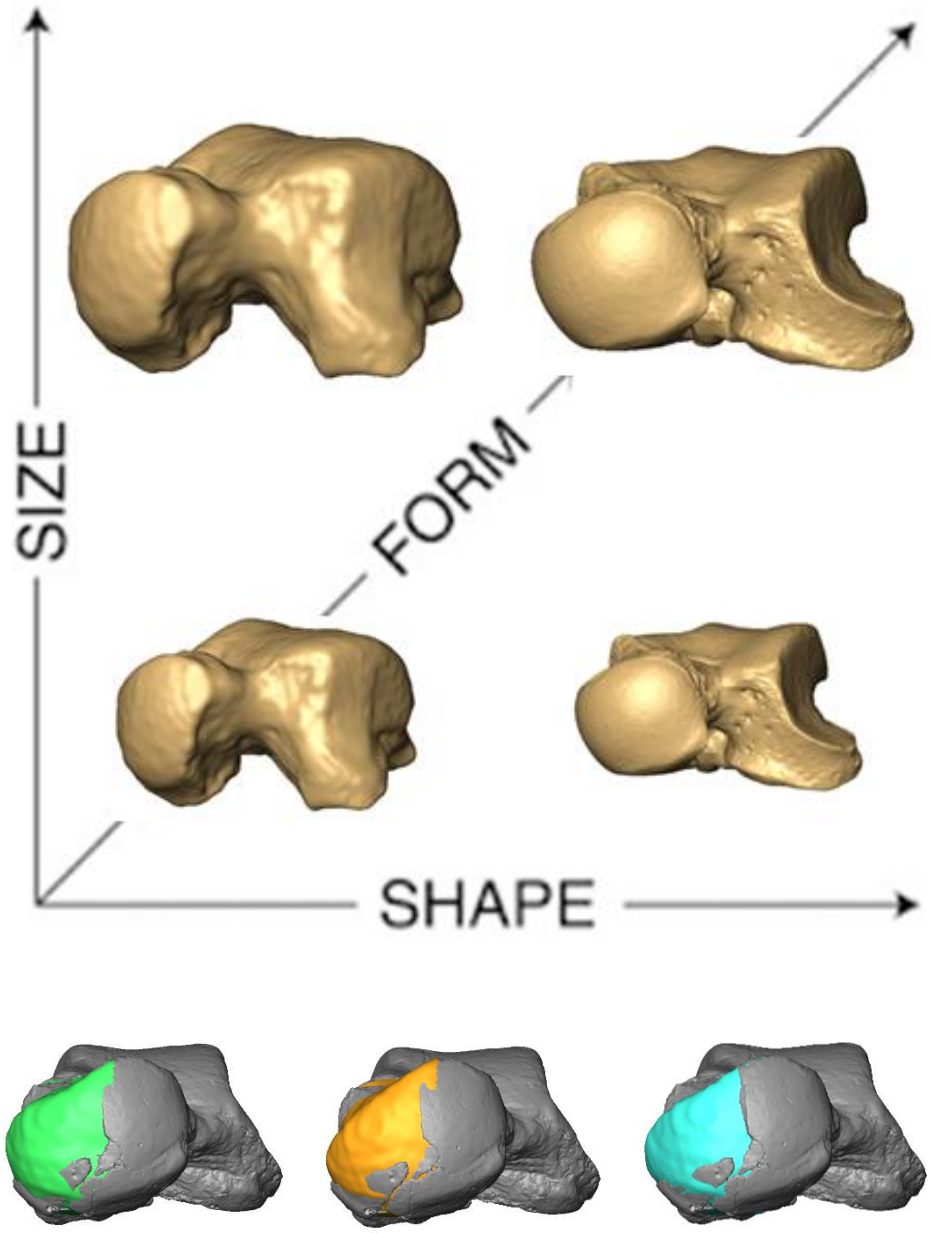

2.1 Paper I

Exploring sexual dimorphism of modern human talus through geometric morphometric methods

R Sorrentino[1,2*], M. Giovanna Belcastro[1,3*], Carla Figus[2], Kevin Turley[4], William Harcourt-Smith[5,6,7,8], Timothy M. Ryan[9], Stefano Benazzi[2,10]

[1]Department of Biological, Geological and Environmental Sciences, University of Bologna, Bologna 40126, Italy.
[2]Department of Cultural Heritage, University of Bologna, Ravenna 48121, Italy.
[3]ADES, UMR 7268 CNRS/Aix-Marseille Université/EFS, Aix-Marseille Université, CS80011, Bd Pierre Dramard, Marseille Cedex 15, 13344, France.
[4]Department of Anthropology, University of Oregon, Eugene, OR, 97403–1218, USA.
[5]Graduate Center, City University of New York, New York, NY 10016.
[6]New York Consortium in Evolutionary Primatology, New York, NY 10024.
[7]Department of Anthropology, Lehman College, New York, NY 10468.
[8]Division of Paleontology, American Museum of Natural History, New York, NY 10024.
[9]Department of Anthropology, Pennsylvania State University, University Park, PA 16802, USA.
[10]Department of Human Evolution, Max Planck Institute for Evolutionary Anthropology, Leipzig 04103, Germany.

* These authors contributed equally to this work.

Corresponding author: Rita Sorrentino, rita.sorrentino2@unibo.it

[Resubmitted after review to Forensic Science International]

Abstract

Sex determination is a pivotal step in both forensic and bioarchaeological fields. Generally, scholars focus on metric or qualitative morphological features, but in the last few years several contributions have applied geometric-morphometric (GM) techniques to overcome limitations of traditional approaches. In this study, we explore sexual dimorphism in modern human tali from three early 20th century populations by means of GM methods. The identified skeletal collections of Sassari and Bologna (Italy) and New York (USA) were analyzed at intra and inter-specific population levels. Our results do not show significant differences in shape between males and females, either considering the pooled sample or the individual populations. Differences in talar morphology due to sexual dimorphism are mainly related to allometry, i.e. size-related changes of morphological traits. Discriminant function analysis using either form space Principal Components or size (i.e., centroid size) correctly classify between 87.7% and 97.2% of the individuals. The result is similar using the pooled sample or the individual population, except for a diminished outcome for the New York group (from 73.9% to 78.2%). Finally, a talus from the Bologna sample was selected to run a virtual resection, followed by two digital reconstructions based on the mean shape of both the pooled sample and the Bologna sample, respectively. The reconstructed talus was correctly classified with a P_{post} between 99.9% and 100%, pointing out that GM is a valuable tool to cope with fragmented tali, which represent a likely condition in forensic and bioarchaeological contexts.

1. Introduction

It is well-known that males have more robust bones and a larger stature than females due to differences in genetics and developmental factors, which overall affect, among other things, growth rates, body composition, lean muscle mass, and hormonal levels [1,2]. Accordingly, sexual dimorphism in human skeletal structures is expressed as differences in both size and shape, and such phenotypic differences are pivotal in bioarchaeology and forensic anthropology to reconstruct the individual biological profile [3–5]. Identification of human remains is the main goal of forensic osteology, and it is a humanitarian need [6–9]. This investigation requires to ascertain the biological profile of one or more individuals whose died for natural, criminal or disaster causes [8,10–14].

Sex assessment is a foremost step for developing reliable biological profile as it represents the prerequisite information for estimating other traits that compose the biological profile, such as age, ancestry and stature [3,7,15,16]. Furthermore, sex assessment contributes in reducing the possible matches by half [17] and is of great importance in paleodemography and paleopathology [18].

When the entire skeleton is preserved, different methods can be exploited for reliable sex determination [19]. Sex assessment is primarily focused on the more dimorphic skeletal elements (i.e., pelvis and cranium) [2,3,18,20–22], but other regions are also observed to strengthen the attribution [1–3]. However, skeletal remains from forensic and archaeological contexts are often incomplete and in fragmentary condition, and very often isolated bones are not associated to an individual skeletal, for example in commingled burials [23,24]. In such circumstances, particularly in the absence of the pelvis and the skull, new methods have been developed to deal with isolated bones [25–31]. Particularly, the pedal remains tend to be discovered in isolation in different scenarios, such as tragic disasters and altered taphonomic contexts [32,33]. Accordingly, several studies have explored sexual dimorphism of foot bones using linear measurements, pointing out the valuable contribution of both the calcaneus and the talus for sex determination [17,32,34–40]. However, linear dimensions are not able to fully characterize the shape of the bones under study, because each measurement loses its relative position with respect to the others [41,42]. Specifically, each linear dimension is measured between two landmarks, but the arrangement of landmarks relative to one another is lost [43]. Landmark-based geometric morphometrics (GM) has the potential to overcome this issue, because it includes the complete information about all pairwise distances between landmarks and possible angles simultaneously [5,27,43–46].

Some further conditions, such as the poor skeletal preservation, severe fragmentation and burning, could make the forensic investigation even more difficult. Bones are usually retrieved broken off and incomplete in mass disasters, crime procedures and postmortem environmental condition [8,10,23,47–49]. Fragmented bones with cracks and/or gaps are usually discarded from traditional analysis because they cannot provide the required information [7,23]. However, new approaches have been developed to cope with them, such as molecular analysis or virtual reconstruction [7,50–53]. With regard to the latter, geometric morphometrics offer the possibility to virtually reconstruct missing data from partially damaged specimens [51,54]. Particularly, the use of semilandmarks allow estimates of missing data from the information that is present using the thin-plate spline

interpolation, ultimately allowing the use of virtually reconstructed specimens for forensic evaluation like sex determination [51,52,55].

In this contribution we use GM methods to explore sexual dimorphism of the talus in three modern human populations (Sassari and Bologna from Italy, and New Yorkers from USA) from osteological collections. First, we test the hypothesis that the amount of sexual dimorphism in the talus is population specific [3]. Second, we investigate the contribution of shape, form (shape + size) and size in determining sexual dimorphism in talar morphology at the intra- and inter-specific population level. Third, we use a digitally-damaged talus with known sex (not included in the previous analysis) and provide a virtual reconstruction of the missing portions using GM techniques. Overall, our extensive morphometric study of the talus aims to assess the most accurate approach for sex discrimination of isolated tali, ultimately providing useful tools for forensic and archaeological investigations.

2. Materials and methods

2.1 Data collection

The tali (N=98) collected in this study belong to three modern human groups of urban societies from the late 19th and early 20th century, for which the sex is known from cemetery and municipal records. The sample consists of 39 individuals from Bologna (18 females and 21 males), 36 individuals from Sassari (17 females and 19 males) and 23 individuals from New York (9 females and 14 males).

The identified skeletal remains (by age, sex, cause of death, occupation) of Sassari and Bologna are part of the Frassetto collection housed at the Museum of Anthropology of the University of Bologna (Italy). The Bologna sample consists of individuals from the Certosa Cemetery (Bologna, Italy) who died between 1898 and 1944 [56]. The Sassari sample (Sardinia, Italy) consists of individuals who died in the first half of the twentieth century and were exhumed from municipal cemeteries [57]. The New York sample is represented by early 20th century post-industrial individuals from New York (USA) stored at the National Museum of Natural History of Smithsonian (Washington, USA) [58].

Left tali were selected for the analysis. In case the left talus was absent or damaged (either fragmented or affected by pathological conditions), the right one, if present, was selected and the digital model (see below) was mirrored to be included in the work.

Three dimensional (3D) digital models of each bone were obtained either by computed tomography (CT) or surface laser scanning. In detail, the Italian sample from the Frassetto collection was CT scanned with a 64 slices Brilliance, Philips Medical System, Eindhoven-the Netherlands at the Department of Diagnostic Imaging of Santa Maria delle Croci Hospital in Ravenna (Italy), and reconstructed using the following voxel sizes: 1) Bologna sample: 0.960 x 0.960 x 0.7 mm; 2) Sassari sample: 0.976 x 0.976 x 0.5 mm. The CT image data were segmented in Avizo 7.1 (Visualization Science Group Inc.) to obtain 3D digital models of each talus. The tali from New York were digitally using a Konica Minolta Vivid 910 surface laser scanner (X: ± 0.22 mm, Y: ± 0.16 mm, Z: ± 0.10 mm). Surface scan data were processed (i.e., mesh alignment, cleaning) using the scanner's associated software (Polygon Editing Tool, Konica Minolta, 2006) and Geomagic Studio 8 (3D Systems).

STL format of 3D models were used to manage the digital sample in Viewbox 4 software.

2.2 Geometric Morphometrics and statistical analysis

A 3D template of 251 (semi)landmarks (15 anatomical landmarks, 105 curve semilandmarks and 131 surface semilandmarks) was created in Viewbox 4 software (Fig.1 and Table 1) and subsequently applied to the targets. The semilandmarks were allowed to slide on the curves (curves semilandmarks) and on the surface (surface semilandmarks) to minimize the thin-plate spline (TPS) bending energy between the target and the template [45,51]. Semiladnamrks are not anatomical landmarks, but thanks to sliding procedures based on TPS interpolation function, they became geometrical homologous between individuals, and they can be analyzed along with traditional landmarks [50,51].

The (semi)landmark coordinates were allowed to slide against recursive updates of the Procrustes consensus and converted into shape coordinates standardizing scale, position, and orientation by means of Generalized Procrustes analysis (GPA) [45,59] using the R package "geomorph"[60]. Size was measured as centroid size (CS), which is the square root of the summed squared distances between each (semi)landmark and the centroid of the (semi)landmark configuration [44,45].

Procrustes coordinates were subjected to Principal Component analysis (PCA) to explore the pattern of morphological variation across the sample. A form-space PCA (i.e., shape + size) was carried out by augmenting the Procrustes shape coordinates by the natural logarithm of CS, hereafter called lnCS [61]. Visualization of shape changes along the principal axes

was obtained by TPS deformation [62] of the Procrustes grand mean shape surface in Avizo 7.1 (Visualization Science Group Inc.).

ANalysis Of VAriance (ANOVA) was performed to identify significant sex differences along the first two PCs (in both shape and form space) and for CS within each population and for the pooled sample. Shape variation related to size (static allometry) was investigated by Pearson product-moment correlation coefficients (r) of shape variables (PCs) against lnCS. Then, multivariate regression of shape and form variables (using all the PCs) on lnCS was carried out to compute the intragroup allometric trajectory across the talar female-male morphospace. Permutation test (N = 1000) on lengths (i.e., magnitude of the variability) and angles between group's trajectories was performed to assess if the amount of sexual dimorphism differs significantly (i.e., $P<0.05$) among populations [63]. For each permutation test, specimens were randomly reassigned with respect to groups (i.e., Sassari, Bologna and New York), and new trajectories were computed.

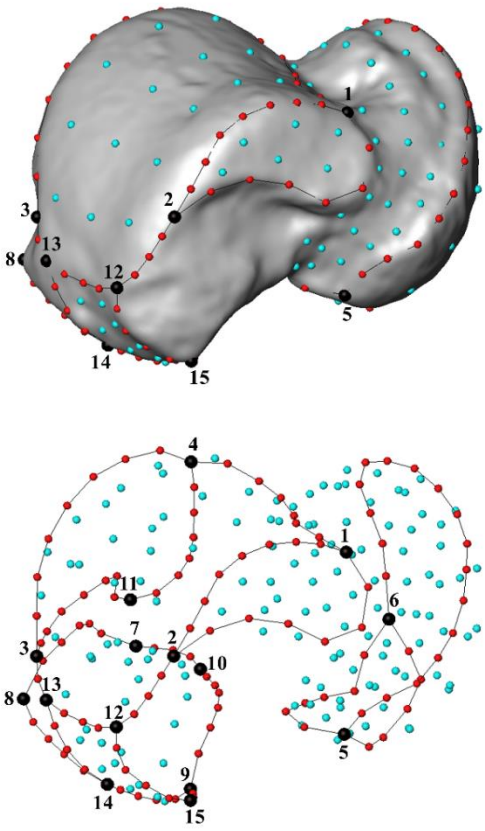

Fig. 1 Template with landmarks (black), curve and surface semilandmarks (red and light blue, respectively) digitized on a left talus. See Table 1 for a detailed description of the anatomical landmarks.

Finally, we used 'leave-one-out' cross validation linear discriminant analysis (LDA) of shape space PC scores, form space PC scores, and CS alone to classify the specimens (i.e., either male or female). The number of PCs used for LDA vary for each analysis in order to find the minimum optimal combination of variables within the first 10 PCs that best discriminate sexes. The data were processed and analyzed through software routines written in R v. 3.5.1 (R Development Core Team, 2018).

Table 1. List of anatomical landmarks of the template for the GM analysis of the talus. Type of landmarks according to Bookstein [62].

Landmarks	Type	Labels
Most distal lateral point of contact between the medial malleolar facet and the trochlear surface	II	1
Most proximal point of contact between the medial malleolar facet and the trochlear surface	II	2
Most proximal point of contact between the lateral malleolar facet and the trochlear surface	II	3
Most distal point of contact between the lateral malleolar facet and the trochlear surface	II	4
Most medial point of contact between the head/navicular facet	III	5
Most lateral point on the head/navicular facet	III	6
Most lateral point on the proximal calcaneal facet	III	7
Deepest (most dorsal) point on the proximal calcaneal facet	III	8
Most proximo-medial point on the proximal calcaneal facet	III	9
Most disto-lateral point on the proximal calcaneal facet	II	10
Most plantar point on the lateral malleolar facet	III	11
Flexor hallucis longus: most distal point on the medial margin	III	12
Flexor hallucis longus: most distal point on the lateral margin	III	13
Flexor hallucis longus: intersection with calcaneus curve	II	14
Flexor hallucis longus: most postero-inferior prominent point	III	15

2.3 Reconstruction of fragmented talus

In order to exploit the power of GM method for virtual reconstruction of a partial talar specimen, we simulate the case in which a fragmented talus does not allow to collect the linear measurements generally used for discriminant function equation [34,35,64], ultimately representing a typical specimen excluded from sex assessment [34].

A female individual of the Bologna sample (BO-F-45), damaged in the talar head and then excluded from the previous PCA, was selected for virtual resection and reconstruction (Fig. 2a). In detail, a portion of the talus (i.e., from the most lateral anterior margin of the trochlea to the mid of the flexor hallucis longus groove) was resected using a cutting plane in Geomagic Design X (3D System) (Fig. 2b), thus adding to the physical damage of the head a more extensive digital fracture. The missing portions were estimated using morphological information from reference specimens

by mean of Thin Plate Spline (TPS) interpolation function in Viewbox 4 software [51,54]. Since the Procrustes mean shape is an effective reference for the reconstruction of missing portions [65], two reconstructions were tested based on two different reference specimens: 1) a reconstruction based on the mean configuration of the Bologna sample (Fig. 2c, d), which represents the ideal condition due to the provenance of the case study; 2) a reconstruction based on the mean of the pooled sample (Fig. 2e, f), which might represent an alternative solution in case the population's provenance of the case study is unknown. In both cases, the virtual reconstruction of the talus was undertaken by estimating the position of the (semi)landmarks that fall in the missing regions (Fig. 2c, e). The virtually reconstructed tali were then projected in the form-space PCA previously computed (i.e., the reconstruction by the mean of the Bologna sample in the Bologna form-space PCA; the reconstruction by the mean of the pooled sample in the pooled form-space PCA), and sex was predicted using the discriminant functions obtained for both the pooled and Bologna samples.

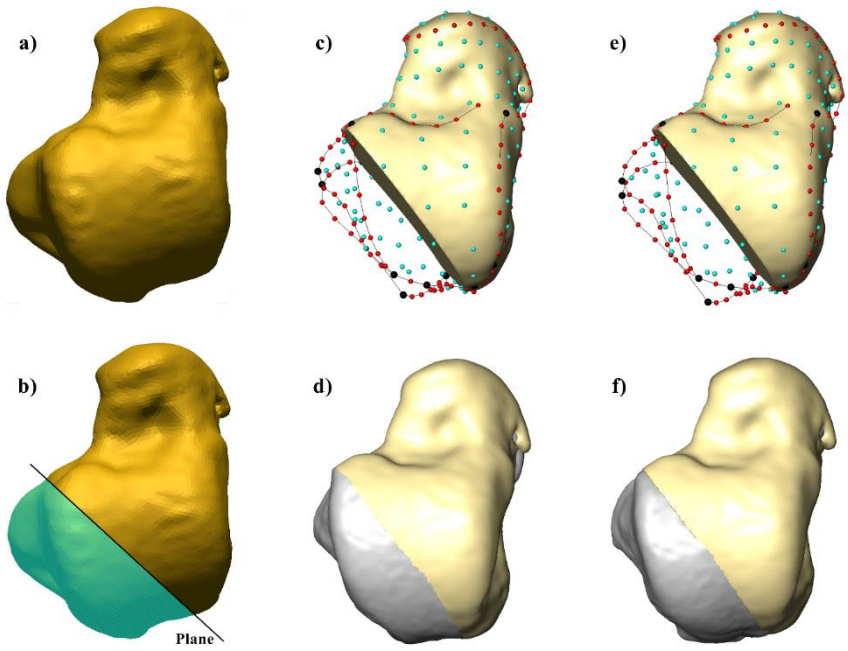

Fig. 2 The left talus of BO-F-45 individual of Bologna (**a**) and the cutting plane used for the virtual resection (resected area in light blue) (**b**). Estimation of (semi)landmarks and reconstruction of the missing portion (in gray) based on the mean of both the Bologna sample (**c, d**) and the pooled sample (**e, f**).

3. Results

3.1 Inter-specific population sex assessment

The shape-space PCA plot of the pooled sample shows a considerable degree of overlap among individuals (Fig.3). The first two PCs account for 24.9% of the total variance and do not contribute to separating males from females (ANOVA; PC1: Df =1, F-test = 1.047, P = 0.30; PC2: Df =1, F-test = 2.162, P = 0.14). Subtle morphological differences are observed in the extreme shape of the PC1 and PC2 axes, in particular the talar head is more expanded on negative PC1 and negative PC2 and reduced on positive

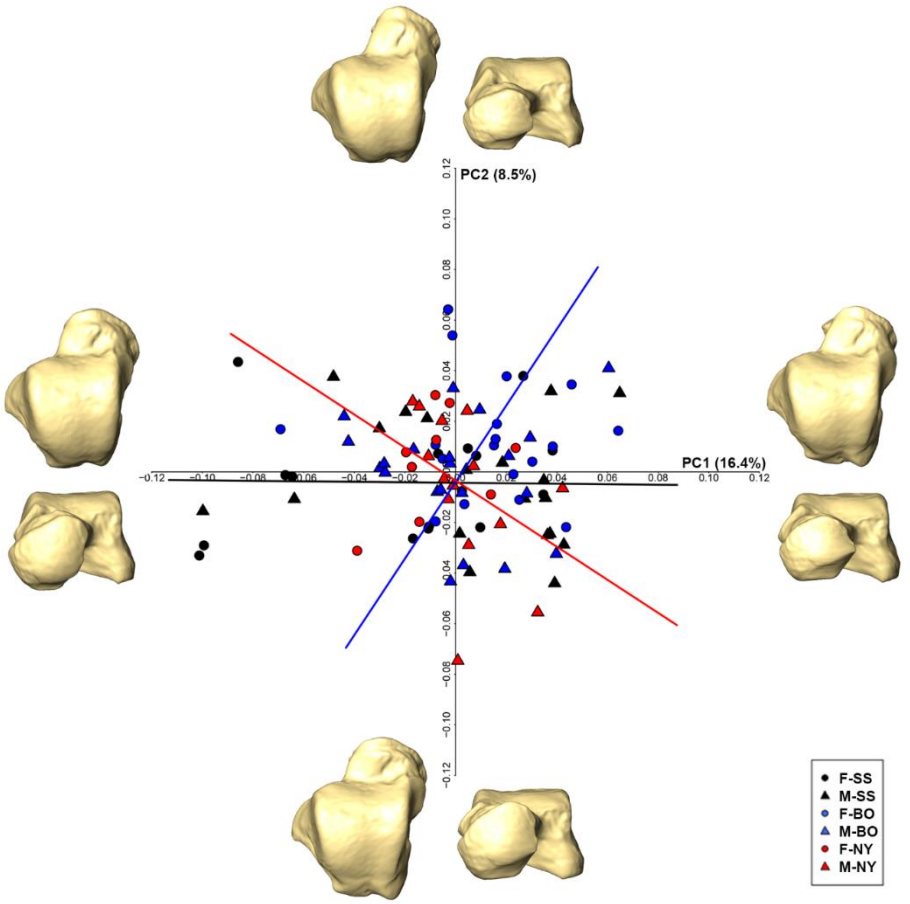

Fig. 3 Shape space PCA plot of the pooled sample and shape warps along axes. Sassari individuals are in black, Bologna individuals in blue and New York individuals in red. Circles represent females and triangles represent males. Intragroup allometric trajectory (black for Sassari, blue for Bologna and red for New York) are shown in the PCA plot. The deformed mean tali in the four directions of the PCs are drawn at the extremity of each axis.

PC1 and positive PC2. A Pearson's correlation test shows that PC1 is correlated with lnCS (r=0.25; P<0.05), i.e., static allometry could account for morphological differences along this axis.

Permutation tests show that angles between group trajectories differ significantly between Sassari and Bologna (α=103.5°, P<0.01), as well as New York and Bologna (α= 97.3°, P<0.05), but not between Sassari and New York (α=57.8°, P= 0.36). No differences in length are observed among the allometric trajectories.

Form space PC1 (48.7%), which retains all size information (r=0.99; P<0.001), significantly separates males and females (ANOVA; Df =1, *F*-test = 147.5, P<0.001) , while PC2 (8.1%) does not account for differences

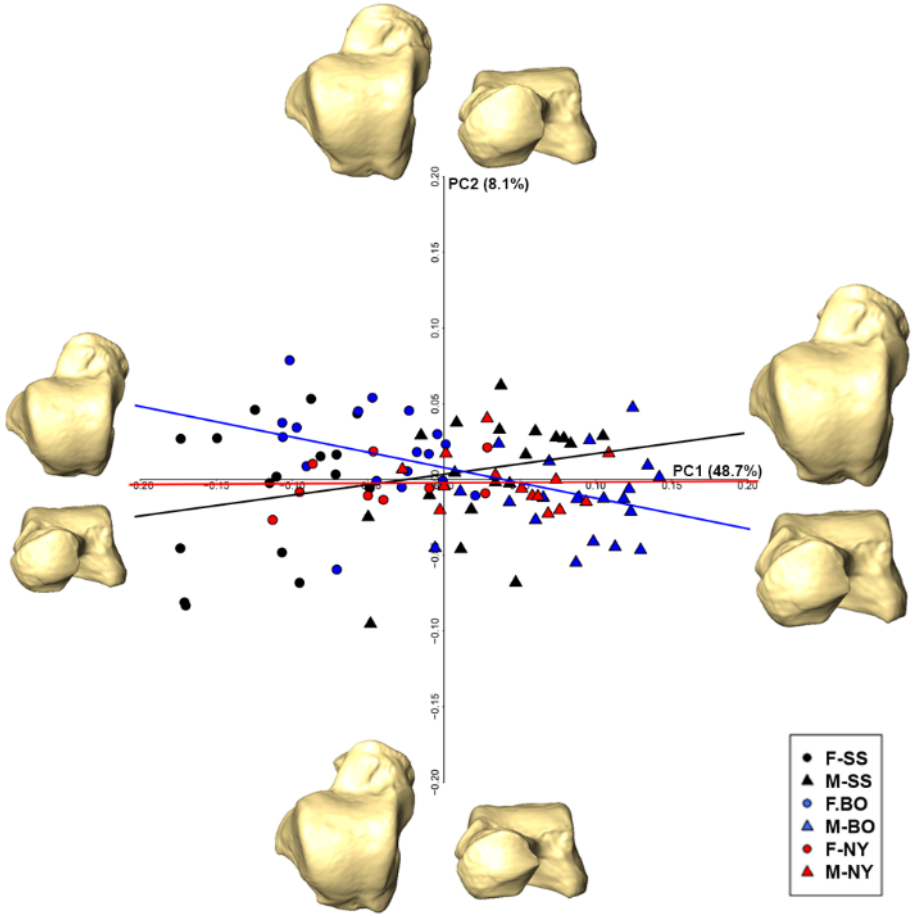

Fig. 4 Form space PCA plot of the pooled sample and shape warps along axes. Sassari individuals are in black, Bologna individuals in blue and New York individuals in red. Circles represent females and triangles represent males. Intragroup allometric trajectory (black for Sassari, blue for Bologna and red for New York) are shown in the PCA plot. The deformed mean tali in the four directions of the PCs are drawn at the extremity of each axis.

among sexes (ANOVA; Df =1, *F*-test = 1.889, P = 0.17) and is not correlated with lnCS (r= -0.05; P = 0.6) (Fig. 4). Positive PC1 accounts for the relative superior-inferior lateral expansion of the talar head and more concave medial malleolar facet (i.e., male shape), while negative PC1 is related to a more rectangular and horizontally-inclined talar head, as well as a less concave medial malleolar facet (i.e., female shape). Allometric trajectories are significantly different between Sassari and Bologna (α=23.7°, P<0.01), as well as New York and Bologna (α= 20.8°, P<0.05), but not between Sassari and New York (α=15.9°, P= 0.53). Furthermore, the magnitude of the intergroups allometric variation differs Sassari from Bologna (P<0.05). Finally, ANOVA shows that CS is significantly different between males and females (ANOVA; Df =1, *F*-test = 151.7, P<0.001).

Cross-validation LDA of the pooled sample returns high accuracy when using the first 6 form space PCA score (91.8%) and CS (87.7%), while the number of correctly classified individuals drops using shape space PCs, the best result obtained with 9 PCs (66.3% of accuracy) (Table 2).

Table 2. Accuracy of classification using shape, form variables and centroid size of each population and pooled sample.

	Predicted group membership				
	Male		Female		Total
	N	%	N	%	%
Sassari					
6 shape-space PCs	15/19	78.9	15/17	88.2	83.3
Centroid size	17/19	89.5	17/17	100	94.4
2 form-space PCs	18/19	94.7	17/17	100	97.2
Bologna					
7 shape-space PCs	16/21	76.2	15/18	83.3	79.4
Centroid size	19/21	90.5	18/18	100	94.9
1 form-space PCs	19/21	90.5	17/18	94.4	92.3
New York					
7 shape-space PCs	11/14	78.6	8/9	88.9	82.6
Centroid size	10/14	71.4	7/9	77.8	73.9
1 form-space PCs	11/14	78.6	7/9	77.8	78.2
Pooled sample					
9 shape-space PCs	37/54	68.5	28/44	63.6	66.3
Centroid size	47/54	87	39/44	88.6	87.7
6 form-space PCs	50/54	92.6	40/44	90.9	91.8

3.2 Intra-specific population sex assessment

Figure 5 shows the PCA plots in both shape and form space for each modern human population and the relative shape changes along the PC axes.

Overall, results in shape space PCA suggest that there are no significant differences (P>0.05) driven by sexual dimorphism in the talar shape of the populations considered in this study (Fig. 5a,b,c). This result is confirmed by the low discriminant accuracy, which ranges from 79.4% to 83.3% (Table 2).

In form space PCA of the Sassari sample (Fig. 5d), PC1 (50.7%) is strongly correlated with lnCS (r=0.98; P <0.001) and significantly segregates males from females (ANOVA; Df =1, *F*-test = 80.17, P<0.001). Negative PC1 (i.e., Sassari females) shows shorter talar neck and medio-laterally extended navicular facet (from dorsal view), as well as less concave and less anteriorly extended medial malleolar facet, compared with positive PC1 (i.e., Sassari males). Discriminant function on the first two form space PCs returns the higher value of accuracy (97.2%) found in this study (Table 2). The importance of size is further supported by significant differences in CS (ANOVA; Df =1, *F*-test = 97.31, P<0.001), which allows to reach 94.4% of accuracy.

Similarly, form space PC1 (52.6%) significantly separates males and females of the Bologna sample (ANOVA; Df =1, *F*-test = 105.6, P<0.001) (Fig. 5e). However, because no relevant allometric shape changes are recognized along the PC1 axis, the separation is basically driven by size (r=-0.99; P <0.001). Discriminant function on the first form space PCs allows to correctly discriminate 92.3% of the individuals, while CS (ANOVA; Df =1, *F*-test = 101.2, P<0.001) reach an accuracy of 94.9% (Table 2).

Similarly, in form-space PCA males and females of the New York sample (Fig. 5f) are significantly different along PC1 (40.8%; ANOVA, Df =1, *F*-test = 22.1, P<0.001), even though the two groups overlap in the middle of the plot. As observed above for the Bologna sample, the separation is mainly driven by size (r=0.99; P <0.001). Sex differences are significant using CS (ANOVA; Df =1, *F*-test = 20.2, P<0.001). Accuracy of the LDA is higher using the first form space PC scores (78.2%) than CS (73.9%), and in both cases are lower than the values obtained for the other two populations.

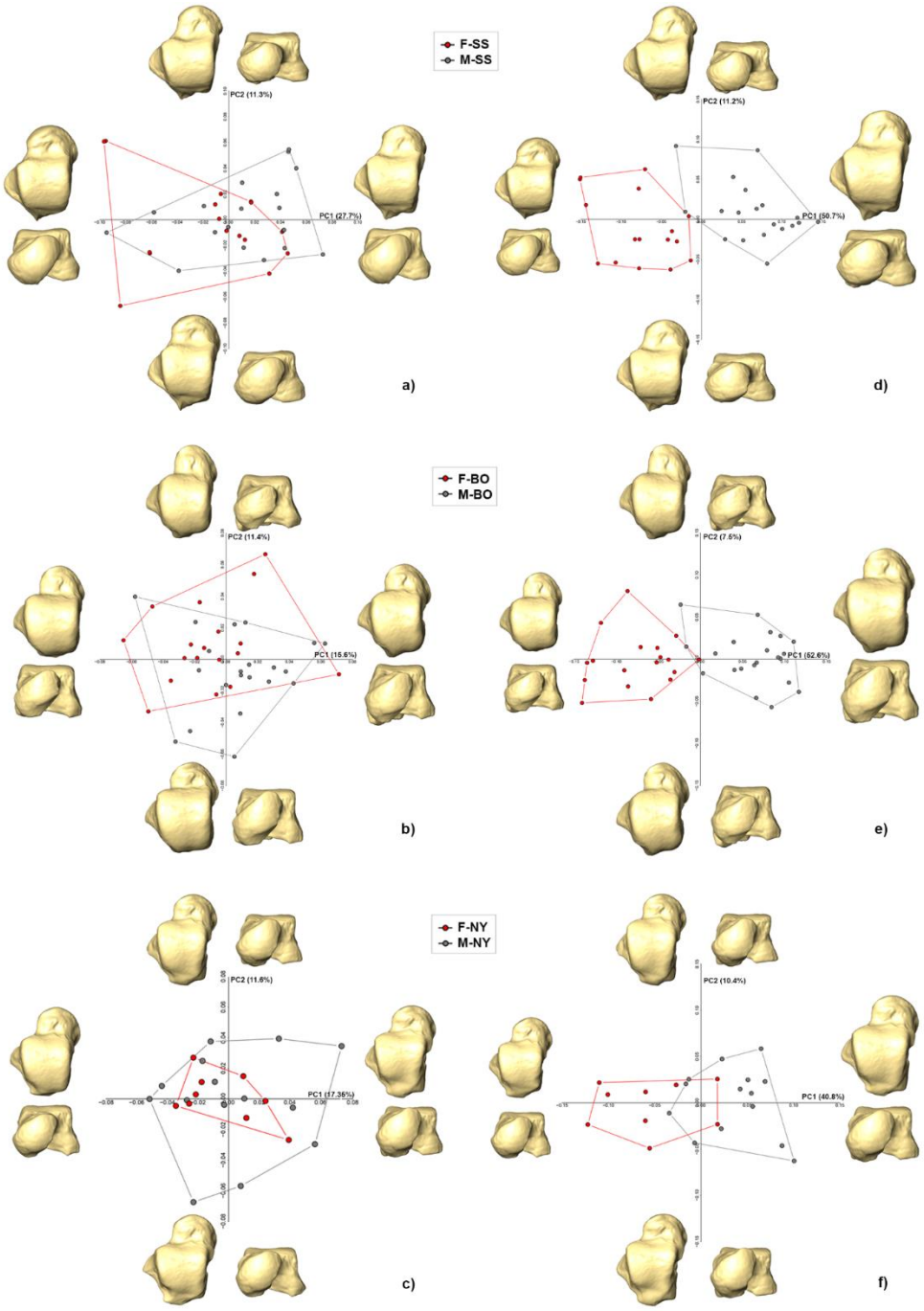

Fig. 5 Shape (left) and form (right) space PCA plots for Sassari (a and d), Bologna (b and e) and New York (c and f). The deformed mean tali in the four directions of the PCs are drawn at the extremity of each axis.

3.3 Sex assessment of virtually reconstructed talus

The two digitally reconstructed tali were projected into the form space PCA plot computed for the Bologna (Fig. 6a) and pooled samples (Fig. 6b), respectively. In both cases, specimen BO-F-45 falls close to the female group.

Indeed, BO-F-45 talus was correctly classified as female (P_{post}=100%) using either 6 form space PCs or CS of the pooled sample. In similar way, the first form space PCs and CS of the Bologna sample predict the sex of this individual as female with 99.9% of probability.

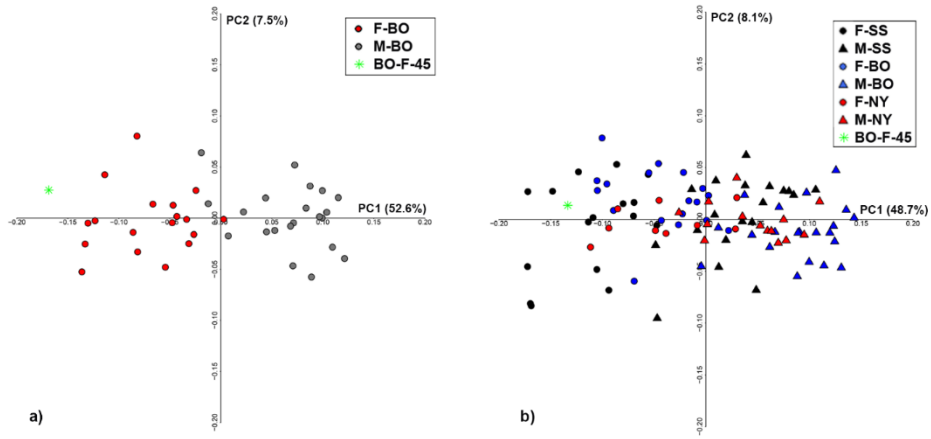

Fig. 6 Form space PCA plots of the Bologna sample (**a**) and pooled sample (**b**). The green star represents the BO-F-45 talus reconstructed based on the pooled sample mean (projected in PCA plot of pooled sample displayed in **a**) and Bologna sample mean (projected in PCA plot of Bologna displayed in **b**).

4. Discussion and conclusions

Human foot bones are often retrieved as isolated elements in both archaeological and forensic contexts [32,33] and consequently they have been the focus of several scientific contributions for sex determination and stature and age estimation [18,22,24,25, 27, 45–50]. Particularly, it is broadly accepted that the talus and the calcaneus are good indicators for the assessment of biological sex due to differences in size related to the weight bearing function of the foot [17,32,34–40]. In this study, we investigate the role of shape, form and size in discriminating biological sex based on geometric morphometric analysis of the talus. Three modern human

populations from the early 20th century (Sassari, Bologna, New York) from different geographical locations (Italy and USA) were analyzed. We followed two different approaches, i.e., 1) considering the populations as a unique sample and exploring sex-related interpopulation trajectories and 2) focusing on each individual population to assess the discriminatory power of the talus for sex determination. Finally, we show that GM methods can be used to cope with fragmented tali, ultimately overcoming intrinsic limits of the traditional approach.

When considering the pooled early 20th century sample, the amount of sexual dimorphism differs significantly among populations (Fig. 3 and 4). Indeed, a permutation test returns significantly different intragroup allometric trajectory between Sassari and Bologna, as well as between New York and Bologna in both shape and form space, while this is not the case between Sassari and New York. This result suggests that a population-specific approach should be used to evaluate sexual dimorphism in modern human tali. In form space PCs of the pooled sample, most of the individuals are correctly classified (about 92%), ultimately emphasizing the crucial role of size for sex determination based on the talus. The same holds when turning to a specific population approach, where either form space PCs or CS provide the best outcome, despite differences in the accuracy of the results among the populations.

Overall, this is in line with the results of Gualdi-Russo [34], who pointed out that male individuals exhibit larger talar measurements than female individuals. However, our study based on a 3D GM approach adds something more to the current debate on sex-related talar morphometric changes. The Sassari sample, for example, shows allometric shape differences in the talar head and neck morphology between males and females. With increasing size, the talar neck become longer, the head is less mediolaterally extended, and the medial malleolar facet is more concave and anteriorly extended. Since this morphological variation was observed only for Sassari, but not for Bologna and New York, it is difficult to provide a functional explanation. These weakly morphological differences may have no adaptive explanation since modern humans (both males and females) are committed bipeds. However, differences in footwear choice and lifestyle factors (e.g., posture, nutrition, daily activity patterns) may affect talar morphological variation [36,72–74].

Finally, in this contribution we emphasize the opportunity offered by (semi)landmark-based methods when dealing with fragmentary tali, which are usually discarded from traditional analyses. We digitally simulated a trivial condition that hampers the collection of fundamental linear measurements (e.g., length and width of the talus, length and breadth of the trochlea, length and breadth of the posterior articular surface for the

calcaneus), and we carried out two digital reconstructions based on the mean of both the pooled sample and the Bologna sample. Since our results on the known sample show that shape differences between males and females are extremely reduced and mainly related to allometry, virtual reconstruction based on a TPS interpolation function will basically scale the reference specimen into the target (i.e., the fragmented talus). Indeed, both virtual reconstructions are very similar and allow correct classification of the sex of the individual with a P_{post} between 99.9% and 100%. Therefore, even though it is desirable to select a reference specimen from the population that the target (i.e., case study) is derived from when possible, our results suggest that, at least based on our sample, the grand mean of the pooled sample might be an effective reference for digital reconstruction of fragmented tali.

In conclusion, the results of this study confirm that the talus is a good indicator of sexual dimorphism and it can be used in those forensic scenarios in which only isolated bones are retrieved (e.g., mass disasters, commingled burials, altered taphonomic contexts). Furthermore, considering that human bones from forensic and archaeological contexts are often retrieved in fragmentary conditions, geometric morphometric approach will give the possibility to virtually reconstruct the specimen under study and undertake, e.g., sex discrimination.

Acknowledgments

This project has received funding from the European Research Council (ERC) under the European Union's Horizon 2020 research and innovation programme (grant agreement No 724046 – SUCCESS); http://www.erc-success.eu/

References

[1] D.W. Frayer, M.H. Wolpoff, Sexual Dimorphism, Annu. Rev. Anthropol. 14 (1985) 429–473. http://doi:10.1146/annurev.an.-14.100185.002241.

[2] G. Acsádi, J. Nemeskéri, History of Human Life, Span and Mortality, Akademial Kiadò, Budapest, 1970.

[3] M.Y. Işcan, Forensic anthropology of sex and body size, Forensic Sci. Int. 147 (2005) 107–112. http://doi:10.1016/j.forsciint.2004.-09.069.

[4] E.H. Kimmerle, L.W. Konigsberg, R.L. Jantz, J.P. Baraybar, Analysis of age at death estimation through the use of pubic symphyseal data, J. Forensic Sci. 53 (2008) 558–568. https://doi.org/10.1111/j.1556-4029.2008.00711.x

[5] E.H. Kimmerle, A. Ross, D. Slice, Sexual dimorphism in America: Geometric morphometric analysis of the craniofacial region, J. Forensic Sci. 53 (2008) 54–57. http://doi:10.1111/j.1556-4029.2007.00627.x.

[6] A. Kemkes-Grottenthaler, The reliability of forensic osteology - A case in point: Case study, Forensic Sci. Int. 117 (2001) 65–72. http://doi:10.1016/S0379-0738(00)00450-3.

[7] K. Krishan, P.M. Chatterjee, T. Kanchan, S. Kaur, N. Baryah, R.K. Singh, A review of sex estimation techniques during examination of skeletal remains in forensic anthropology casework, Forensic Sci. Int. 261 (2016) 165.e1-165.e8. http://doi:10.1016/j.forsciint.-2016.02.007.

[8] K.J. Reichs, Forensic osteology: advances in the identification of human remains, Charles C. Thomas, Springfield, 1998.

[9] D.H. Ubelaker, International Advances in Identification of Human Remains, in: New Perspect. Forensic Hum. Skelet. Identif., Elsevier, 2018: pp. 295–300.

[10] C. Cattaneo, Forensic anthropology: developments of a classical discipline in the new millennium, Forensic Sci. Int. 165 (2007) 185–193. http://doi:10.1016/j.forsciint.2006.05.018.

[11] M.M. Holland, D.L. Fisher, L.G. Mitchell, W.C. Rodriquez, J.J. Canik, C.R. Merril, V.W. Weedn, Mitochondrial DNA sequence analysis of human skeletal remains: identification of remains from the Vietnam War, J. Forensic Sci. 38 (1993) 542–553. https://doi.org/10.1520/JFS13439J.

[12] M. Suhani, M. Noor, L. See, W. Za, Z. Alias, A. Ha, M. Azaini, M. Shah, The clandestine multiple graves in Malaysi: The first mass identification operation of human skeletal remains, Forensic Sci. Int. 278 (2017) 1–9. http://doi:10.1016/j.forsciint.2017.05.014.

[13] S. Theresa, D. Ellingham, P. Perich, M. Tidball-binz, The fate of human remains in a maritime context and feasibility for forensic humanitarian action to assist in their recovery and identification, Forensic Sci. Int. 279 (2017) 229–234. http://doi:10.1016/-j.forsciint.2017.07.039.

[14] A. Ambers, Improved Y-STR typing for disaster victim identification , missing persons investigations , and historical human skeletal remains, Int. J. Legal Med. 132 (2018) 1545–1553. https://doi.org/10.1007/s00414-018-1794-8.

[15] S. Schlager, A. Rüdell, Sexual Dimorphism and Population Affinity in the Human Zygomatic Structure - Comparing Surface to Outline Data, Anat. Rec. 300 (2017) 226–237. https://doi:10.1002/ar.23450.

[16] T. White, P. Folkens, The human bone manual, Elsevier Academic Press, 2005.

[17] M.A. Bidmos, M.R. Dayal, Sex Determination from the Talus of South African Whites by Discriminant Function Analysis, Am. J. Forensic Med. Pathol. 24 (2003) 322–328. http://doi:10.1097/01-.paf.0000098507.78553.4a.

[18] P.N. González, V. Bernal, S. Ivan Perez, G. Barrientos, Analysis of dimorphic structures of the human pelvis: its implications for sex estimation in samples without reference collections, J. Archaeol. Sci. 34 (2007) 1720–1730. http://doi:10.1016/j.jas.2006.12.013.

[19] W.M. Krogman, M.Y. Işcan, The human skeleton in forensic science, CC Thomas Springf. (1986).

[20] J. Bruzek, A method for visual determination of sex, using the human hip bone, Am. J. Phys. Anthropol. 117 (2002) 157–168. https://doi.-org/10.1002/ajpa.10012.

[21] P. Murail, J. Bruzek, F. Houët, E. Cunha, DSP: A tool for probabilistic sex diagnosis using worldwide variability in hip-bone measurements, Bull. Mémoires La Société d'Anthropologie Paris. 17 (2005) 167–176.

[22] L. Betti, N. Von Cramon-taubadel, A. Manica, S.J. Lycett, Global Geometric Morphometric Analyses of the Human Pelvis Reveal Substantial Neutral Population History Effects , Even across Sexes, PloS one 8 (2013) e55909.8. http://doi:10.1371/journal.pone.-0055909.

[23] C. Garrido Varas, M. Intriago Leiva, Managing commingled remains from mass graves: Considerations, implications and recommendations from a human rights case in Chile, Forensic Sci. Int. 219 (2012) e19–e24. http://doi:10.1016/j.forsciint.2011.11.035.

[24] A.J. Osterholtz, K.M. Baustian, D.L. Martin, Commingled and Disarticulated Human Remains, Springer, 2014.

[25] S. Benazzi, C. Maestri, S. Parisini, F. Vecchi, G. Gruppioni, Sex assessment from the acetabular rim by means of image analysis, Forensic Sci. Int. 180 (2008) 7–9. http://doi:10.1016/j.forsciint.-2008.06.007.

[26] S. Benazzi, C. Maestri, S. Parisini, F. Vecchi, G. Gruppioni, Sex assessment from the sacral base by means of image processing, J. Forensic Sci. 54 (2009) 249–254. http://doi:10.1111/j.1556-4029.2008.00947.x.

[27] E.F. Kranioti, M. Bastir, A. Sánchez-Meseguer, A. Rosas, A

geometric-morphometric study of the cretan humerus for sex identification, Forensic Sci. Int. 189 (2009) 2–9. http://doi:10.1016-/j.forsciint.2009.04.013.

[28] J. Albanese, A metric method for sex determination using the hipbone and the femur., J. Forensic Sci. 48 (2003) 263–273. http://doi:10.1111/j.1556-4029.2008.00855.x.

[29] K.J. Carlson, F.E. Grine, O.M. Pearson, Robusticity and sexual dimorphism in the postcranium of modern hunter-gatherers from Australia, Am. J. Phys. Anthropol. 134 (2007) 9–23. https://-doi.org/10.1002/ajpa.20617.

[30] T.L. Kivell, I. Guimont, C.E. Wall, Sex-Related Shape Dimorphism in the Human Radiocarpal and Midcarpal Joints, 30 (2013) 19–30. https://doi:10.1002/ar.22609.

[31] H. Brzobohat, Sex Classification Using the Three-Dimensional Tibia Form or Shape Including Population Specificity Approach, J. Forensic Sci. 60 (2015) 29-40. https://doi:10.1111/1556-4029.12641.

[32] C.M. Davies, L. Hackman, S.M. Black, The foot in forensic human identification - A review, Foot. 24 (2014) 31–36. https://doi:10.-1016/j.foot.2013.12.001.

[33] T. Kanchan, K. Krishan, A. Sharma, R.G. Menezes, A study of correlation of hand and foot dimensions for personal identification in mass disasters, Forensic Sci. Int. 199 (2010) 112. https://doi:10.1016/j.forsciint.2010.03.002.

[34] E. Gualdi-Russo, Sex determination from the talus and calcaneus measurements, Forensic Sci. Int. 171 (2007) 151–156. https://doi:-10.1016/j.forsciint.2006.10.014.

[35] S.M. Harris, D.T. Case, Sexual Dimorphism in the Tarsal Bones: Implications for Sex Determination, J. Forensic Sci. 57 (2012) 295–305. https://doi:10.1111/j.1556-4029.2011.02004.x.

[36] R.S. Kidd, C.E. Oxnard, Patterns of Morphological Discrimination in Selected Human Tarsal Elements, Am. J. Phys. Anthropol. 181 (2002) 169–181. https://doi:10.1002/ajpa.10021.

[37] T. Riepert, T. Drechsler, H. Schild, B. Nafe, R. Mattern, Estimation of sex on the basis of radiographs of the calcaneus, Forensic Sci. Int. 77 (1996) 133–140. https://doi:10.1016/0379-0738(95)01832-8.

[38] D.G. Steele, The Estimation of Sex on the Basis of the Talus and Calcaneus, Am. J. Phys. Anthropol. 45 (1976) 581–588. https://doi.org/10.1002/ajpa.1330450323.

[39] M. A. Bidmos, M.R. Dayal, Further evidence to show population specificity of discriminant function equations for sex determination using the talus of South African blacks., J. Forensic Sci. 49 (2004)

1165–1170. https://doi.org/10.1520/JFS2003431.

[40] D. Nathena, E. Michopoulou, E.F. Kranioti, Sexual dimorphism of the calcaneus in contemporary Cretans, Forensic Sci. Int. 277 (2017) 260.e1-260.e8. https://doi:10.1016/j.forsciint.2017.04.005.

[41] U.Y. Lee, I.B. Kim, D.S. Kwak, Sex determination using discriminant analysis of upper and lower extremity bones: New approach using the volume and surface area of digital model, Forensic Sci. Int. 253 (2015) 135.e1-135.e4. https://doi:10.1016-/j.forsciint.2015.05.017.

[42] E. Ruiz Mediavilla, B. Perea Pérez, E. Labajo González, J.A. Sánchez Sánchez, A. Santiago Sáez, E. Dorado Fernández, Determining sex by bone volume from 3D images: Discriminating analysis of the tali and radii in a contemporary Spanish reference collection, Int. J. Legal Med. 126 (2012) 623–631. https://doi:-10.1007/s00414-012-0715-5.

[43] D.C. Adams, F.J. Rohlf, D.E. Slice, Geometric morphometrics: Ten years of progress following the 'revolution,' Ital. J. Zool. 71 (2004) 5–16. https://doi:10.1080/11250000409356545.

[44] P.O. Higgins, The study of morphological variation in the hominid fossil record : biology , landmarks and geometry, J Anat 197 (2000) 103–120.

[45] D.E. Slice, Modern Morphometrics in Physical Anthropology, Springer, Boston, MA, 2005.

[46] E. Pretorius, M. Steyn, Y. Scholtz, Investigation into the usability of geometric morphometric analysis in assessment of sexual dimorphism, Am. J. Phys. Anthropol. 129 (2006) 64–70. https://doi:10.1002/ajpa.20251.

[47] S.A. Asala, M.A. Bidmos, M.R. Dayal, Discriminant function sexing of fragmentary femur of South African blacks, Forensic Sci. Int. 145 (2004) 25–29. https://doi:10.1016/j.forsciint.2004.03.010.

[48] A.Z. Mundorff, Integrating forensic anthropology into disaster victim identification, Forensic Sci. Med. Pathol. 8 (2012) 131–139. https://doi:10.1007/s12024-011-9275-0.

[49] D.H. Ubelaker, The forensic evaluation of burned skeletal remains: A synthesis, Forensic Sci. Int. 183 (2009) 1–5. https://doi:10.1016/-j.forsciint.2008.09.019.

[50] P. Gunz, P. Mitteroecker, F.L. Bookstein, Semilandmarks in three dimensions, in: Mod. Morphometrics Phys. Anthropol., Springer, 2005: pp. 73–98.

[51] P. Gunz, P. Mitteroecker, Semilandmarks: A method for quantifying curves and surfaces, Hystrix. 24 (2013) 103–109. https://doi:10.44-04/hystrix-24.1-6292.

[52] P. Mitteroecker, P. Gunz, Advances in Geometric morphometrics, Evol. Biol. 36 (2009) 235–247. https://doi:10.1007/s11692-009-9055-x.

[53] A.Z. Mundorff, E.J. Bartelink, E. Mar-Cash, DNA preservation in skeletal elements from the world trade center disaster: Recommendations for Mass Fatality Management, J. Forensic Sci. 54 (2009) 739–745. https://doi:10.1111/j.1556-4029.2009.01045.x.

[54] S. Benazzi, F.L. Bookstein, D.S. Strait, G.W. Weber, A new OH5 reconstruction with an assessment of its uncertainty, J. Hum. Evol. 61 (2011) 75–88. https://doi:10.1016/j.jhevol.2011.02.005.

[55] J.H. Arbour, C.M. Brown, Incomplete specimens in geometric morphometric analyses, Methods Ecol. Evol. 5 (2014) 16–26. https://doi:10.1111/2041-210X.12128.

[56] M.G. Belcastro, B. Bonfiglioli, M.E. Pedrosi, M. Zuppello, V. Tanganelli, V. Mariotti, The History and Composition of the Identified Human Skeletal Collection of the Certosa Cemetery (Bologna, Italy, 19th–20th Century), Int. J. Osteoarchaeol. 27 (2017) 912–925. https://doi:10.1002/oa.2605.

[57] S.M. Hens, E. Rastelli, G. Belcastro, Age estimation from the human os coxa: A test on a documented Italian collection, J. Forensic Sci. 53 (2008) 1040–1043. https://doi:10.1111/j.15564029.2008.0081-8.x.

[58] S.R. Turley, K., White, F.J., Frost, Phenotypic Plasticity : The Impact of Habitat and Behavior (Substrate Use) on Adult Talo-Crural Appositional Articular Joint Shape Both Between and Within Closely Related Hominoid Species ., Hum. Evol. 30 (2015) 49–67. https://doi:10.14673/HE201512002.

[59] F.J. Rohlf, D. Slice, Extensions of the Procrustes method for the optimal superimposition of landmarks, Syst. Biol. 39 (1990) 40–59. https://doi.org/10.2307/2992207.

[60] D.C. Adams, E. Otárola-Castillo, Geomorph: An r package for the collection and analysis of geometric morphometric shape data, Methods Ecol. Evol. 4 (2013) 393–399. https://doi:10.1111/2041-210X.12035.

[61] C.P. Klingenberg, Size, shape, and form: concepts of allometry in geometric morphometrics, Dev. Genes Evol. 226 (2016) 113–137. https://doi:10.1007/s00427-016-0539-2.

[62] F.L. Bookstein, Morphometric tools for landmark data: geometry and biology, Cambridge University Press, 1991.

[63] S.E. Bailey, S. Benazzi, J.J. Hublin, Allometry, merism, and tooth shape of the upper deciduous M2 and permanent M1, Am. J. Phys. Anthropol. 154 (2014) 104–114. https://doi:10.1002/ajpa.22477.

[64] U.Y. Lee, S.H. Han, D.K. Park, Y.S. Kim, D.I. Kim, I.H. Chung, M.H. Chun, Sex Determination from the Talus of Koreans by Discriminant Function Analysis, J. Forensic Sci. 57 (2012) 166–171. https://doi:10.1111/j.1556-4029.2011.01914.x.

[65] S. Senck, M. Coquerelle, G.W. Weber, S. Benazzi, Virtual Reconstruction of Very Large Skull Defects Featuring Partly and Completely Missing Midsagittal Planes, Anat. Rec. 296 (2013) 745–758. https://doi:10.1002/ar.22693.

[66] L. Scheuer, S. Black, A. Christie, Bone development, Dev. Juv. Osteol. Acad. Press. Londres. (2000).

[67] M.C. Schaefer, S. Black, J.L. Scheuer, Juvenile osteology, London: Academic Press (2009).

[68] J.M. Whitaker, L. Rousseau, T. Williams, R.A. Rowan, W.C. Hartwig, Scoring system for estimating age in the foot skeleton, Am. J. Phys. Anthropol. 118 (2002) 385–392. https://doi:10.1002/-ajpa.10109.

[69] L. Hackman, C.M. Davies, S. Black, Age Estimation Using Foot Radiographs from a Modern Scottish Population, J. Forensic Sci. 58 (2013) 146–150. https://doi:10.1111/1556-4029.12004.

[70] T.D. Holland, Brief Communication Estimation of Adult Stature From the Calcaneus and Talus Am. J. Phys. Anthropol. 96 (1995) 315–320. https://doi.org/10.1002/ajpa.1330960308.

[71] M. Bidmos, Adult stature reconstruction from the calcaneus of South Africans of European descent, J. Clin. Forensic Med. 13 (2006) 247–252. https://doi:10.1016/j.jcfm.2005.11.010.

[72] W.C.H. Parr, A. Ruto, C. Soligo, H.J. Chatterjee, Allometric shape vector projection: A new method for the identification of allometric shape characters and trajectories applied to the human astragalus (talus), J. Theor. Biol. 272 (2011) 64–71. https://doi:10.1016/-j.jtbi.2010.11.030.

[73] W.E.H. Harcourt-Smith, Form and function in the hominoid tarsal skeleton, University of London, PhD Thesis. (2002).

2.2 Paper II

The influence of mobility strategy on the modern human talus

Rita Sorrentino[1,2], Nicholas B. Stephens[3], Kristian J. Carlson[4,5], Carla Figus[2], Luca Fiorenza[6,7], Stephen Frost[8], William Harcourt-Smith[9,10,11,12], William Parr[13], Jaap Saers[14], Kevin Turley[8], Stephen Wroe[15], M. Giovanna Belcastro[1,16], Timothy M. Ryan[3], Stefano Benazzi[2,17]

[1]Department of Biological, Geological and Environmental Sciences, University of Bologna, Bologna 40126, Italy.
[2]Department of Cultural Heritage, University of Bologna, Ravenna 48121, Italy.
[3]Department of Anthropology, Pennsylvania State University, University Park, PA 16802, USA.
[4]Evolutionary Studies Institute, University of the Witwatersrand, Palaeosciences Centre, Private Bag 3, Wits 2050, South Africa.
[5]Department of Integrative Anatomical Sciences, Keck School of Medicine, University of Southern California, Los Angeles 90089, USA.
[6]Department of Anatomy and Developmental Biology, Monash University, Clayton, VIC 3800, Australia.
[7]Earth Sciences, University of New England, Armidale NSW 2351 Australia.
[8]Department of Anthropology, University of Oregon, Eugene, OR, 97403–1218, USA.
[9]Graduate Center, City University of New York, New York, NY 10016, USA.
[10]New York Consortium in Evolutionary Primatology, New York, NY 10024, USA.
[11]Department of Anthropology, Lehman College, New York, NY 10468, USA.
[12]Division of Paleontology, American Museum of Natural History, New York, NY 10024, USA.
[13]Surgical and Orthopaedic Research Laboratory, Prince of Wales Hospital, University of New South Wales, Sydney 1466, Australia.
[14]PAVE Research Group, Department of Archaeology & Anthropology, University of Cambridge, Pembroke Street, Cambridge CB2 3ER, United Kingdom.
[15]Function, Evolution and Anatomy Research Laboratory, Zoology Division, School of Environmental and Rural Science, University of New England, New South Wales 2351, Australia.
[16]ADES, UMR 7268 CNRS/Aix-Marseille Université/EFS, Aix-Marseille Université, CS80011, Bd Pierre Dramard, Marseille Cedex 15, 13344, France.
[17]Department of Human Evolution, Max Planck Institute for Evolutionary Anthropology, Leipzig 04103, Germany.

Corresponding author: Rita Sorrentino, rita.sorrentino2@unibo.it

[Under review in Scientific Reports]

Abstract

Although the human (*Homo sapiens*) talus -located at the ankle- is morphologically specialized for bipedal walking, its morphology varies in accordance with behavior. Here we apply (semi)landmark-based methods and whole-bone trabecular analysis to tali of modern human populations with different subsistence economies and lifestyles to explore how cultural and environmental factors influence external shape and internal trabecular structure. Our results show distinct differences in shape and structure between highly mobile hunter-gatherers and more sedentary groups belonging to a mixed post-agricultural/industrial background. Hunter-gatherers exhibit a more "flexible" talar shape with high bone volume fraction, which we interpret as reflecting long-distance walking strictly performed barefoot, or wearing minimalistic footwear, along uneven ground. The talus of the post-industrial population exhibits a "stable" profile with low bone volume fraction, as a consequence of sedentary lifestyle and use of stiff footwear. We conclude that modern human tali vary with differences in locomotor and cultural behavior.

Introduction

Humans are the only obligate bipeds among extant primates. Morphologically, this shift in locomotion has led to substantial changes in the hominin skeleton, differentiating us from other extant great apes[1,2]. Among all the derived anatomical features associated with this locomotor change, the human foot is among the most specialized, with the talus playing a key role in bearing body weight and maintaining stability during bipedal walking[2–4]. Moreover, humans have retained the ability to use their feet for other activities, such as climbing, running, striding, and limited grasping[5]. Overall, the locomotor strategy pursued by modern humans is highly variable between populations and environments. Consequently, human feet must adapt to these differences.

Aside from development, bone morphology is affected by differences in the loading regime, activity level and distances covered in a day[6–9]. Comparison between hunter-gatherers and agriculturalists indicate that the latter are characterized by less robust skeletal elements associated with a reduction in activity[6,10–15]. Similarly, skeletal gracilization of internal bone structure has been observed in Holocene *Homo sapiens*, which is thought to be a consequence of decreased mechanical stimuli resulting in reduced

apposition of bone tissue[7,8,16]. While most studies have investigated cross-sectional differences in cortical bone, similar reductions in trabecular bone structure have been reported for the lower and upper limbs[7,8,11,12,17–20]. Differences in the intrinsic proportions of the foot have been noted between human groups with different levels of locomotor performance. Sprinters show a shorter rearfoot, resulting in shorter moment arms (i.e., lever arm), that increases plantar flexor work and reduces energetic costs[21,22].

Aside from physiological variation, cultural and technological factors also influence the ways in which humans use their feet to interact with their environment. The most notable of these is the widespread use of stiff shoes or boots to protect feet, as in industrial societies, which contrasts with the practice of prehistoric societies and modern hunter-gatherers, who tend to walk barefoot or use soft footwear[23]. It has been demonstrated that prolonged use of constrictive foot coverings results in structural changes to the bones of the feet, which may manifest as pathological conditions[23–26], with the forefoot showing the highest incidence of pathology (e.g. hallux valgus, reductions in bone strength, and abnormal metatarsal/matatarsophalangeal modifications). Furthermore, while the transmission of mechanical forces through the foot during the stance phase of walking seems the same in shod and unshod feet, there is a loss of pliability in plantar arches for shod individuals[23,27,28]. Biomechanically, unshod individuals tend to have wider feet (Fig.1) that more equally distribute peak pressures during walking, which may help limit injury[29]. The foot strike patterns in runners tend to vary between shod and unshod individuals as well, with shod individuals more often striking at the heel and barefoot runners more often

Fig. 1 | Comparison of a) unshod and b) shod feet. An unshod foot exhibits a wider profile, flatter forefoot and toes that are spread out compared to a shod foot that exhibits a narrow forefoot, elevated arch and crowded toes.

striking at the midfoot, thus avoiding damage to the heel from high impacts against hard substrates[28,30,31].

It has recently been shown that hominid talar shape varies according to different locomotor modes and substrate uses[32–37]. However, less is known about variation in talar morphology within modern humans[32,37,38]. Here, we test the hypothesis that aspects of talar morphology reflect variation in mobility strategy (active vs. sedentary), substrate (flat vs. uneven) and footwear (shod vs. unshod/minimally shod). To our knowledge, this work is the first to assess at the same time how the external and internal morphology of the talus varies among groups of modern humans (Table 1). Morphological data were collected by means of a 3D configuration consisting of 251 (semi)landmarks covering the entire external surface of the talus (Fig.2 and Table 2). The functional significance of internal morphological differences was assessed by quantifying trabecular bone structure (i.e., bone volume fraction (BV/TV), degree of anisotropy (DA), and elastic modulus (E)), which are known to vary in relation to habitual mechanical loading (38).

Finally, this work aims to determine anatomical pedal changes related to different human behaviors during bipedal walking.

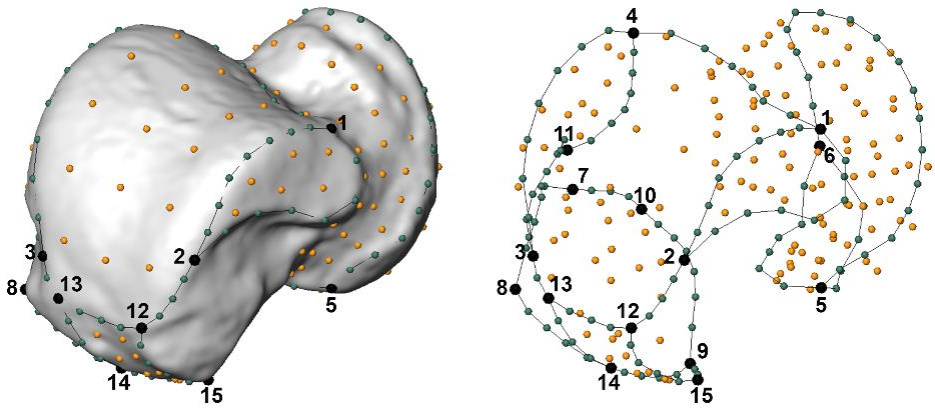

Fig. 2 | Talar configuration of 251 (semi)landmarks. Landmarks are the black spheres, curve and surface semilandmarks are dark green and orange spheres, respectively.

Table 1 | Sample examined in the present study.

Sample	Number	Period	Geografical location	Subsistence	Typical Footwear	Collections[1]
UP/LSA[2]	6	Upper Paleolithic/ Late Stone Age	Italy; Ethiopia	hunter-gatherers	Unshod/soft covering	DBP/ NHMP
Black Earth	15	3000 B.C.	Illinois, USA	hunter-gatherers	Unshod/soft covering	SIU
Californian	9	Shell Midden Cultures (~1500 B.C. - 500 A.D.)	California, USA	hunter-gatherers	Unshod/soft covering	PAHM
Norris Farms	10	Late Prehistoric North America (1300 A.D.)	Illinois, USA	mixed agriculture and foraging	Unshod/soft covering	ISM
Point Hope	8	~1600 - 500 B.C.	Alaska, USA	maritime subsistence	Seal Skin Boots	AMNH
Egyptian	7	~600 - 350 B.C.	Egypt	farmers/maritime subsistence	Thin Leather Shoes	AMNH
Paleo Pueblo	6	~1000 B.C.	New Mexico, USA	mountain dwellers	Heavy Double Yucca Sandal	AMNH
Roccapelago	15	17th-18th century	Italy	mountain dwellers	Socks with reinforced soles/ shoes	SAPAB
Nguni	6	20th century	Southern Africa	Farmers	Sandals	BiGeA
Bologna	39	19th-20th century	Italy	post-industrial	Heavy Leather Shoes/Boots	BiGeA
New York	21	early 20th Century	New York, USA	post-industrial	Heavy Leather Shoes/Boots	NMNH

[1]DBP, Department of Biology, University of Pisa, Pisa; NHMP, The Natural History Museum, Department of Earth Sciences, London; SIU, Southern Illinois University, Carbondale; PAHM, P. A. Hearst Museum Collections, University of California, Berkeley; ISM, Illinois State Museum, Springfield; AMNH, American Museum of Natural History, New York; SAPAB, Soprintendenza Archeologia, Belle Arti e Paesaggio per la città metropolitana di Bologna e le province di Modena, Ferrara e Reggio Emilia; BiGeA, Department of Biological, Geological and Environmental Sciences, University of Bologna, Bologna; NMNH, National Museum of Natural History, Smithsonian, Washington.
[2]UP, Upper Paleolithic (Romito7, Romito 8, Romito 9, Veneri 2 and Villabruna); LSA, Late Stone Age (Clark Howell Omo, Ethiopia).

Table 2. Landmarks of talar configuration.

Landmarks	Type	Labels in Fig. 2
Most distal lateral point of contact between the medial malleolar facet and the trochlear surface	II	1
Most proximal point of contact between the medial malleolar facet and the trochlear surface	II	2
Most proximal point of contact between the lateral malleolar facet and the trochlear surface	II	3
Most distal point of contact between the lateral malleolar facet and the trochlear surface	II	4
Most medial point of contact between the head/navicular facet	III	5
Most lateral point on the head/navicular facet	III	6
Most lateral point on the proximal calcaneal facet	III	7
Deepest (most dorsal) point on the proximal calcaneal facet	III	8
Most proximo-medial point on the proximal calcaneal facet	III	9
Most disto-lateral point on the proximal calcaneal facet	II	10
Most plantar point on the lateral malleolar facet	III	11
Flexor hallucis longus: most distal point on the medial margin	III	12
Flexor hallucis longus: most distal point on the lateral margin	III	13
Flexor hallucis longus: intersection with calcaneus curve	II	14
Flexor hallucis longus: most postero-inferior prominent point	III	15

Results

External talar morphology. Overall, our results show that talar morphology varies among modern human groups. The shape space PCA plot (Fig. 3) depicts a trend in separating hunter-gatherers from early agriculturalist/post-industrial populations along PC1 (45.3%). ANOVAs with Tukey post hoc tests (Supplementary Table 1) indicate significant differences between the more mobile Upper Paleolithic/Late Stone Age group, Californian, Black Earth, Norris Farms (with generally positive PC1 scores) versus the more sedentary groups of Bologna ($P<0.001$) and New York (from $P<0.005$ to $P<0.001$) with more negative values PC1 scores. The other modern human groups (Roccapelago, Point Hope, Egyptian, Paleo Pueblo, Nguni) are intermediate, overlapping both higher and lower mobility groups, as they are probably intermediate in mobility (e.g., Norris Farms). However, most of these intermediate groups are significantly

different from post-industrial populations (from P<0.05 to P<0.001), except for Nguni with both Bologna and New York, as well as Egyptians with the New York sample. In a similar way, the Norris Farms, Point Hope, Egyptian, Roccapelago, and Nguni samples differ from Californian and/or Black Earth groups (Supplementary Table 1).

Positive scores along PC1 (hunter-gatherers) reflect shorter talar length, a trochlea that deviates slightly laterally from the midline of the talus, a mediolaterally wider anterior margin of the trochlea with an anterior extension of the medial margin, a laterally extended and curved lateral malleolar facet, a relatively more cupped medial malleolar facet that extends further anteriorly with a marked anteromedial edge for the attachment of the anterior tibiotalar ligament, an enlarged talar neck and head that are more medially oriented, and a more concave and coronally

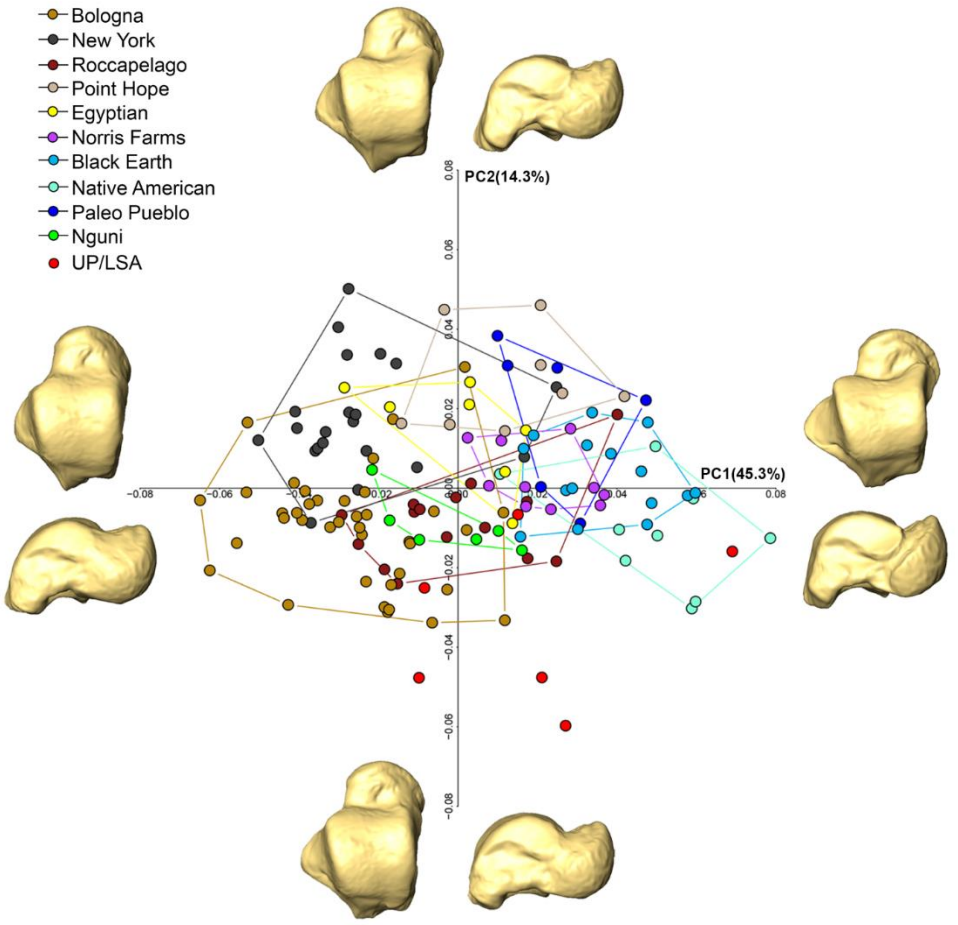

Fig. 3 | Shape space PCA plot and the surface warps of left tali along the PC axes.

oriented posterior calcaneal facet when compared to negative scores along PC1 (sedentary groups) (Fig.3 and Supplementary Fig. 1). Principal component 2 accounts for 14.3% of shape variability with positive scores reflecting a more oval and concave posterior calcaneal facet, an antero-posteriorly longer medial trochlear edge, and a posterior extension of the medial and lateral tubercles when compared to those with negative PC2 scores. There is overlap among groups, although the American groups tend to occupy the positive end, with Europeans and Africans (aside from Egyptians) occupying the negative end of the axis.

Procrustes ANOVA showed significant effects of shape variation due to typical footwear ($F = 7.72$, $R^2 = 0.099$, $df= 2$, $p= 0.001$), substrate ($F =10.91$, $R^2 = 0.072$, $df= 1$, $p= 0.001$) and mobility strategy ($F = 7.66$, $R^2 = 0.099$, $df= 2$, $p= 0.001$). The respective R^2 indicate that both factors corresponding to typical footwear and mobility strategy are responsible for 9.9% of overall variation, whereas substrate accounts for 7.2% of overall variation.

A Pearson's correlation indicates that only PC1 is correlated with the logarithm of centroid size, i.e. static allometry ($r=-0.38$; $P<0.001$). Results of centroid size on the boxplot (Supplementary Fig. 2 and Supplementary Table 2) and an ANOVA with Tukey post hoc tests (Supplementary Table 3) show that the Bologna, Upper Paleolithic/Late Stone Age, and New York samples have larger tali than those from the Black Earth group (from $P<0.05$ to $P<0.001$). The size distribution of Bologna differs also from those of Norris Farms and Egyptians ($P<0.05$, Supplementary Table 3).

In the form space PCA, the first two PCs explain 77.7% of total variability (Supplementary Fig. 3). PC1 (66.5%) accounts for variation in overall size, whereas PC2 tends to separate sedentary groups (positive scores) from more mobile modern humans (negative scores), as previously described for shape space PC1.

Based on the results obtained by the PCA in shape space, individuals at the observed extremes for each PC (i.e., positive and negative extreme individuals for PC1 and PC2) were selected for the analysis of trabecular structure (Supplementary Table 4).

Trabecular structure. Figure 4 illustrates the PCA plot of two populations used for the trabecular analysis. Tali located on the extremes of PC axes represent trabecular bone volume fraction (BV/TV) distribution. The Black Earth talus (extreme of PC1 positive) expressed visibly higher BV/TV with

more expansive regions in respect to the Bologna talus (extreme of PC1 negative).

Results from a Mann Whitney-U test for BV/TV and elastic modulus (E) found significant differences between Bologna (n = 8) and Black Earth (n = 6) individuals (BV/TV, U = 45 p = 0.005; E, U = 45 p = 0.005), but no differences were found for degree of anisotropy (DA). In both cases the Black Earth population have higher BV/TV and E, indicating the likelihood of more robust talar bones overall (Supplementary Table 4).

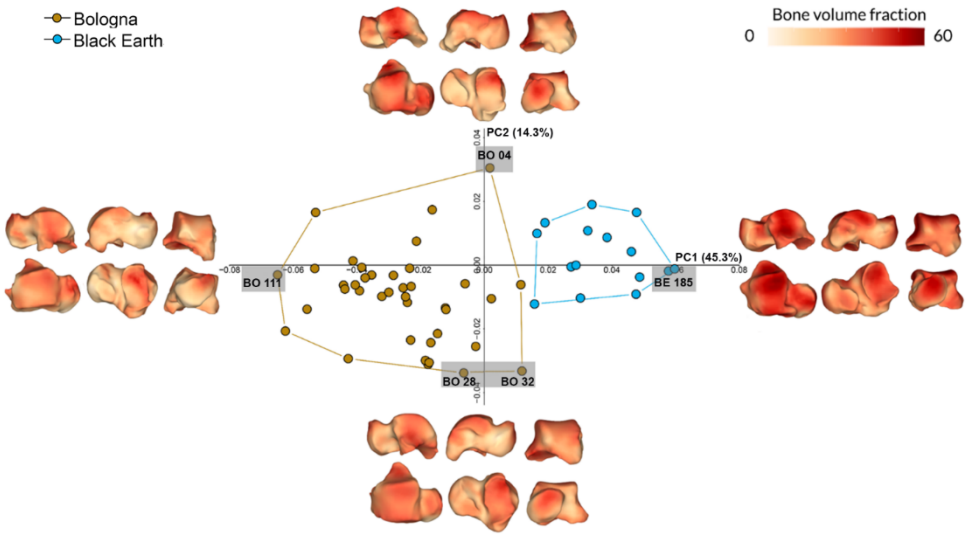

Fig. 4 | Trabecular bone volume fraction distribution for the left tali located at the extremes of the principal component axes. Shaded boxes indicate selected individuals. Note that the PC2 negative represents an average of BO28 and BO32.

Discussion

Our results point to relevant morphological differences between hunter-gather populations and post-industrial people (Fig. 3, 4, Supplementary Fig. 1). It is likely that these reflect biomechanical differences in response to differences in locomotor behavior. Generally, hunter-gatherers show relatively shorter tali when compared to individuals from post-industrial Bologna and New York groups (Fig 3 and Supplementary Fig. 1). Studies on rearfoot relative proportions find that runners tend to have shorter

plantarflexor moment arms[21] and that shorter calcaneal tubers are correlated with more efficient running[22]. Although there are no controlled studies, that we are aware of, that examine how talar length is related to effective endurance running, our results suggest that there may be a relationship. Further research should explore this dynamic, as it is relevant to the evolution of running capabilities in the genus *Homo*[39].

Other notable shape differences exist between the various groups (Fig 3 and Supplementary Fig. 1). The post-industrial populations (Bologna and New York) show a square-shaped trochlea, whereas hunter-gatherers (especially Californian and Black Earth) are characterized by a mediolaterally expanded anterior trochlea with an anterior extension of the medial margin, as well as an anterior extension of the medial malleolar facet. The extension of both the medial malleolar surface and the medial edge of the trochlea are associated with dorsiflexion of the ankle joint[40,41]. Similarly, talar corpora, as seen in lateral view, are relatively more dorsally convex in hunter-gatherers, allowing for a broader range of ankle excursion in the parasagittal plane (dorsal and plantar flexion)[42]. Interpretation of differences in width of the anterior margin of the trochlea is more difficult. In African apes the anterior aspect of the talocural joint is mediolaterally broad, which is thought to relate to the need for dissipating peak compressive forces associated with greater dorsiflexion during climbing[42,43]. DeSilva[43] hypothesizes that the same would be true for hominins engaging in vertical climbing. However, Venkataraman and colleagues[44,45] did not observe differences between the dimensions of the anterior margin of hunter-gatherers who climb trees and those of humans from industrialized societies. Anterior medio lateral width increase also causes wedging, preventing over rotation in dorsiflexion of the talus in the talocrural joint[46]. This could be related to habitual passive dorsiflexion extremes during development (for example during squatting). Due to these conflicting results, further research is needed to understand the functional significance of an expanded anterior trochlear margin.

The talocrural joint in hunter-gatherers also reflects lateral displacement of the lateral malleolar facet, a more cupped medial malleolar facet and a slightly laterally deviated trochlea. This configuration likely indicates eversion of the foot while standing and walking and likely increased anterior wedging[26,46] and -as expressed by the marked anteromedial edge of the medial malleolar facet in hunter-gatherers (Fig. 3 and Supplementary Fig. 1)- this likely implies stress on the deltoid ligament (particularly the tibiotalar ligament), which stabilizes the ankle and restricts excessive eversion of the foot[47,48]. The posterior extension of the medial limit of the head facet (Fig. Supplementary Fig. 1), which contacts the spring ligament during eversion, may also be linked to increased

loading through an everted talus. In contrast, the configuration of the tibiotalar joint in post-industrial groups shows the trochlear axis is more parasagittally oriented, reflecting a relatively more vertical tibia with less range of motion at the ankle joint[42,43,46,49].

The talar neck and head in hunter-gatherers are more medially displaced with respect to the trochlea, while they are more orthogonally oriented in the post-industrial populations. This may be an indicator of a habitually adducted hallux as a consequence of routinely wearing rigid shoes[3,26,50]. Scholars have shown increased medial deviation of the first metatarsal in barefoot individuals and lateral deviation of the hallux in shod feet, which may ultimately cause a valgus hallux[23–26] (Fig. 1). Hunter-gatherers display an enlarged talar neck and more rounded, broader navicular facets. It is known that, during toe-off, the transmission of body weight shifts from the talar head to the first and second metatarsals[2,38]. Trinkaus[23] showed that unshod Native Americans have more robusticity in hallucal proximal phalanges compared to habitually shod Inuit and modern Euroamericans. He found that the use of footwear reduces the role of the hallux during toe-off, dissipating the ground reaction force across the plantar aspect of the foot, ultimately resulting in decreased robusticity of hallucal phalanges. This is consistent with our results for the decreased dimensions of the talar neck and head, where the involvement of the big toe, working in conjunction with a stiff shoe, at toe-off has reduced the need for a robust talar neck and head.

Further differences are observed on the posterior portion of the talus, where the calcaneal facet appears more concave and coronally oriented in hunter-gatherers, allowing more eversion-inversion capabilities at the subtalar joint[2,38]. In addition, the anterior and middle calcaneal facets are separated by a ridge that, together with the posterior calcaneal facet, forms a tripod facet configuration that increases stability at the subtalar joint[51].

When taken together, these traits suggest that the tali of hunter-gatherers provided a more “flexible” shape (i.e., a shape configuration that provides flexibility of joint movement), when compared to the more “stable” shape of the tali (i.e., a talar shape that guarantees stability at the joints) of post-industrial people[32]. However, it should also be noted that some differences seen in hunter-gatherers (e.g. medially extending head, trochlea-head alignment) may have an allometric origin since PC1 is correlated, although weakly, with size and the hunter gatherer tali are (generally) smaller than the tali of post-industrial populations[52].

Hence, overall, we suggest that morphological differences in the talus between hunter-gatherers and post-industrial individuals reflect different levels of mobility and mechanical loading (Fig. 4). This is supported by trabecular bone structure of the analyzed populations, where lower BV/TV

and E of the more sedentary post-industrial sample indicates reduced routine loading compared to that of the highly mobile hunter-gatherers[8,16]. In site-specific BV/TV maps, the talar facets echo shape results described above, with the tali of hunter-gatherers showing expanded regions of BV/TV along the lateral aspect of the trochlea, the medial aspect of the subtalar surface, and the antero-superior aspect of the head. These results agree with previous assessments of BV/TV distribution in humans[53] and, together with the morphological differences noted above, support the idea that these features are related to differences in locomotion and load distribution between the sedentary groups and highly mobile groups. More broadly, these results are consistent with progressive gracilization of the human lower limb from the Holocene onward as a consequence of decreased mobility and activity levels and mechanical loading (e.g., 17, 47). In addition to greater distance travelled, talar robusticity in hunter-gatherers may reflect adaptation to uneven terrain that increases mediolateral movement, thus requiring higher stability[20]. Individuals from post-industrial societies, in contrast, who walk on packed roads or asphalt do not have to stabilize the foot over such uneven terrain, but may have to compensate for higher ground reaction forces from the stiffer substrate. A stiff, albeit less flexible, shoe may be beneficial under these circumstances. Thus, the use of heavy leather shoes and boots may work to reduce dorsal and plantar flexion, as well as eversion and inversion excursion, by blocking the region around the ankle and decreasing the space in which the foot can move (remaining constricted by the shoe). All these movements are reflected in morphology of the talus of hunter-gatherers. For highly mobile and unshod individuals, the stability of the talus appears to be reinforced by the tripod configuration of the calcaneal facet[51], as well as by the strength of medial ligaments[47].

Individuals with intermediate levels of mobility (Fig. 3), also adopt an intermediate footwear of non-restrictive sandals/skin boots with soft soles. While this style of footwear does not strongly compress the foot[26], the soft soles allow the foot to adapt to the ground during running or walking. However, even if they do not walk on hard packed surfaces (e.g., asphalt roads or concrete/packed soil) they also do not walk strictly barefoot along uneven ground. Consequently, their talar morphology reflects this intermediate level of mobility, as well as intermediate degrees of foot covering and substrate use. Indeed, the talar neck and head are relatively smaller than those of hunter-gatherers, while they are larger than in post-industrial populations. Additionally, the lateral and medial malleolar facets are less concave than in more mobile people, but more concave with respect to those of sedentary populations.

However, other variables could play a role in differentiating modern human tali. Variation in talar morphology may also stem from ancestry, as seen in the separation of American from European and African groups along PC2 of the shape space PCA (Fig.3). However, once again, these differences may also indicate variation in individual activities. Indeed, trabecular structure varies among individuals of the same population (i.e., Bologna), as a result of intraspecific population variation (Fig. 4, Supplementary Table 4).

In conclusion, our results quantitatively demonstrate the critical functional role that the talus plays in facilitating mobility, with variation in external shape and internal trabecular structure indicating that both plastically respond to variation in locomotor behaviors and activity. Here we show that human talar shape and internal bone structure varies in ways consistent with loading differences driven by variation in footwear use and terrain (i.e., highly mobile barefoot/minimal covering vs. sedentary stiff footwear). These results are relevant to interpretations of the fossil record, and may be useful in inferring the ranges of joint movements (arthrokinematics), mobility patterns, and the behavior of extinct hominin taxa.

Methods

Samples. The sample consists of 142 tali from 11 modern human groups (Table 1). For each group, we collected information on geographical location, chronology, subsistence economies, and footwear use. Collection records or anthropological analysis have been used to select only adult individuals. When present, left tali were preferred in the selection, otherwise right tali were mirrored to be included in the work. Each talus has been controlled to exclude the presence of pathological condition such as osteoarthritic growth, bone anomalies and fractures.

The oldest sample includes a Late Stone Age individual (Clark Howell Omo) from Ethiopia[54] and middle Upper Paleolithic humans from Italy (Romito, Veneri and Villabruna). Since they lived before the Neolithic revolution, it is assumed that their subsistence economy was based on hunting and gathering and they were habitually barefoot or used minimalistic footwear[23]. Other hunter-gatherer populations in the sample are Black Earth from Illinois and Californian (Shell Midden Cultures) from San Francisco Bay (California). The Black Earth hunter-gatherers occupied multi-season base camps[55]. The Shell Midden group lived close to the mud flats and estuaries collecting mollusks and fishing in the region[32]. The Norris Farms #36 site (Illinois) is dated to approximately 1300 A.D. and

archaeological records suggest a mixed economy based on both agriculture and foraging, with an intermediate level of mobility[8,56].

Inferring footwear use in archaeological contexts is very difficult. However, the archaeological record attests to the use of sandals in the North American Southwest around ca. 9000 B.P.[57], whereas post-contact reports suggest that they were completely unshod[32]. In any case, footwear used in the pre-contact period was highly unlikely to be hard soled and rigid like modern shoes. Rather, this footwear may have consisted of soft sandals and skin boots that guarantee freedom of ankle motion allowing adaptability of the foot to the substrate[23].

The Point Hope sample are Paleo-Inuit individuals (Alaska) with a maritime subsistence[58]. Ethnohistorical records suggest that they protect their feet from the cold using sealskin boots with stiff sealskin soles[23,32]. Also, Egyptians from El Hesa had a maritime existence around the Nile River, but they also practiced agriculture and commerce. They would wear sandals or soft leather boots or be unshod[32]. Two mountain dweller groups are present in the sample. The first one consists of a Paleo Pueblo group (New Mexico) that occupied stone dwellings constructed in the Canyon de Chelly. They wore double layer woven yucca sandals[32,59].

The second one consists of individuals from Roccapelago (Italy, 17th-18th century). Anthropological and historical evidence suggests gender division in their occupational activities at Roccapelago. Men were mainly involved in husbandry of cattle, materials handling and transport, while women performed domestic tasks[60,61]. Generally, the activities were carried out while barefoot or minimally shod (with socks reinforced on the plant and on the heels). Shoes with rigid soles were worn only when going to the city or during holidays[62].

The six Nguni individuals in the sample were originally collected by Raymond A. Dart (Dart Collection, Department of Anatomical Sciences, University of the Witwatersrand, South Africa) and then, in 1926, they were donated to the Anthropological Collection of the University of Bologna managed by Prof. Fabio Frassetto. Nguni are South African people of pre- European colonization (20th century). They were herders and farmers and, despite the importance of cattle breeding in their economy, they were generally sedentary. Their clothes were made with animal skins and their traditional sandals are called “imbadada”[63].

The last two groups are post-industrial individuals from Bologna (Italy) and from New York (USA). Both represent modern urban societies of the beginning of the 20th century in which the cities are surmounted by steel infrastructures and crossed by asphalt roads and concrete sidewalks. The economy is based on different labors and specializations (agrarian,

maritime, agricultural, urban). Contemporary humans are considered to have worn heavy leather shoes and boots[32,64].

Data acquisition. The sample was virtually acquired using laser, CT and microCT scans. The Upper Paleolithic samples from Italy (Romito 7, Romito 8, Romito 9, Veneri 2 and Villabruna) were surface scanned at the Department of Cultural Heritage (University of Bologna) with a 3D ARTEC scanner. The Late Stone Age talus of Clark Howell (Omo deposits, Ethiopia), as well as Californian, Point Hope, Egyptian, Paleo Pueblo, New York tali were acquired with a Konica Minolta Vivid 910 surface laser scanner (X: ± 0.22 mm, Y: ± 0.16 mm, Z: ± 0.10 mm) and were processed using Geomagic Studio 8.

Roccapelago (voxel size: 0.470 x 0.470 x 0.6 mm), Bologna (voxel size: 0.960 x 0.960 x 0.7 mm) and Nguni (voxel size: 0.976 x 0.976 x 0.5 mm) were scanned with medical CT at Department of Diagnostic Imaging of Santa Maria delle Croci Hospital in Ravenna (Italy).

Scans for Norris Farms, Black Earth, and a subsample of the Bologna tali were scanned using the industrial microCT (OMNI-X HD600 High-Resolution X-ray computed tomography - HRCT) at the Center for Quantitative Imaging (CQI) at the Pennsylvania State University using source energy settings 180 kV, 110 μA, and between 2800 and 4800 views (0.030-0.057 μm). Data from CT and microCT scans were reconstructed from the projections and Avizo 7.1 (Visualization Science Group Inc.) was used to generate isosurfaces.

Geometric Morphometric analysis. External talar surfaces were investigated through landmark-based geometric morphometric methods (GMM). A 3D-template of 251 (semi) landmarks (15 anatomical landmarks, 105 curve semilandmarks and 131 surface semilandmarks) was created in Viewbox 4 software on a specimen of Roccapelago group (Fig.2 and Table 2). The template configuration was applied to the targets, allowing the semilandmarks to slide on the curves (curves semilandmarks) and on the surface (surface semilandmarks) to minimize thin-plate spline (TPS) bending energy[65] between the target and the template. As a result, semilandmarks can be considered geometrical homologous[66]. The (semi)landmark configurations were superimposed by Generalized Procrustes Analysis (GPA)[67] using the R package "geomorph"[68]. Procrustes coordinates were subjected to Principal Component (PC) analysis based on the group mean covariance following the function in the R package "Morpho"[69] to explore shape differences among modern human

tali. ANalysis Of VAriance (ANOVA) with Tukey's post hoc test was used to identify group differences along each PC (Supplementary Table 1). Shape variation related to static allometry was investigated by Pearson product-moment correlation coefficients (r) of shape variables (PCs) against the natural logarithm of centroid size. Procrustes ANOVA with permutation procedures (n=1000) was performed to assess group shape variation attributable to typical footwear (unshod/minimally shod vs. non-restrictive sandals/skin boots with soft soles vs. heavy leather shoes/boots), substrate (asphalt vs. uneven terrain) and mobility strategy (high vs. intermediate vs. low mobility).

Differences in size (i.e., centroid size, defined as the square root of the summed squared distances between each landmark to the centroid) among populations was evaluated through ANOVA Post Hoc tests and box plot analyses (Supplementary Table 2 and Supplementary Table 3, Supplementary Fig. 2).

Following GPA, a Procrustes form analysis was performed adding the logarithm of centroid size (CS) as another variables (Supplementary Fig. 3)[70].

Data analysis were written in R software[71].

Trabecular analysis. Subsample from Bologna (n= 8) and Black Earth (n= 6) were selected for whole bone trabecular analysis[72]. Image sequences from microCT data were down-sampled to 8-bit in ImageJ and then manually cleaned in AVIZO using the paintbrush tool (e.g., removing sediment and matrix). Segmentation of volumes was performed using the MIA-Clustering algorithm[73], while quantification and visualization of BV/TV, DA, and E were performed using Medtool v4.2 (Dr. Pahr Ingenieurs e.U, 2018)[72]. Herein a series of masks were used to remove the cortical mask from the 3D mask, which allows for quantification of trabecular volume to total volume (BV/TV) and, relative orientation (DA) via a series 7.5mm volumes of interest (VOI) at each node of 3.5mm grid overlaid onto the 3D volume. From these values elastic modulus (E) of the trabecular bone is modeled to estimate mean stiffness for each analyzed bone[74]. Hereafter mapping of BV/TV was performed by interpolating the results from the VOIs onto a tetrahedral mesh of the trabecular volume[72].

Acknowledgments. This project has received funding from the European Research Council (ERC) under the European Union's Horizon 2020 research and innovation programme (grant agreement No 724046 – SUCCESS; www.erc-success.eu). We are grateful to Francesco Feletti,

Luisa Mingozzi and Denis Nicolini of the Unit of Radiology (S. Maria delle Croci Hospital of Ravenna) for providing scans for Italian collections; Natasha Johnson and Paolo Pellegatti of the P.A. Hearst Museum, UC Berkeley, for access to Native American collection; Norman Macleod for access to the NHM's Konica Minolta scanner. We thank the curators of the Museo Delle Mummie di Roccapelago for access to Roccapelago sample and Mirko Traversari for anthropological and historical information provided for this population.

References

1. Harcourt-Smith, W. H. E. The first hominins and the origins of bipedalism. *Evol. Educ. Outreach* **3,** 333–340 (2010).

2. Aiello, L. C., Dean, C. *An introduction to human evolutionary anatomy*. (Academic Press, 1990).

3. Kidd, R. Evolution of the rearfoot. A model of adaptation with evidence from the fossil record Evolution of the Rearfoot. *J. Am. Podiatr. Med. Assoc.* **89**, 1–17 (1999).

4. Harcourt-Smith, W. E. H. & Aiello, L. C. Fossils, feet and the evolution of human bipedal locomotion. *J. Anat.* **204**, 403–416 (2004).

5. Ingold, T. Culture on the ground: The world perceived through the feet. *J. Mater. Cult.* **9,** 315–340 (2004).

6. Hagihara, Y. & Nara, T. Morphological features of the fibula in Jomon hunter-gatherers from the shell mounds of the Pacific coastal area. *Am. J. Phys. Anthropol.* **160,** 708–718 (2016).

7. Chirchir, H. *et al.* Recent origin of low trabecular bone density in modern humans. *Proc. Natl. Acad. Sci. U.S.A.* **112,** 366-371 (2015).

8. Saers, J. P. P., Cazorla-bak, Y., Shaw, C. N., Stock, J. T. & Ryan, T. M. Trabecular bone structural variation throughout the human lower limb. *J. Hum. Evol.* **97,** 97–108 (2016).

9. Von Cramon-taubadel, N. Global human mandibular variation re fl ects differences in agricultural and hunter-gatherer subsistence strategies. *Proc. Natl. Acad. Sci. U.S.A.* **108**, 7–12 (2011).

10. Spencer Larsen, C. Biological Changes in Human Populations with

Agriculture. *Annu. Rev. Anthropol.* **24,** 185–213 (1995).

11. Püschel, T. A. & Benítez, H. A. Femoral functional adaptation: A comparison Bbetween hunter gatherers and farmers using Geometric Morphometrics. *Int. J. Morphol.* **32,** 627–633 (2014).

12. Marchi, D. Relationships between lower limb cross-sectional geometry and mobility: The case of a Neolithic sample from Italy. *Am. J. Phys. Anthropol.* **137,** 188–200 (2008).

13. Ruff, C. B. *et al.* Body size, body proportions, and mobility in the Tyrolean "Iceman". *J. Hum. Evol.* **51,** 91–101 (2006).

14. Stock, J. T. Hunter-gatherer postcranial robusticity relative to patterns of mobility, climatic adaptation, and selection for tissue economy. *Am. J. Phys. Anthropol.* **131,** 194–204 (2006).

15. Saers, J. P.P., Ryan, T. M., Stock, J. T. Trabecular bone functional adaptation and sexual dimorphism in the human foot. *Am. J. Phys. Anthropol.* (2018). doi:DOI: 10.1002/ajpa.23732

16. Ryan, T. M. & Shaw, C. N. Gracility of the modern *Homo sapiens* skeleton is the result of decreased biomechanical loading. *Proc. Natl. Acad. Sci. U.S.A.* **112,** 372–377 (2015).

17. Wescott, D. J. Effect of mobility on femur midshaft external shape and robusticity. *Am. J. Phys. Anthropol.* **130,** 201–213 (2006).

18. Stock, J. & Pfeiffer, S. Linking structural variability in long bone diaphyses to habitual behaviors: Foragers from the southern African Later Stone Age and the Andaman Islands. *Am. J. Phys. Anthropol.* **115,** 337–348 (2001).

19. Shaw, C. N. & Stock, J. T. The influence of body proportions on femoral and tibial midshaft shape in hunter-gatherers. *Am. J. Phys. Anthropol.* **144,** 22–29 (2011).

20. Carlson, K. J., Grine, F. E. & Pearson, O. M. Robusticity and sexual dimorphism in the postcranium of modern hunter-gatherers from Australia. *Am. J. Phys. Anthropol.* **134,** 9–23 (2007).

21. Baxter, J. R., Novack, T. A., Werkhoven, H. V., Pennell, D. R. & Piazza, S. J. Ankle joint mechanics and foot proportions differ between human sprinters and non-sprinters. *Proc. Biol. Sci.* **279**, 2018–2024 (2012).

22. Raichlen, D. A., Armstrong, H. & Lieberman, D. E. Calcaneus

length determines running economy: Implications for endurance running performance in modern humans and Neandertals. *J. Hum. Evol.* **60,** 299–308 (2011).

23. Trinkaus, E. Anatomical evidence for the antiquity of human footwear use. *J. Archaeol. Sci.* **32,** 1515–1526 (2005).

24. Zipfel, B. & Berger, L. R. Shod versus unshod: The emergence of forefoot pathology in modern humans? *Foot* **17,** 205–213 (2007).

25. Barnett, C. H. The normal orientation of the human hallux and the effect of footwear. *J. Anat.* **96,** 489 (1962).

26. Hoffmann, P. Conclusions drawn from a comparative study of the feet of barefooted and shoe-wearing peoples. *J. Bone Jt. Surg. Am.* **2,** 105–136 (1905).

27. Kadambande, S., Khurana, A., Debnath, U., Bansal, M. & Hariharan, K. Comparative anthropometric analysis of shod and unshod feet. *Foot* **16,** 188–191 (2006).

28. Lieberman, D. E. Strike type variation among Tarahumara Indians in minimal sandals versus conventional running shoes. *J. Sport Heal. Sci.* **3,** 86–94 (2014).

29. D'Août, K., Pataky, T. C., De Clercq, D. & Aerts, P. The effects of habitual footwear use: Foot shape and function in native barefoot walkers. *Footwear Sci.* **1,** 81–94 (2009).

30. Larson, P. Comparison of foot strike patterns of barefoot and minimally shod runners in a recreational road race. *J. Sport Heal. Sci.* **3,** 137–142 (2014).

31. Hatala, K. G., Dingwall, H. L., Wunderlich, R. E. & Richmond, B. G. Variation in foot strike patterns during running among habitually barefoot populations. *PLoS One* **8,** 4–9 (2013).

32. Turley, K., White, F.J., Frost, S. R. Phenotypic plasticity: The impact of habitat and behavior (substrate use) on adult talo-crural appositional articular joint shape both between and within closely related Hominoid species. *Hum. Evol.* **30,** 49–67 (2015).

33. Knigge, R. P., Tocheri, M. W. & Orr, C. M. Three-dimensional geometric morphometric analysis of talar morphology in extant gorilla taxa from highland and lowland habitats. *Anat. Rec.* **298,** 277–290 (2015).

34. Turley, K. & Frost, S. R. The appositional articular morphology of the talo-crural joint : The influence of substrate use on joint shape. *Anat. Rec.* **297,** 618–629 (2014).

35. Shaw, C. N. & Ryan, T. M. Does skeletal anatomy reflect adaptation to locomotor patterns? cortical and trabecular architecture in human and nonhuman anthropoids. *Am. J. Phys. Anthropol.* **147,** 187–200 (2012).

36. Turley, K. & Frost, S. R. The shape and presentation of the Catarrhine talus: a geometric morphometric analysis. *Anat. Rec.* **296,** 877–890 (2013).

37. Turley, K. *Ankle Morphology: Interface of Genetics, Ontogeny and Use*. (University of Oregon, 2013).

38. Harcourt-Smith, W. E. H. *Form and function in the hominoid tarsal skeleton.* (University of London, 2002).

39. Bramble, D. M. & Lieberman, D. E. Endurance running and the evolution of Homo. *Nature* **432,** 345–352 (2004).

40. Oygucu, I. H., Kurt, M. A., Ikiz, I., Erem, T. & Davies, D. C. Squatting facets on the neck of the talus and extensions of the trochlear surface of the talus in late Byzantine males. *J. Anat.* **192,** 287–291 (1998).

41. Trinkaus, E. Squatting among the Neandertals: A problem in the behavioral interpretation of skeletal morphology. *J. Archaeol. Sci.* **2**, 327–351 (1975).

42. Latimer, B., Ohman, J. C. & Lovejoy, C. O. Talocrural joint in African hominoids: Implications for Australopithecus afarensis. *Am. J. Phys. Anthropol.* **74,** 155–175 (1987).

43. DeSilva, J. M. Functional morphology of the ankle and the likelihood of climbing in early hominins. *Proc. Natl. Acad. Sci. U.S.A.* **106**, 6567-6572 (2009).

44. Venkataraman, V. V., Kraft, T. S., DeSilva, J. M. & Dominy, N. J. Phenotypic Plasticity of Climbing-Related Traits in the Ankle Joint of Great Apes and Rainforest Hunter-Gatherers. *Hum. Biol.* **85,** 309–328 (2013).

45. Venkataraman, V. V, Kraft, T. S. & Dominy, N. J. Tree climbing and human evolution. *Proc. Natl. Acad. Sci. U.S.A.* **110,** 1237–1242

(2013).

46. Barnett, C. H. & Napier, J. R. The axis of rotation at the ankle joint in man; its influence upon the form of the talus and the mobility of the fibula. *J. Anat.* **86,** 1–9 (1952).

47. Panchani, P. N. *et al.* Anatomic study of the deltoid ligament of the ankle. *Foot Ankle Int.* **35,** 916–921 (2014).

48. Gibson, V. & Prieskorn, D. The valgus ankle. *Foot Ankle Clin.* **12,** 15–27 (2007).

49. Parr, W. C. H., Chatterjee, H. J. & Soligo, C. Calculating the axes of rotation for the subtalar and talocrural joints using 3D bone reconstructions. *J. Biomech.* **45,** 1103–1107 (2012).

50. Day, M. H. & Wood, B. A. Functional affinities of the Olduvai Hominid 8 talus. *Man* **3,** 440–455 (1968).

51. Namburu, B. S. P., Kaavya, H. & Reddy, S. M. A study of morphology of talus and its calcaneal facets. *Int. J. Anat. Res.* **5,** 4570–4574 (2017).

52. Parr, W. C. H., Ruto, A., Soligo, C. & Chatterjee, H. J. Allometric shape vector projection: A new method for the identification of allometric shape characters and trajectories applied to the human astragalus (talus). *J. Theor. Biol.* **272,** 64–71 (2011).

53. Tsegai, Z. J. *et al.* Trabecular and cortical bone structure of the talus and distal tibia in Pan and Homo. *Am. J. Phys. Anthropol.* **163,** 784–805 (2017).

54. Parr, W. C. H., Chatterjee, H. J. & Soligo, C. Inter- and intra-specific scaling of articular surface areas in the hominoid talus. *J. Anat.* **218**, 386–401 (2011).

55. Jefferies, R. W. *The archaeology of Carrier Mills: 10,000 years in the Saline Valley of Illinois*. (SIU Press, 2013).

56. Santure, S. K., Harn, A. D. & Esarey, D. *Archaeological investigations at the Morton Village and Norris Farms 36 cemetery*. (Illinois State Museum, 1990).

57. Geib, P. R. Sandal types and Archaic prehistory on the Colorado Plateau. *Am. Antiq.* **65,** 509–524 (2000).

58. Dumond, D. E. *Archaeology on the Alaska Peninsula: The Northern*

Section: Fifty Years Onward. (Museum of Natural and Cultural History and Department of Anthropology, University of Oregon, 2011).

59. Kankainen, K. & Casjens, L. *Treading in the Past: Sandals of the Anasazi*. (Univ of Utah Pr, 1995).

60. Lugli, F. *et al.* C4-Plant Foraging in Northern Italy: Stable Isotopes, Sr/Ca and Ba/Ca data of human osteological samples from Roccapelago (16th–18th Centuries AD). *Archaeometry* **59,** 1119–1134 (2017).

61. Traversari, M. Ricostruzione del profilo bioculturale e biodemografico di una piccola comunita'montana del XVI-XVIII secolo attraverso i dati archeoantropologici e documentari: il caso degli inumati di Roccapelago (Modena). (alma, 2017).

62. Anselmi, S. *Contadini marchigiani del primo Ottocento. Un'inchiesta del Regno Italico* (Sapere Nuovo Senigallia, 1995).

63. Gentili, A. M. *Il leone e il cacciatore. Storia dell'Africa sub-sahariana* (Carocci editore, 1995).

64. Belcastro, M. G. *et al.* The history and composition of the identified human skeletal collection of the Certosa Cemetery (Bologna, Italy, 19th–20th century). *Int. J. Osteoarchaeol.* **27,** 912–925 (2017).

65. Slice, D. E. *Modern morphometrics in physical anthropology*. (Springer Science & Business Media, 2006).

66. Gunz, P. & Mitteroecker, P. Semilandmarks: A method for quantifying curves and surfaces. *Hystrix* **24,** 103–109 (2013).

67. Rohlf, F. J. & Slice, D. Extensions of the Procrustes method for the optimal superimposition of landmarks. *Syst. Biol.* **39,** 40–59 (1990).

68. Adams, D. C. & Otárola-Castillo, E. Geomorph: An r package for the collection and analysis of geometric morphometric shape data. *Methods Ecol. Evol.* **4,** 393–399 (2013).

69. Schlager, S. *Morpho and Rvcg - Shape Analysis in R: R-Packages for Geometric Morphometrics, Shape Analysis and Surface Manipulations. Statistical Shape and Deformation Analysis: Methods, Implementation and Applications* (Elsevier Ltd, 2017).

70. Klingenberg, C. P. Size, shape, and form: concepts of allometry in geometric morphometrics. *Dev. Genes Evol.* **226,** 113–137 (2016).

71. Team, R. C. R: A language and environment for statistical computing. Vienna, Austria: R Foundation for Statistical Computing (2017).

72. Gross, T., Kivell, T. L., Skinner, M. M., Nguyen, N. H. & Pahr, D. H. A CT-image-based framework for the holistic analysis of cortical and trabecular bone morphology. *Palaeontol. Electron.* **17,** 1–13 (2014).

73. Dunmore, C. J., Wollny, G. & Skinner, M. M. MIA-Clustering: a novel method for segmentation of paleontological material. *PeerJ* **6,** e4374 (2018).

74. Gross, T., Pahr, D. H. & Zysset, P. K. Morphology-elasticity relationships using decreasing fabric information of human trabecular bone from three major anatomical locations. *Biomech. Model. Mechanobiol.* **12,** 793–800 (2013).

SUPPLEMENTARY INFORMATION

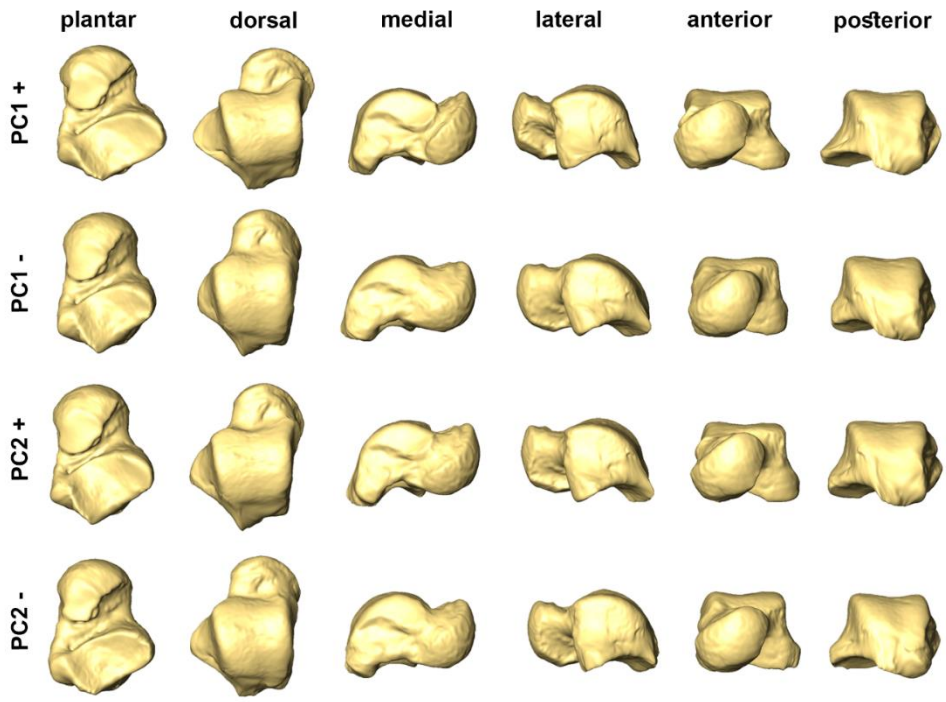

Supplementary Figure 1 | Shape changes of left tali along the first two shape space PC axes.

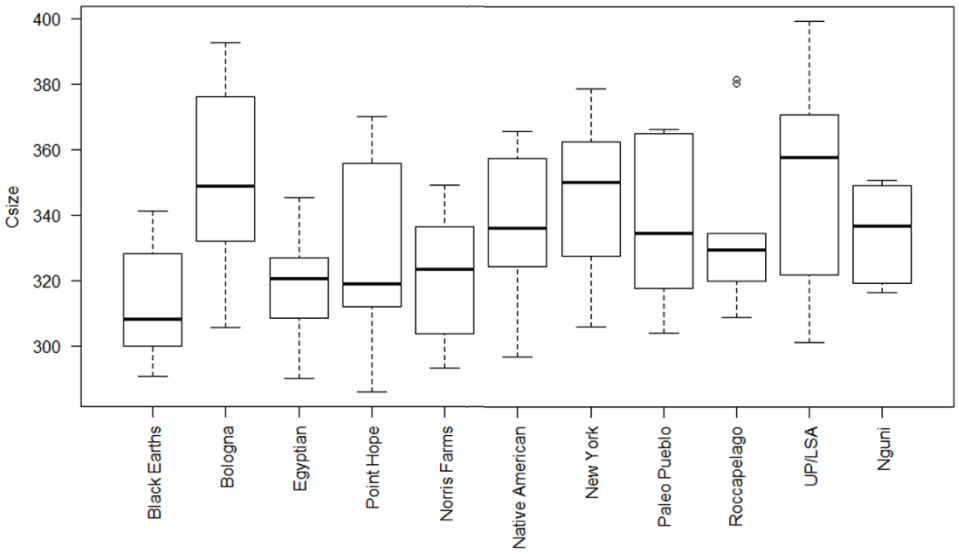

Supplementary Figure 2 | Box-plot distributions of centroid size of left tali belonging to different populations showing the median (the box horizontal line), the upper and lower quartiles (the ends of the box), the highest and lowest value excluding outliers (the whiskers extending from the box), the outliers (the circles).

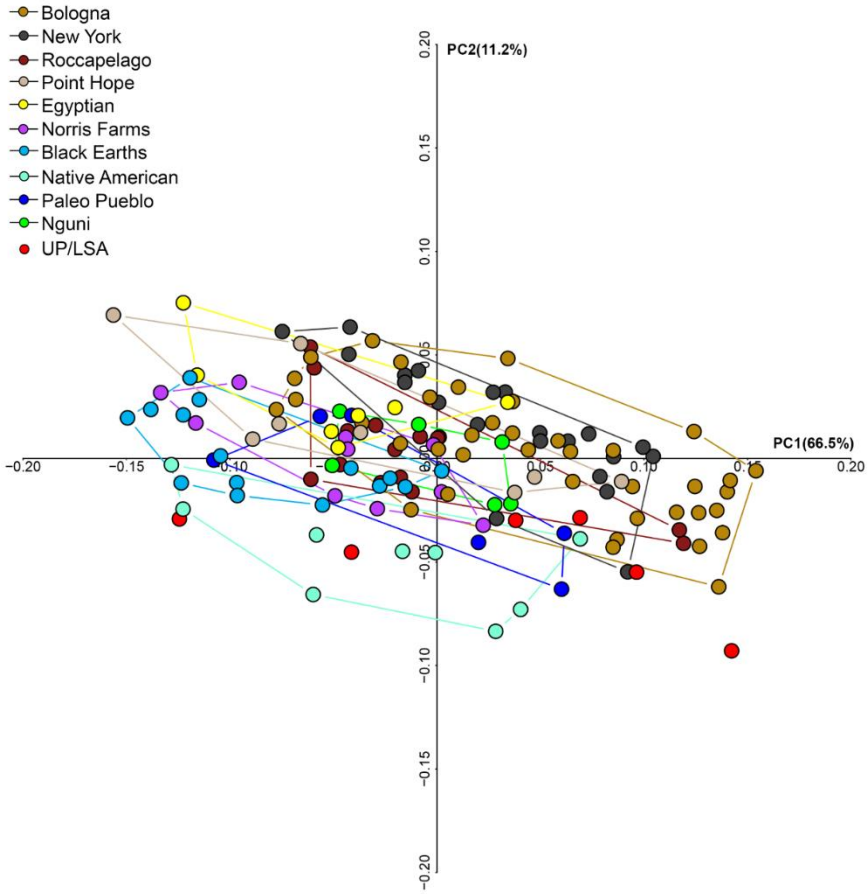

Supplementary Figure 3 | Form space PCA plot of modern human left tali.

Supplementary Table 1 | P-values for post hoc (ANOVA) comparisons of shape space scores of PC1 (above the diagonal) and PC2 (below the diagonal) among modern human groups.

Sample[1]	UP/LSA	BE	CA	NF	PH	EG	PP	RO	NG	BO	NY
UP/LSA	x	0.634	0.053	1	0.999	0.746	0.999	0.452	0.575	0.000*	0.005*
BE	0.634	x	0.808	0.598	0.098	0.001*	0.945	0.000*	0.000*	0.000*	0.000*
CA	0.053	0.808	x	0.030*	0.002*	0.000*	0.218	0.000*	0.000*	0.000*	0.000*
NF	1	0.598	0.030*	x	0.995	0.403	0.999	0.100	0.256	0.000*	0.000*
PH	0.999	0.098*	0.002*	0.995	x	0.963	0.981	0.821	0.876	0.000*	0.000*
EG	0.746	0.001*	0.000*	0.403	0.963	x	0.382	1	0.999	0.019*	0.059
PP	0.999	0.945	0.218	0.999	0.981	0.382	x	0.134	0.248	0.000*	0.000*
RO	0.452	0.000*	0.000*	0.100	0.821	1	0.134	x	1	0.000*	0.000*
NG	0.575	0.000*	0.000*	0.256	0.876	0.999	0.248	1	x	0.123	0.242
BO	0.000*	0.000*	0.000*	0.000*	0.000*	0.019*	0.000*	0.000*	0.123	x	1
NY	0.000*	0.000*	0.000*	0.000*	0.000*	0.059	0.000*	0.005*	0.242	1	x

[1]UP/LSA, Upper Paleolithic and Late Stone Age; BE, Black Earth; CA, Californian; NF, Norris Farms; PH, Point Hope; EG, Egyptian; PP, Paleo Pueblo; RO, Roccapelago; NG, Nguni; BO, Bologna; NY, New York.
*Significant P-value ($P < 0.05$).

Supplementary Table 2 | Mean and standard deviation of centroid sizes of tali.

Sample	Mean (mm)	SD
UP/LSA	351.45	35.1
Black Earth	313.01	17
Californian	334.41	25.1
Norris Farms	322.22	18.4
Point Hope	328.74	28.8
Egyptian	318.14	18.8
Paleo Pueblo	337.09	26
Roccapelago	332.57	21.4
Nguni	334.85	15.2
Bologna	351.33	27.5
New York	345.14	21.4

Supplementary Table 3 | P-values for post hoc (ANOVA) comparisons of centroid size among modern human groups.

Sample[1]	UP/LSA	BE	CA	NF	PH	EG	PP	RO	NG	BO	NY
UP/LSA	x	0.043*	0.957	0.397	0.802	0.313	0.993	0.865	0.981	1	0.999
BE		X	0.565	0.997	0.917	0.999	0.592	0.482	0.723	0.000*	0.005*
CA			x	0.989	0.999	9.958	1	1	1	0.709	0.988
NF				x	0.999	0.999	0.981	0.992	0.994	0.031*	0.318
PH					x	0.998	0.999	0.999	0.999	0.355	0.858
EG						x	0.940	0.964	0.974	0.037*	0.268
PP							x	0.999	1	0.956	0.999
RO								x	1	0.270	0.898
NG									x	0.891	0.997
BO										x	0.996
NY											x

[1]UP/LSA, Upper Paleolithic and Late Stone Age; BE, Black Earth; CA, Californian; NF, Norris Farms; PH, Point Hope; EG, Egyptian; PP, Paleo Pueblo; RO, Roccapelago; NG, Nguni; BO, Bologna; NY, New York.
*Significant P-value ($P < 0.05$).

Supplementary Table 4 | Trabecular variables.

Population	Specimen	Ontoitem	BV/TV	Anisotropy	Modulus(Mpa)
Black Earth	BE 142	Talus	0.33	0.22	3760.94
Black Earth	BE 185	Talus	0.37	0.17	4212.30
Black Earth	BE 187	Talus	0.26	0.30	2362.13
Black Earth	BE 19	Talus	0.35	0.21	4055.73
Black Earth	BE 1	Talus	0.33	0.20	3574.10
Black Earth	BE 86	Talus	0.36	0.20	4094.08
Bologna	BO 111	Talus	0.23	0.21	1807.64
Bologna	BO 112	Talus	0.19	0.22	1258.88
Bologna	BO 28	Talus	0.25	0.20	2135.84
Bologna	BO 32	Talus	0.27	0.26	2443.13
Bologna	BO 38	Talus	0.22	0.29	1786.33
Bologna	BO 4	Talus	0.29	0.19	2593.65
Bologna	BO 51	Talus	0.30	0.18	2945.59
Bologna	BO 84	Talus	0.18	0.25	1104.91

2.3 Paper III

The evolutionary history of the hominid talus

Rita Sorrentino[a,b,1], Caterina Minghetti[b], Eugenio Bortolini[b], Kristian J. Carlson[c,d], Francesco Feletti[e], Luca Fiorenza[f,g], Stephen Frost[h], Tea Jashashvili[i,j], William Parr[k], Colin Shaw[l], Anne Su[m], Kevin Turley[h], Stephen Wroe[n], Timothy M. Ryan[o], M. Giovanna Belcastro[a,p], Stefano Benazzi[b,q]

[a]Department of Biological, Geological and Environmental Sciences, University of Bologna, Bologna 40126, Italy.
[b]Department of Cultural Heritage, University of Bologna, Ravenna 48121, Italy.
[c]Department of Integrative Anatomical Sciences, Keck School of Medicine, University of Southern California, Los Angeles 90089, USA.
[d]Evolutionary Studies Institute, University of the Witwatersrand, Palaeosciences Centre, Private Bag 3, Wits 2050, South Africa.
[e]Department of Diagnostic Imaging, Ausl Romagna, S.Maria delle Croci Hospital, Ravenna 48121, Italy.
[f]Department of Anatomy and Developmental Biology, Monash University, Clayton, VIC 3800, Australia.
[g]Earth Sciences, University of New England, Armidale NSW 2351, Australia.
[h]Department of Anthropology, University of Oregon, Eugene, OR, 97403–1218, USA.
[i]Molecular Imaging Center, Department of Radiology, Keck School of Medicine, University of Southern California, Los Angeles 90089, USA.
[j]Department of Geology and Paleontology, Georgian National Museum, 0105 Tbilisi, Georgia.
[k]Surgical and Orthopaedic Research Laboratory, Prince of Wales Hospital, University of New South Wales, Sydney 1466, Australia.
[l]PAVE Research Group, Dept. of Archaeology & Anthropology, University of Cambridge, Cambridge CB2 3QG, United Kingdom.
[m]School of Health Sciences, Cleveland State University, Cleveland, OH 44195, USA.
[n]Function, Evolution and Anatomy Research Laboratory, Zoology Division, School of Environmental and Rural Science, University of New England, New South Wales 2351, Australia.
[o]Department of Anthropology, Pennsylvania State University, University Park, PA 16802, USA.
[p]ADES, UMR 7268 CNRS/Aix-Marseille Université/EFS, Aix-Marseille Université, CS80011, Bd Pierre Dramard, Marseille Cedex 15, 13344, France.
[q]Department of Human Evolution, Max Planck Institute for Evolutionary Anthropology, Leipzig 04103, Germany.

[1]Corresponding author: Rita Sorrentino, rita.sorrentino2@unibo.it

[Under review in PNAS]

Abstract

Morphology of the talus is critical for understanding the evolution of bipedalism in humans. Here, we investigate morphological variability of extinct and extant hominid tali using a 3D geometric morphometrics approach. The evolutionary timing and appearance of modern human-like features and their contributions to bipedal locomotion were evaluated on the talus as a whole, each articular facet separately, and multiple combinations of talar facets. Distinctive suites of morphological features are consistently indicative of bipedal locomotion in all fossil hominins, despite the presence of substantial variation between species. A modern human-like condition evolved in navicular and lateral malleolar facets early in the hominin lineage compared to other facets, which demonstrated broader variation within Hominidae. The combination of the trochlea, navicular and posterior calcaneal facets distinguish *Australopithecus* from *Homo*, suggesting that in the former the medial longitudinal arch had not fully developed yet. Based on these results we offer a model of talar changes over the course of the acquisition of bipedalism and its transition from a facultative to an obligate condition.

Significance

The adoption of bipedalism is a key element in human evolution that in part depends on talar morphology. We trace the evolutionary emergence of talar features in the human lineage that are linked to the biomechanical demands of bipedalism. We show that a more everted foot and stable medial midtarsal region are early adaptive modifications that coincide with the emergence of bipedalism, while a high medial longitudinal arch emerges comparatively more recently in the human evolutionary lineage. This study provides novel insights on the emergence of pedal morphological traits required for selectively adaptive terrestrial bipedalism.

Introduction

Modern humans and at least some extinct hominins are the only primates that engaged in routine or obligate bipedal locomotion. How and when terrestrial bipedalism emerged is one of the longest-standing questions in palaeoanthropology, but this feature remains the primary evolutionary hallmark used to separate extinct and extant hominins from apes (1, 2).

While the capacity for upright walking (3–7) in the earliest hominins between 7 Ma and 4 Ma (i.e., *Sahelanthropus tchadensis, Orrorin tugenensis, Ardipithecus kadabba, Ardipithecus ramidus)* is still debated (4, 8, 9), it is broadly accepted that australopiths engaged in selectively adaptive terrestrial bipedalism (10–13), as confirmed by the 3.6 Ma footprints from Laetoli, generally attributed to *A. afarensis* (14–16). However, australopiths also maintain skeletal characteristics selectively adaptive to arboreality (11, 17, 18), suggesting that multiple locomotor repertories evolved in Africa between 4 and 2 Ma (11, 19).

It is accepted that most members of the genus *Homo* are obligate bipeds, but there are divergent opinions about the bipedal capability of the first members of the genus. Some have interpreted derived post-cranial morphology in early *Homo* (e.g., increased relative hindlimb length, plantar arch) as critical for long distance walking and running (20–23). Others have noted that pre-*erectus Homo* (23) share morphological features and skeletal proportions with *Australopithecus,* suggesting that obligate, fully-committed terrestrial bipedalism only emerged with *H. ergaster/erectus* (23–26). However, primitive retentions present in Late Pleistocene *H. naledi* (e.g., pedal phalanges more curved than in *H. sapiens),* and *H. floresiensis* (e.g., long foot relative to the leg and short hallux) suggest that modern human gait and posture may even be unique to *H. sapiens* (27–29). Despite this uncertainty, it is clear that over a time-span of approximately 7 million years hominins evolved a suite of specialized anatomical features (e.g., anteriorly placed foramen magnum, S-shape vertebral column, broad and flattened ribcage, wide and short pelvis, long lower limb, stable knee, relatively long and robust ankle region, arched foot), which together facilitated an efficient bipedal gait and upright stance (1, 21, 30).

Among all adaptations that have evolved in the hominin locomotor system, those of the foot are the most highly specialized and unique among primates since it represents the only structure that directly interfaces with the ground during locomotion (11, 30–32). During a single step of the gait cycle, the human foot transitions from a compliant shock absorber at heel strike to a rigid lever at toe-off (i.e., windlass mechanism) (33). Structurally, the human foot is defined as a twisted plate forming transverse and longitudinal arches (34). When standing, the human foot is an elastic, arched structure that actively works to maintain the body's stability, adjusting itself with small sideward displacements of the talus (35).

The human talus (36) occupies a key position in the ankle, as: 1) it is the tenon of the ankle mortise, 2) it sustains the body's entire weight while distributing the load anteriorly to the navicular and inferiorly to the calcaneus, 3) it allows plantar- and dorsal flexion, as well as some degree of abduction-adduction and pronation-supination of the foot, and 4) it is

part of the medial longitudinal arch (30, 33, 35).

Because the talus is a common element in the fossil record and its morphology is clearly linked to locomotor behavior (37–40), there is considerable literature evaluating derived bipedal features in extinct hominins with respect to talar morphology (5, 11, 18, 26, 28, 29, 41–49).

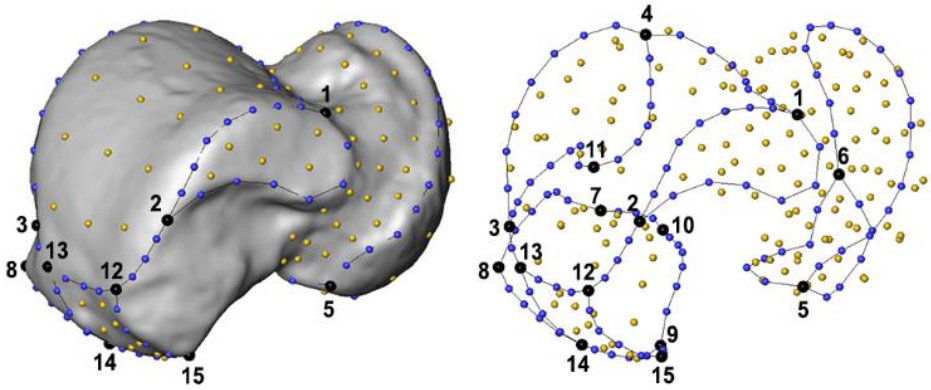

Fig. 1. Talar configuration of landmarks and semilandmarks: 15 fixed landmarks (black), 105 curve semilandmarks (blue) and 131 surface semilandmarks (orange).

Table 1. Landmarks of talar configuration. Labels are depicted in Fig. 1.

Landmarks	**Labels**
Most distal lateral point of contact between the medial malleolar facet and the trochlear surface	1
Most proximal point of contact between the medial malleolar facet and the trochlear surface	2
Most proximal point of contact between the lateral malleolar facet and the trochlear surface	3
Most distal point of contact between the lateral malleolar facet and the trochlear surface	4
Most medial point of contact between the head/navicular facet	5
Most lateral point on the head/navicular facet	6
Most lateral point on the proximal calcaneal facet	7
Deepest (most dorsal) point on the proximal calcaneal facet	8
Most proximo-medial point on the proximal calcaneal facet	9
Most disto-lateral point on the proximal calcaneal facet	10
Most plantar point on the lateral malleolar facet	11
Flexor hallucis longus: most distal point on the medial margin	12
Flexor hallucis longus: most distal point on the lateral margin	13
Flexor hallucis longus: intersection with calcaneus curve	14
Flexor hallucis longus: most postero-inferior prominent point	15

However, these studies have considered the whole talus, not the distinct articular facets and the timing of their evolution, i.e., their individual and combined importance in the acquisition of terrestrial bipedalism.
In the present study, we aim to: 1) quantify hominid talar variation using a (semi)landmark-based approach and compare the results with previous work, 2) determine an order of evolutionary appearance of human-like talar characteristics, and 3) formally assess the contribution of individual and combined facets in identifying bipedal features.

A template of 251 (semi)landmarks (Fig. 1, Table 1) was used to analyze 161 specimens, including *H. sapiens* (81), lowland *Gorilla gorilla* (31), *Pan troglodytes* (29), and extinct hominins (20; Tables S1 and S2). The extinct sample includes *Australopithecus afarensis* (A.L. 288-1), *Australopithecus africanus* (StW 88, StW 363, StW 486), *Australopithecus sediba* (U.W. 88-98), *Paranthropus robustus* (TM 1517), *Homo habilis/ Paranthropus boisei* (OH8), *Homo* spp. / *Paranthropus boisei* (KNM-ER 1464, KNM-ER 1476), *Homo* sp. (KNM-ER 813), *Homo erectus* (KNM-ER 5428, D4110), *Homo naledi* (U.W. 101-1417, U.W. 101-1417), *Homo neanderthalensis* (EM 3519, Krapina 235, Krapina 237, SP4B, Ferrassie 1, Ferrasie 2), and *Homo floresiensis* (LB1-15). Cartesian coordinates were converted to shape coordinates by Generalized Procrustes Analysis (GPA) and Principal Component Analysis (PCA) was performed to explore shape and form variation of the whole talus and of individual and combined talar facets among hominids (see Methods).

Results

Whole talus. The first three PCs in shape space describe 47.6% of the total variance (Fig. 2a). Talar shape scores on PC1 (34.7%) are significantly different between African apes and *H. sapiens* (ANOVA, Df= 2, *F*-test = 618, $P < 0.001$, Table S3), and account for significant allometric shape variation (r=0.4535, $P < 0.001$) due to an enlarged talus in *H. sapiens*. Individuals yielding positive scores on PC1 (i.e., *H. sapiens*) display a taller talar body with an inclined and wider lateral head, a flatter navicular facet, a shorter neck, a squared and flatter trochlea, a flatter posterior calcaneal facet, vertical orientation of the lateral malleolar facet, a flat medial malleolar facet, and a vertical flexor hallucis longus (FHL) groove. Individuals with negative PC1 scores (i.e., African apes) exhibit shorter talar bodies, dorsally extended talar heads, rounded navicular facets, elongated necks, posteriorly narrowed and grooved trochleae with dorsally elevated lateral margins, more concave posterior

calcaneal facets, flared lateral malleolar facets, cupped and distally elongated medial malleolar facets, and oblique and deep FHL grooves (Fig. 2c).

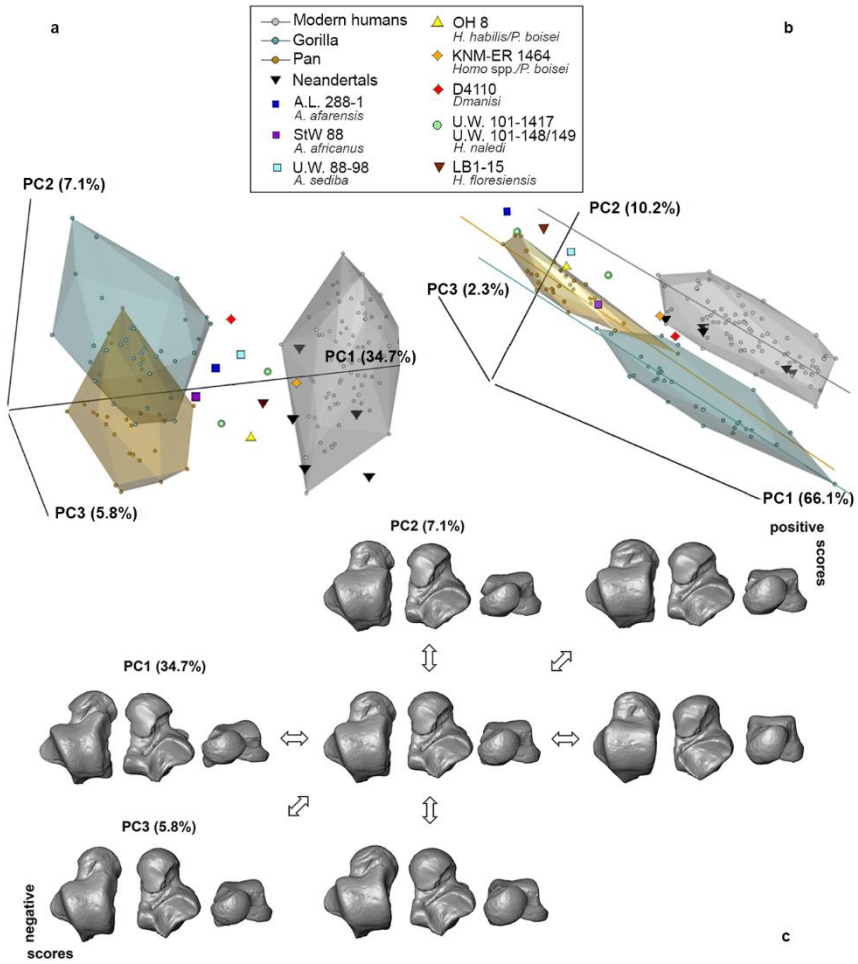

Fig. 2. Whole talus. Shape space 3D PCA plot (**a**) and form space 3D PCA plot (**b**). Shape changes along the first three shape PCs (**c**) in dorsal, plantar and frontal views (from left to right). At the center of each cluster is mean shape.

PC2 (7.1%) separates *Gorilla* from *Pan* (ANOVA, Df = 2, F-test = 66.97, P < 0.001, Table S3). Positive scores (i.e., *Gorilla*) indicate shorter talar body, smaller and flatter navicular facets, which are also mediolaterally extended, more symmetrical trapezoidal trochleae with shallower central grooves and dorsally elevated lateral margins and shallower posterior calcaneal facets. Negative scores (i.e., *Pan*) are related to relative taller corpora in respect to positive scores (i.e., *Gorilla*), a

rounder and larger navicular facet, an oblique trochlear axis relative to the head, a grooved trochlea with equally elevated lateral and medial margins, a distally elongated medial facet and a deeper posterior calcaneal facet (Fig. 2c). PC3 (5.8%) significantly differentiates *Pan* and *H. sapiens* (ANOVA, Df = 2, F-test = 3.773, $P < 0.05$; Table S3) (Fig. 2c), with the latter showing a shorter and wider talus (Fig. 2c). For some talar characteristics *H. sapiens* and *Gorilla* are more similar than *H. sapiens* and *Pan*, especially concerning the curvature of the navicular facet, the shape of the trochlea and posterior calcaneal facet.

Among the fossils, australopiths are generally more similar to African apes, while fossil *Homo* specimens are closer to *H. sapiens*. In accordance with previous work (11, 17, 18, 45, 48), australopiths show a mosaic of ape-like and human-like talar features and some show a more mixed individually than others (e.g., compare StW 88 and the *A. sediba* talus) (Fig.2c), such as an ape-like long neck and concave posterior calcaneal facet, and, at the same time, flared lateral malleolus facet and more vertical FHL grooves. *Homo habilis* (OH 8) and D4110 (Dmanisi) plot between *H. sapiens* and African apes in PC1, suggesting that some primitive features are still present in these early *Homo* specimens, but they are separated along PC2. The talus of OH8 shows a deep, central, grooved trochlea and elevated lateral margin, suggesting an arcuate ape-like path of the leg during the stance phase. Even if the Dmanisi talus shares some features with modern human tali (e.g., flat trochlea, inclined head, no cup-shaped medial malleolus), other traits it exhibits are ape-like (e.g., an elongated neck, antero-posterior narrowed posterior calcaneal facet which is slightly more concave than in humans). The two *H. naledi* tali are quite different in shape from each other, as was previously suggested (28). The U.W. 101-148/149 specimen plots close to *H. habilis*, probably due to its slightly grooved trochlea and relatively higher lateral rim and elongated neck. U.W. 101-1417, KNM-ER 1464, and LB1-15 cluster near the range of variation expressed by *H. sapiens,* while the Neandertal sample overlaps with the range exhibited by *H. sapiens*.

In the form space PCA, the first three PCs explain 78.6% of total variance (Fig. 2b). PC1 (66.1%) accounts for variation in overall size, separating *Pan* from *Gorilla* and *H. sapiens*. PC2 (10.2%) differentiates between African apes and *H. sapiens,* as previously described for shape space PC1 and PC2. *Homo sapiens* and *Pan* have different (evolutionary) allometric trajectories ($\alpha = 20.9$, $P < 0.01$; magnitude $P<0.01$), while no differences were found between *H. sapiens* and *Gorilla*. *Pan* and *Gorilla* also differ in their allometric trajectory ($\alpha = 22.1$, $P < 0.01$; magnitude $P<0.01$). Except for *A. africanus* (StW 88), which plots inside the *Pan*

range, all other australopiths and early *Homo* fall outside the ranges of both African apes and *H. sapiens*.

Individual articular facets. Even though the talar facets are highly integrated (1 to 0.981; P< 0.001; iterations = 1000), distinct facets diversely contribute in discriminate between forms of bipedalism (Supplementary Text 1 and Figs. S1-S3). However, navicular and lateral malleolar facets provide the most informative results.

Navicular facet. For the navicular facet, the first three PCs account for 70% of morphological variation (Fig. 3a)**.** A significant positive correlation with logged centroid size (lnCS) was found for PC1 (r=0.4656, $P < 0.001$), while significant negative correlations were observed for PC2 (r= -0.1624,

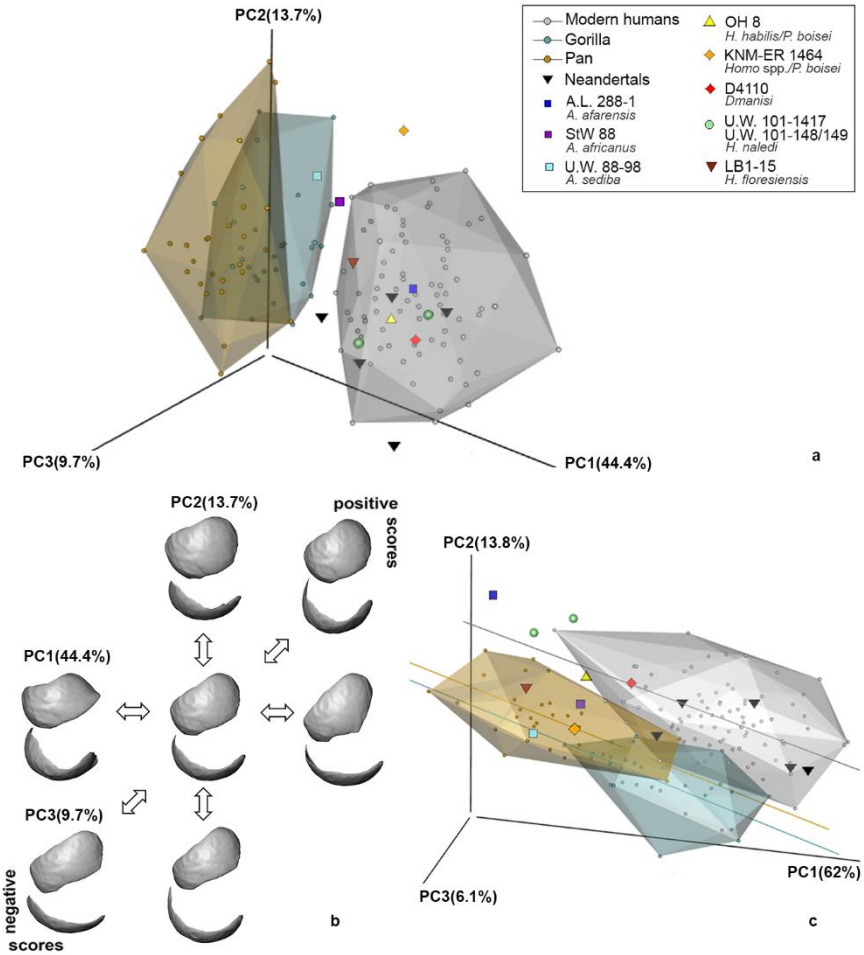

Fig. 3. Navicular facet. Shape space 3D PCA plot (**a**) and form space 3D PCA plot (**c**). Shape changes along the first three shape PCs (**b**) in frontal (above) and dorsal (down) views.

$P = 0.041$) and PC3 (r= -0.2626, P< 0.001). PC1 describes 44.4% of variation and segregates African apes from *H. sapiens* (ANOVA, Df = 2, *F*-test = 190, $P < 0.001$, Table S3) by discriminating the rounded and dorsally extended navicular facet typical of African apes (greater dorsiflexion and rotation at the talonavicular joint) from the flared and laterally expanded navicular facet of *H. sapiens* (stable midtarsal region) associated with efficient bipedalism (Fig. 3b). While all extinct *Homo* specimens, except possibly KNM-ER 1464, fall inside or at the edge of the human variation, australopiths (StW 88 and U.W. 88-98) are adjacent to African apes except for A.L. 288-1 (*A. afarensis*), which plots perfectly within the *H. sapiens* range.

PC2 (ANOVA, Df = 2, *F*-test = 2.975, $P < 0.1$) does not discriminate among extant taxa, while PC3 (ANOVA, Df = 2, *F*-test = 31.34, $P < 0.001$) accounts for significant differences between the more terrestrial forms (*Gorilla* and *H. sapiens*) and the more arboreal form (*Pan*) (Table S3). Specifically, positive values along PC3 are associated with tali exhibiting rounded spherical navicular facets (i.e., suggestive of a broad range of motion in the joint) and negative values associated with tali exhibiting flatter rectangular navicular facets (i.e., suggestive of reduced manoeuvrability of the joint).

In form space, the first three PCs describe 81.9% of variation (Fig. 3c). PC1 (62%) tends to separate larger species (*Gorilla* and *H. sapiens*) from smaller-bodied forms (*Pan*), while PC2 distinguishes between African apes as a group and *H. sapiens*. Most of the small hominins (U.W 88-98, StW88, KNM-ER 1464, LB1-15) plot close to the *Pan* range, except for A.L. 288-1 (*A. afarensis*), which follows the *H. sapiens* allometric trajectory (Fig. 3c). No differences in angles of trajectories have been found among taxa in the extant sample. *Pan* and *H. sapiens* significantly differ only in allometric magnitude of trajectories (P< 0.01), as well as *Gorilla* and *Pan* (P< 0.05).

Lateral malleolar facet. The shape space 3D PCA plot for the lateral malleolar facet depicts a trend separating bipedal species from arboreal species (Fig. 4a)**.** There are significant differences between African apes and *H. sapiens* on PC1 (ANOVA, Df = 2, *F*-test = 35.81, $P < 0.001$, Table S3) and PC2 (ANOVA, Df = 2, *F*-test = 49.64, $P < 0.001$, Table S3), while PC3 (ANOVA, Df = 2, *F*-test = 5.032, $P < 0.01$, Table S3) accounts for differences between *Pan* and *Gorilla* (Table S3). Most of the fossil hominins tend to plot within or closer to (i.e., A.L. 288-1, U.W. 88-98, D4110) the modern human range, and only KNM-ER 1464 (*Homo* spp./ *P. bosei*) falls inside the area of overlap between *Gorilla* and *H. sapiens*. Distally extended and concave lateral malleolar facets yielded negative scores on PC1, while inferior-superiorly larger and flatter lateral malleolar surfaces return positive scores (Fig. 4c). Morphology along PC2 displays a

lateral malleolar facet with the apex distally extended in larger-bodied forms (PC2 negative) and plantarly extended in smaller-bodied forms (PC2 positive). Negative scores on PC3 are associated with an extension of the inferior apex (i.e., *Pan*) compared to larger and inferior-superiorly compressed surface along positive PC3 scores (i.e., *Gorilla*).

The first three form space PCs explain 77% of variability (Fig.4b). PC1 (54.8%) separates *H. sapiens* and *Gorilla* from *Pan*, while both PC2 (13.5%) and PC3 (8.7%) show overlap among extant taxa, manly between *Gorilla* and *H. sapiens*. Fossil hominins are characterized by a high degree of variability in form space. Only *Gorilla* and *H. sapiens* significantly differ in allometric trajectories (α= 18.5, P< 0.05), which converge with increasing talar size (Fig.4b).

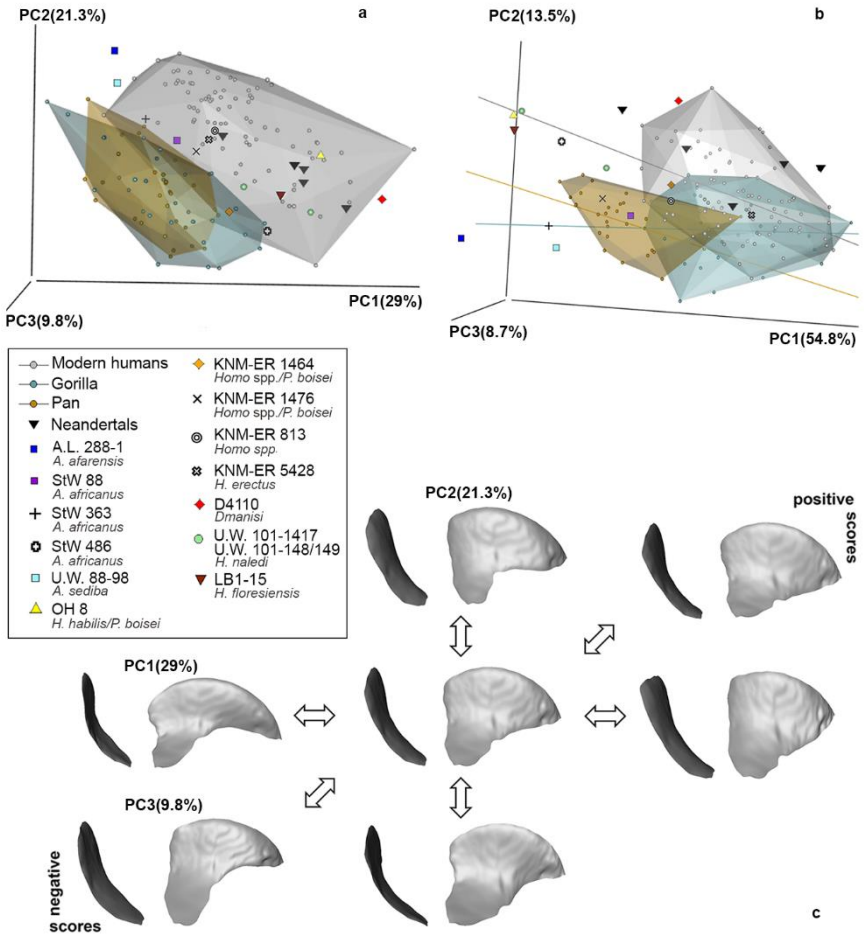

Fig. 4. Lateral malleolar facet. Shape space 3D PCA plot (**a**) and form space 3D PCA plot (**b**). Shape changes along the first three shape PCs (**c**) in frontal (left) and lateral (right) views.

Combined facets. The combination of trochlea, navicular and posterior calcaneal facets provides the best results in terms of separation between australopiths and *Homo* specimens (see also Supplementary text 2 and Figs S3-S10). The first three PCs in shape space account for almost 50% of the observed variation among extant taxa (Fig. 5a). PC1 (36.6%) provides significant differences between *H. sapiens* and African apes (ANOVA, Df = 2, *F*-test = 613.8, $P < 0.001$; Table S3). *Homo sapiens* is characterized by an inclined plantar navicular facet relative to a taller talar corpus, which increases the distance of the tibiotalar joint (i.e., the ankle joint) from the ground (Fig. 5c). Australopiths are generally more similar to African apes, while most fossil *Homo* specimens are closer to *H. sapiens*, except for Neandertals that fall just inside the *H. sapiens* range. PC2 accounts for differences among all three extant groups

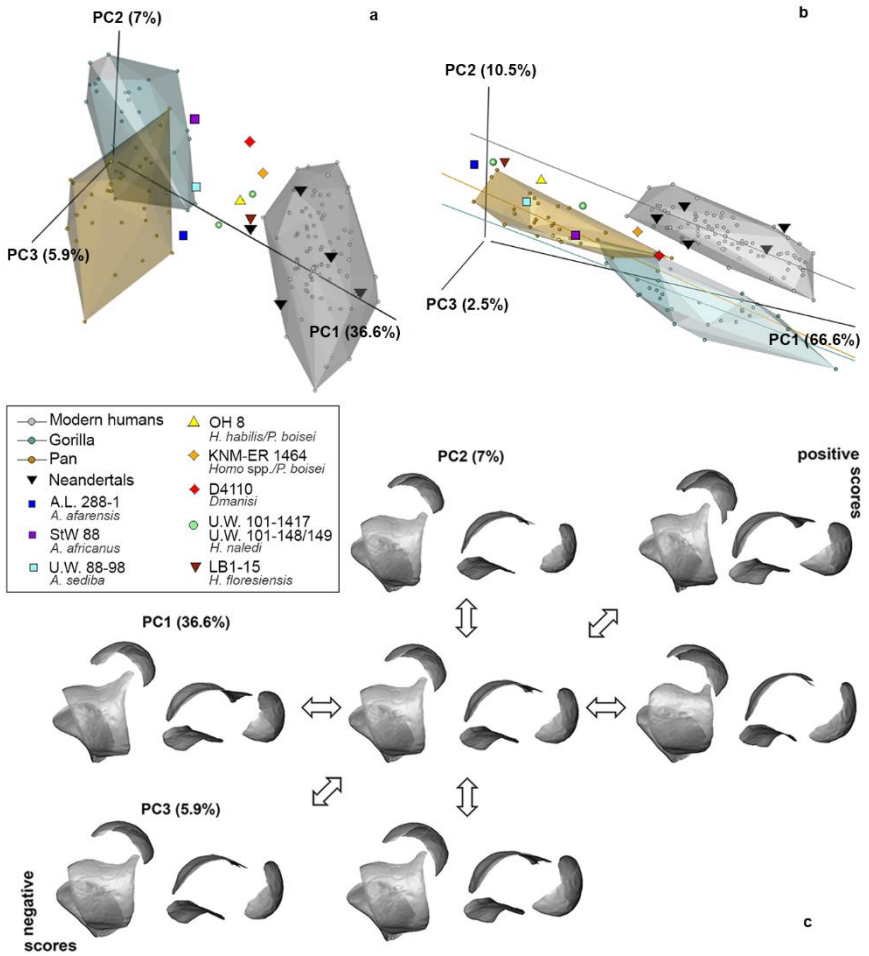

Fig. 5. Combined trochlea, navicular and posterior calcaneal facets. Shape space 3D PCA plot (**a**) and form space 3D PCA plot (**b**). Shape changes along the first three shape PCs (**c**) in dorsal (left) and medial (right) views.

(ANOVA, Df = 2, *F*-test = 10.9, $P < 0.001$, Table S3), whereas PC3 separates *Pan* on one side from *Gorilla* and *H. sapiens* on the other (ANOVA, Df = 2, *F*-test = 18.2, $P < 0.01$, Table S3). In the first three PCs, shape correlates with lnCS (PC1, r= 0.4452, P< 0.001; PC2, r= 0.2657, P< 0.001; PC3, r= -0.22429, P< 0.01) and this relationship results in enlarged articular surfaces in larger-bodied individuals to lessen peak compressive forces through any one point in the joint.

In form space, PCA mirrors results obtained in shape space, even though no significant differences in allometric trajectories were found among extant taxa. Extinct *Homo* fall between *H. sapiens* and African apes, australopiths are closer to *Pan*, and Neandertals fall within the range of *H. sapiens* variation.

Discussion

Results obtained for the whole talus (Fig. 2) are consistent with those of previous studies (28, 29, 38, 39, 50) showing that differences in talar shape among hominids are due to different locomotor behaviors (bipedalism *versus* knuckle-walking and climbing). However, our results differ from some recent analyses on hominid talus (28, 29, 39) showing that no fossil hominins fall within the ape range, likely reflecting their own unique combination of locomotor modes which is not ape-like (11, 19, 32, 51). In addition, neither A.L. 288-1 (*A. afarensis*) nor KNM-ER 1464 (*Homo* or *P. boisei*) are within the *H. sapiens* range, while the talus LB1-15 attributed to *H. floresiensis* (one of the geologically youngest species of genus *Homo*) plots closer to *H. sapiens* in shape space than has been suggested in other recent works (28, 29). OH8 (potentially *H. habilis*) and D4110 (Dmanisi) exhibit a mosaic of human-like and ape-like talar features. Since the fossil remains from Dmanisi are attributed to *H. erectus*, this suggests that early Eurasian *Homo* retained primitive features in the foot but still exhibited a structural capability of sustained long-distance walking (11, 22, 52). In contrast with previous results (53), Neandertals are generally similar to our *H. sapiens* sample, which was specifically selected to account for diversity in subsistence strategies, locomotor activity, landscape use, and chronology.

Individual facets have varying potential to distinguish features associated with bipedal locomotion from other forms of locomotion. For example, the medial malleolar facet and the anterior-medial calcaneal facet (Supplementary Text 1 and Fig. S1) show considerable clusters overlapping in shape space between African apes and *H. sapiens* morphologies, suggesting that these two facets are conservative and cannot

be considered as markers of derived bipedal features. Similarly, even though to a lesser extent, African apes and *H. sapiens* clusters tend to overlap in shape space when considering the morphology of the posterior calcaneal facet and trochlea respectively (Supplementary Text 2 and Fig. S2). Overall, we show that fossil hominins have a broad range of variation in the above-mentioned facets, suggesting that they were not universally under strict selection for the acquisition of bipedalism, or selection was being opposed by other forces, such as developmental plasticity. Ultimately, this suggests they are less informative for functional/locomotor interpretation.

The navicular facet best discriminates between *H. sapiens* and African apes (Figure 3). This facet is a key element for enhancing stability of the midtarsal region (28, 30, 38, 39, 50, 54) as decreasing curvature of the navicular facet represents a derived feature of modern human toe-off (18, 30, 55, 56). Most fossil hominins show modern human-like navicular morphology, including *A. afarensis*. This suggests that *A. afarensis* could have achieved a stable medial midtarsal region in addition to lacking midtarsal break typical of great apes (15, 18, 42, 45, 50, 57–59). The medial column is thought to have changed more recently in the human evolutionary lineage, after the early adaptive modification of the lateral column of the foot (7, 31, 32, 57, 60), even if additional evidence suggests that the evolutionary trajectory of the lateral column is not so simple (52). Here, the talonavicular joint of *A. afarensis* reveals the appearance of an increasing relative stiffness of the medial column by at least 3.2 million years ago. *Australopithecus africanus* (but see DeSilva (56) for an alternative view) and *A. sediba*, however, retain a navicular facet morphology more similar to that of African apes, and specifically to *Gorilla* (18). This suggests that *A. africanus* and *A. sediba* may have exhibited more talonavicular joint mobility and an ape-like loading of the lateral region during the last half of the stance phase (61). Size correlation with the first three PCs could be related to the transmission of body weight from the talar head through the navicular, to the first ray at toe-off (62, 63). Indeed, even if the navicular facet of *A. afarensis* is smaller compared to those of *H. sapiens*, its morphology follows the *H. sapiens* allometric trajectory. Thus, the navicular facet of *A. afarensis* suggests that this hominin had a modern human-like propulsion during toe-off (18) and this adaptation is maintained by *Homo* specimens. Other postcranial findings indicate that *A. afarensis* share more similar postcranial characteristics with *Homo* than more recent specimens such as *A. africanus* and *A. sediba* (18, 39, 48, 64–66).

The lateral malleolar facet (Fig. 4) seems to effectively discriminate between fossil hominins and African apes. High concavity and greater

lateral projection of the lateral malleolar facet in African apes (Figure 4b) likely prevents the distal fibular dislocation when the foot is inverted during dorsiflexion in arboreal environments (i.e., during climbing) (17, 38, 61, 67). Furthermore, the foot of African apes has an inverted posture during locomotion on flat surface and, consequently, the lateral malleolar facet of the talus is subjected to downward forces which may determine this flaring morphology (30, 39, 61). Fossil hominins lack these morphological characteristics as a consequence of decreasing arboreality, reduced inversion posture of the foot and emphasis on ankle stability. As argued by Gebo and Schwartz (43), and confirmed by our results, the lateral facet does not distinguish australopiths from *Homo*. Indeed, the lateral facet seems to evolve toward a bipedal form with australopiths. This is in line with the work of DeSilva (17), suggesting the poor adaptation of the hominin ankle joint to modern ape-like vertical climbing. Furthermore, recent studies of Venkataraman and colleagues (68, 69) on habitually climbing modern human populations suggest that ankle traits related to facultative arborealism can be obscured by increased stabilization demands in terrestrial locomotion. Therefore, even if the potential for arboreality could be retained in fossil hominin postcranial skeleton (11, 17, 18, 70), it could be obscured by the effect of bipedal locomotion on the lateral facet of the talus.

The combination of trochlea, navicular and posterior calcaneal facets suggests a progressive development of the medial longitudinal arch from African apes to *H. sapiens*, passing first through australopiths and then through *Homo* fossil specimens (Fig. 5a). In *H. sapiens*, the trochlea is dorsally elevated with respect to the posterior calcaneal facet, resulting in a taller talar corpus, while the talar head is plantarly oriented (i.e., declined). Following Prang (45), the relative arrangement of these talar facets might be a proxy for inferring the presence of a medial longitudinal arch, which is absent in African apes while it is a derived feature of the modern human foot (30). Because australopiths are more similar to African apes in this regard, our results suggest that the medial longitudinal arch could be absent or extremely reduced in australopiths (contra 14, 15, 45, 55, 57), implying that it is a derived feature that only characterizes the genus *Homo* (26, 28, 39, 42, 43, 45, 51, 58). Indeed, to the best of our knowledge, the oldest direct (i.e., a footprint) evidence of a clearly developed longitudinally arched foot comes from Ileret, Kenya, dated to 1.5 Ma and potentially attributed to *H. erectus* (24, 71). The development of a high medial longitudinal arch in *Homo* specimens represent a selected adaptation for storing much elastic energy, which is helpful in long-distance walking and running (21, 51). However, the evolution of the longitudinal arch is controversial since many authors have argued for the

presence of a longitudinal arch in *A. afarensis* based on foot bone characteristics (14, 45, 55, 57) and the 3.6 Ma Laetoli footprints (Tanzania) (15, 72, 73), even though reduced when compared to *H. sapiens* (16, 45, 51, 71, 74, 75). Despite the uncertainty in the expression of the medial longitudinal arch (i.e., absent or low), our results suggest that the stability achieved at the talonavicular joint in *A. afarensis* might have favored a human-like push-off.

In summary, this study provides a more comprehensive understanding of bipedal locomotor adaptations in the hominin foot, as it appears from change over time in the talus, and thus sheds light on one of the evolutionary steps that strictly defined modern humans. Joints, such as those implicated by the lateral malleolar and navicular facets, seem to evolve towards a modern human-like form (i.e., structured for bipedal efficiency) earlier than others. More specifically, during the first phases of the evolution of bipedalism selective pressure acted towards a more stable talonavicular joint, thus promoting weight transfer along the medial column of the foot during push-off, and a less inverted foot. The combined trochlea, navicular and posterior calcaneal facets, instead, reflect a gradual expression of the longitudinal arch from australopiths to *Homo*, marking the transition from facultative to obligate bipedalism.

Materials and Methods

Data collection. Fossil and extant samples are shown in Tables S1 and S2. In this study we considered left tali when present, otherwise right tali were mirrored and analyzed when substitution was necessary. Original bones or casts (e.g., fossils) were subjected to computed tomography (CT), microCT or laser scanning to generate 3D surface models. The modern human samples of Italian Medieval (Guidizzolo, North Italy) and Renaissance (Roccapelago) period (voxel size: 0.470 x 0.470 x 0.6 mm), as well as the 20th century individuals from the Frassetto Collection, i.e. sample from Bologna (76) (voxel size: 0.960 x 0.960 x 0.7 mm) and Nguni (voxel size: 0.976 x 0.976 x 0.5 mm), were scanned with medical CT at the Department of Diagnostic Imaging of Santa Maria delle Croci Hospital in Ravenna (Italy). The tali from the Norris Farms #36 collection (Late Prehistoric North America, 1300 A.D.) were scanned on the OMNI-X HD600 industrial microCT system at the Penn State Center for Quantitative Imaging. Data were collected with energy settings of 180kV and 0.11 mA, inline pixel sizes of 0.048 mm, and slice thickness and spacing of 0.051 mm. Three-dimensional surface reconstructions were made from the CT data using Avizo 9.0 (Visualization Science Group).

The Upper Palaeolithic sample from Italy (Romito 7, Romito 8, Romito 9 and Veneri 2) were surface scanned at the Department of Cultural Heritage with a 3D ARTEC scanner.

Casts of the Late Stone Age talus of Clark Howell Omo (Omo deposits, Ethiopia), as well as Native American (California, Shell Midden Cultures, ~1500 B.C. - 500 A.D.), *Gorilla* and *Pan* sample, and hominin fossil casts of EM3519 and SPB4 (*H. neanderthalensis*), A.L.-288-1 (*A. afarensis*), OH8 talus (*H. habilis / P. boisei?*), Koobi Fora specimens KNM-ER 1464 and KNM-ER 1476 (*Homo* spp. / *P. boisei?*) from the Natural History Museum, London, Palaeontology department collection were scanned with a Konica Minolta Vivid 910 surface laser scanner (X: ± 0.22 mm, Y: ± 0.16 mm, Z: ± 0.10 mm). Surface scan data were processed using the scanner's associated software (Polygon Editing Tool, Konica Minolta, 2006) and Geomagic Studio 8 (3D Systems).

Fossils casts of KNM-ER 813 (*Homo* spp.) and KNM-ER 5428 (*H. erectus*) were scanned with an Artec Spider (Artec 3D). Scan parameters and protocols for StW 88, StW 363, StW 486, and TM 1517 are given by Su and Carlson (61). The Malapa talus was generated from high resolution CT data with energy settings of 130kV and 390µA, 4000 projections, isotropic voxel dimensions of 57.1 µm and 1.2 mm of copper was used to prefilter the beam hardening setting.

LB1-15 (*H. floresiensis*) was scanned using a NextEngine 3D Scanner (macro setting, 16 scans per orientation, minimum two orientations per bone). Triangular meshes of the bone were created in ScanStudio HD PRO software and then aligned and merged in Geomagic Studio software.

CT data of the Dmanisi talus (D4110) were acquired in the Department of Computed Tomography, Research Institute of Clinical Medicine (Todua Clinic) using s Siemens Somatom Sensation 64 medical CT scanner. The Spine Routine protocol was used for image acquisition. Relevant scan parameters for this fossil include: 120kVp, a tube exposure time 750, a slice thickness of 1.00mm, and a reconstruction increment of 0.4mm. Subsequent to the acquisition of these raw data, image data were reconstructed as 16-bit singed DICOM images using a bone reconstruction algorithm (i.e. a "B60s" Convolution kernel). A 3D model was reconstructed using a -200 threshold gray value. Virtual models of *H. naledi* tali (U.W. 101-148/149 and U.W. 101-1417) are from www.morphosource.org.

CT data of Krapina 235 were obtained from the NESPOS (Neanderthal Studies Professional Online Service) Database (voxel size: 0.154 x 0.154 x 0.4 mm).

CT data of La Ferrassie 1 (voxel size: 0.219 x 0.219 x 0.4 mm) and La Ferrassie 2 (voxel size: 0.251 x 0.251 x 0.5 mm) were kindly provided by

Museum National d'Histoire Naturelle, *Département Hommes, Natures, Sociétés,* Paris. Digital three- dimensional (3D) models were virtually obtained generating isosurface reconstruction in Avizo 9.0.

Landmark and Semilandmark Data. A 3D-template of 15 anatomically homologues landmarks, 105 curve semilandmarks and 131 surface semilandmarks was created in Viewbox 4 software on a specimen of the Roccapelago modern human group (Fig.1 and Table 1). All (semi) landmarks were chosen to best represent the entire morphology of the talus as well as to allow extrapolation of the talar articular facets (i.e., the navicular facet, anterior and medial calcaneal facets, the trochlea, the posterior calcaneal facet, the medial malleolar facet, and the lateral malleolar facet) and combined facets (i.e., the trochlea and navicular facet; the posterior calcaneal and navicular facets; the posterior calcaneal facet and trochlea; the trochlea, posterior calcaneal and navicular facets; the trochlea and lateral malleolar facet; the trochlea and medial malleolar facet; the trochlea, lateral and medial malleolar facets; the trochlea, posterior calcaneal, lateral and medial malleolar facets). Beside the whole talus, we decided to analyse individual and combined facets to disentangle subtle morphological differences (size, shape, degree of curvature and orientation) in our hominid sample.

The (semi)landmark configuration of the template was applied to targets, allowing the semilandmarks to slide on curves (curves semilandmarks) and on the surface (surface semilandmarks) in order to minimize thin-plate spline (TPS) bending energy (77, 78) between the target and the template. As a result, semilandmarks can be considered geometrically homologous.

Fragmentary fossils and (semi) landmark estimation procedure. Digital reconstructions were used to estimate missing regions of partially damaged fossils using a TPS interpolation function in Viewbox 4 software (78, 79).

The reconstruction was performed for the whole talus, or for singular/combined facets (Table S4), in order to include as many fossils as possible in each analysis (i.e., analyses for the whole talus and for individual and combined facets).

Reliability of the individual reconstructions was tested by comparing the reconstruction based on the grand mean (mean of the entire extant sample) against reconstructions obtained by using the mean of *Gorilla, Pan* and *H. sapiens*, respectively. If differences were observed (i.e., if the reconstructions fell in different areas of the PCA plots), then reference choice was determined to have affected the final outcome and the fossil

was removed from the analysis. For example, this was the case with KNM-ER 813 (*Homo* spp.) for the posterior calcaneal facet and for the combined posterior calcaneal facet and trochlea, as well as for StW 486 (*A. africanus*) for the medial malleolar facet. Otherwise, if the reference choice did not affect the results, the reconstruction based on the grand mean was used for analyses. The only exception to this protocol was with respect to Krapina 235 (*H. neanderthalensis*), which was reconstructed using the *H. sapiens* mean.

Geometric morphometrics and statistical analyses. The (semi)landmark coordinates were allowed to slide against recursive updates of the Procrustes consensus and converted into shape coordinates by means of Generalized Procrustes analysis (GPA) (77). Separate GPAs of the raw coordinates of the whole talus, as well as of each separate talar facet and multiple combinations of talar facets were performed. Shape and form (matrix of shape coordinates augmented by the logarithm of centroid size – lnCS) space PCAs were calculated using the Procrustes coordinates of the extant sample, while fossil specimens were projected into this space to evaluate their morphological variation in relation to *Pan*, *Gorilla* and *H. sapiens*.

Differences among extant group means (*H. sapiens*, *Pan*, *Gorilla*) were evaluated for the first three PCs through ANOVA and Tukey's post hoc test was used to identify between species differences (80) (Table S4).
Allometric shape variation was investigated by the Pearson product-moment correlation coefficient (r) of shape variables (PCs) against lnCS.
Since centroid size is considered a proxy of body mass (37, 50), angles between (evolutionary) allometric trajectories of non-human ape taxa and *H. sapiens* were computed in form space PCA, and a permutation test (n=1000) was used to assess the statistical significance of the trajectory angle (81).

The degree of morphological integration between an individual facet and the rest of the talar configuration was evaluated while accounting for phylogenetic relationships among taxa (82). Shape data were previously aligned using Generalized Procrustes Analysis (GPA). Then, morphological covariation was statistically assessed permuting data per 1000 iterations. We assumed that each individual talar structure is strongly correlated with overall talar shape since the talus acts like a modulus.
Further analyses were performed to investigate some specific findings of the present work.

For trochlea and combined trochlea and medial malleolar facet analyses, three *A. africanus* specimens (StW 88, StW 363 and StW 486) were included. Phenetic distance analysis was performed to test the hypothesis

that *A. africanus* variability is greater than variability observed in the extant groups. Phenetic distance among *A. africanus* (K=3) was compared against phenetic distance based on random resampling of K subsamples (permutation test n=1000) of each extant sample ($S_{i,k}$). Then, statistical significance ($P< 0.05$) was assigned if phenetic distance of *A. africanus* ($S_{0,k}$) was greater than or equal to 95‰ ($N+/N > 95‰$) of the resampled distances (83). Moreover, we compared phenetic distance of the other three australopiths ($S_{0,k}$) in our sample (A.L. 288-1, U.W. 88-98, TM1517) with those of the extant sample and those of the three tali that have been attributed to *A africanus*. We tested the hypothesis that some *A. africanus* tali could have an erroneous taxonomic designation, as another species has been suggested as present at Sterkfontein (84). Figure S3 shows histograms depicting shape distances in extant taxa, *A. africanus* (StW 88, StW 363 and StW 486) and the *Australopitecus/Paranthropus* group (A.L. 288-1, U.W. 88-98, TM1517).

Data processing and analysis routines were written in R software (85) and using the R packages "geomorph" (86) and "Morpho" (87).

Acknowledgments. This project has received funding from the European Research Council (ERC) under the European Union's Horizon 2020 research and innovation programme (grant agreement No 724046 – SUCCESS; www.erc-success.eu). We are grateful to the Liang Bua Team" and "The National Research Centre for Archaeology, Indonesia" for access to the model of LB1-15. We thank Norman Macleod for access to the NHM's Konica Minolta scanner and the following curators and their institutions for access to material: Christophe Soligo, Department of Anthropology, UCL; Richard Kraft and Mike Schweissing, Zoologische Staatssammlung München; Malcolm Harman, Powell Cotton Museum, Kent; Paula Jenkins, Daphne Hills and Louise Tomsett, Department of Zoology, NHM, London; Illinois State Museum; Yohannes Haile-Selassie and Lyman Jellman, CMNH; Bernhard Zipfel, University of the Witwatersrand; Linda K. Gordon and Darrin P. Lunde, NMNH; Natasha Johnson, Mike Black and Paolo Pellegatti of the P.A. Hearst Museum, UC Berkeley, for access to Native American collection; Museo delle Mummie di Roccapelago. We thank Luisa Mingozzi and Denis Nicolini of the Unit of Radiology (S. Maria delle Croci Hospital of Ravenna) for assistance during the scanning of Italian collections.We thank the Dmanisi research team for support and access during data collection at Dmanisi Museum-Reserve Georgian National Museum. We thank Drs. David Miminoshvili and Giorgi Tsivtsivadze, the Department of Computed Tomography, Research Institute of Clinical Medicine (Todua Clinic) for allowing us to

scan the Dmanisi talus in their facility. Access to the Krapina sample was made possible by the NESPOS (Neanderthal Studies Professional Online Service) Database (https://www.nespos.org/display/openspace/Home). We thank P. Mennecier and A. Froment (Museum National d'Histoire Naturelle, Departement Hommes, Natures, Societes) for providing digital models of La Ferrassie 1 and 2.

References

1. Harcourt-Smith WHE (2010) The first hominins and the origins of bipedalism. *Evol Educ Outreach* 3:333–340.

2. Kivell TL, Schmitt D (2009) Independent evolution of knuckle-walking in African apes shows that humans did not evolve from a knuckle-walking ancestor. *Proc Natl Acad Sci* 106:14241–14246.

3. Richmond BG, Jungers WL (2008) *Orrorin tugenensis* femoral morphology and the evolution of hominin bipedalism. *Science* 319:1662–1665.

4. Zollikofer CPE, et al. (2005) Virtual cranial reconstruction of *Sahelanthropus tchadensis*. *Nature* 434:755–759.

5. White TD, et al. (2009) *Ardipithecus ramidus* and the paleobiology of early hominids. *Science* 326:64–86.

6. Haile-Selassie Y (2001) Late Miocene hominids from the Midle Awash, Ethiopia. *Nature* 412:178.

7. Lovejoy CO, Latimer B, Suwa G, Asfaw B, White TD (2009) Combining prehension and propulsion: The foot of *Ardipithecus ramidus*. *Science* 326: 72-72e8.

8. Wolpoff MH, Senut B, Pickford M, Hawks J (2002) Palaeoanthropology: *Sahelanthropus* or '*Sahelpithecus*'? *Nature* 419:581–582.

9. Crompton RH (2016) The hominins: A very conservative tribe? Last common ancestors, plasticity and ecomorphology in Hominidae. Or, what's in a name? *J Anat* 228:686–699.

10. Ward CV (2002) Interpreting the posture and locomotion of *Australopithecus afarensis*: Where do we stand? *Am J Phys Anthropol* 119:185–215.

11. Harcourt-Smith WEH, Aiello LC (2004) Fossils, feet and the evolution of human bipedal locomotion. *J Anat* 204:403–416.

12. Drapeau MSM, Harmon EH (2013) Metatarsal torsion in monkeys, apes, humans and australopiths. *J Hum Evol* 64:93–108.

13. Ryan TM, et al. (2018) Human-like hip joint loading in *Australopithecus africanus* and *Paranthropus robustus*. *J Hum Evol* 121:12–24.

14. Stern JT, Susman RL (1983) The locomotor anatomy of *Australopithecus afarensis*. *Am J Phys Anthropol* 60:279–317.

15. Raichlen DA, Gordon AD, Harcourt-Smith WEH, Foster AD, Randall W (2010) Laetoli footprints preserve earliest direct evidence of human-like bipedal biomechanics. *PLoS One* 5: e9769.

16. Hatala KG, Demes B, Richmond BG (2016) Laetoli footprints reveal bipedal gait biomechanics different from those of modern humans and chimpanzees. *Proc R Soc B Biol Sci* 283: 20160235.

17. DeSilva JM (2009) Functional morphology of the ankle and the likelihood of climbing in early hominins. *Proc Natl Acad Sci* 106: 6567-6572.

18. Prang TC (2016) The subtalar joint complex of *Australopithecus sediba*. *J Hum Evol* 90:105–119.

19. Haile-Selassie Y, et al. (2012) A new hominin foot from Ethiopia shows multiple Pliocene bipedal adaptations. *Nature* 483:565–569.

20. Haeusler M, McHenry HM (2004) Body proportions of *Homo habilis* reviewed. *J Hum Evol* 46:433–465.

21. Bramble DM, Lieberman DE (2004) Endurance running and the evolution of *Homo*. *Nature* 432:345–352.

22. Pontzer H (2012) Ecological energetics in early *Homo*. *Curr Anthropol* 53:S346–S358.

23. Antón SC, Potts R, Aiello LC (2014) Evolution of early *Homo*: An integrated biological perspective. *Science* 345: 1236828-1–1236828-13.

24. Hatala KG, et al. (2016) Footprints reveal direct evidence of group behavior and locomotion in *Homo erectus*. *Sci Rep* 6:1–9.

25. Ruff C (2008) Femoral/humeral strength in early African *Homo*

erectus. *J Hum Evol* 54:383–390.

26. Pontzer H, et al. (2010) Locomotor anatomy and biomechanics of the Dmanisi hominins. *J Hum Evol* 58:492–504.

27. Harcourt-Smith WEH (2016) Early hominin diversity and the emergence of the genus *Homo*. *J Anthropol Sci* 94:19–27.

28. Harcourt-Smith WHE, et al. (2015) The foot of *Homo naledi*. *Nat Commun* 6:1–8.

29. Jungers WL, et al. (2009) The foot of *Homo floresiensis*. *Nature* 459:81–84.

30. Aiello LC, Dean C (1990) *An introduction to human evolutionary anatomy* (Academic Press).

31. Kidd R (1999) Evolution of the rearfoot. A model of adaptation with evidence from the fossil record. *J Am Podiatr Med Assoc* 89:1–17.

32. McNutt EJ, Zipfel B, DeSilva JM (2018) The evolution of the human foot. *Evol Anthropol* 27:197–217.

33. Griffin NL, Miller CE, Schmitt D, Ao KD (2015) Understanding the evolution of the windlass mechanism of the human foot from comparative anatomy: insights, obstacles, and future directions. *Am J Phys Anthropol* 156:1–10.

34. Sarrafian SK (1987) Functional characteristics of the foot and plantar aponeurosis under tibiotalar loading. *Foot Ankle* 8:4–18.

35. Huson A (1991) Functional anatomy of the foot. *Disord foot ankle* 1:409–431.

36. Steele DG, Bramblett CA (1988) *The anatomy and biology of the human skeleton* (Texas A&M University Press).

37. Parr WCH, Chatterjee HJ, Soligo C (2011) Inter- and intra-specific scaling of articular surface areas in the hominoid talus. *J Anat* 218:386–401.

38. Turley K, Frost SR (2013) The shape and presentation of the Catarrhine talus: a geometric morphometric analysis. *Anat Rec* 296:877–890.

39. Harcourt-Smith WEH (2002) Form and function in the hominoid tarsal skeleton. Dissertation (University of London).

40. Turley K, Frost SR (2014) The appositional articular morphology of the talo-crural joint: the influence of substrate use on joint shape. *Anat Rec* 297:618–629.

41. Latimer B, Ohman JC, Lovejoy CO (1987) Talocrural joint in African hominoids: Implications for *Australopithecus afarensis*. *Am J Phys Anthropol* 74:155–175.

42. DeSilva JM, Throckmorton ZJ (2010) Lucy's flat feet: The relationship between the ankle and rearfoot arching in early hominins. *PLoS One* 5: e14432.

43. Gebo DL, Schwartz GT (2006) Foot bones from Omo: implications for hominid evolution. *Am J Phys Anthropol* 129:499–511.

44. Kidd RS, O'Higgins P, Oxnard CE (1996) The OH8 foot: a reappraisal of the functional morphology of the hindfoot utilizing a multivariate analysis. *J Hum Evol* 31: 269-291

45. Prang TC (2015) Rearfoot posture of *Australopithecus sediba* and the evolution of the hominin longitudinal arch. *Sci Rep* 5: 17677.

46. Rhoads JG, Trinkaus E (1977) Morphometrics of the Neandertal talus. *Am J Phys Anthropol* 46:29–43.

47. Day MH, Wood BA (1968) Functional affinities of the Olduvai hominid 8 talus. *Man* 3:440–455.

48. Zipfel B, et al. (2011) The foot and ankle of *Australopithecus sediba*. *Science* 333:1417–1420.

49. Su A, Wallace IJ, Nakatsukasa M (2013) Trabecular bone anisotropy and orientation in an Early Pleistocene hominin talus from East Turkana , Kenya. *J Hum Evol* 64 (6):667–677.

50. Parr WCH, et al. (2014) Three-dimensional shape variation of talar surface morphology in hominoid primates. *J Anat* 225:42–59.

51. Holowka NB, Lieberman DE (2018) Rethinking the evolution of the human foot: insights from experimental research. *J Exp Biol* 221:jeb174425.

52. Dowdeswell MR, et al. (2017) Adaptation to bipedal gait and fifth metatarsal structural properties in *Australopithecus*, *Paranthropus*, and *Homo*. *Comptes Rendus Palevol* 16:585–599.

53. Rosas A, et al. (2017) Neandertal talus bones from El Sidrón site

(Asturias, Spain): A 3D geometric morphometrics analysis. *Am J Phys Anthropol* 164:394–415.

54. Holowka NB, O'Neill MC, Thompson NE, Demes B (2017) Chimpanzee and human midfoot motion during bipedal walking and the evolution of the longitudinal arch of the foot. *J Hum Evol* 104:23–31.

55. Lamy P (1986) The settlement of the longitudinal plantar arch of some African Plio-Pleistocene hominids: a morphological study. *J Hum Evol* 15:31–46.

56. DeSilva JM (2010) Revisiting the "midtarsal break". *Am J Phys Anthropol* 141:245–258.

57. Ward CV, Kimbel WH, Johanson DC (2011) Complete fourth metatarsal and arches in the foot of *Australopithecus afarensis*. *Science* 331:750–753.

58. Holowka NB, O'Neill MC, Thompson NE, Demes B (2017) Chimpanzee and human midfoot motion during bipedal walking and the evolution of the longitudinal arch of the foot. *J Hum Evol* 104:23–31.

59. Nowak MG, Carlson KJ, Patel BA (2010) Apparent density of the primate calcaneo-cuboid joint and its association with locomotor mode, foot posture, and the "midtarsal break". *Am J Phys Anthropol* 142:180–193.

60. Fernández PJ, et al. (2018) Evolution and function of the hominin forefoot. *Proc Natl Acad Sci* 115: 8746-8751.

61. Su A, Carlson KJ (2017) Comparative analysis of trabecular bone structure and orientation in South African hominin tali. *J Hum Evol* 106:1–18.

62. Griffin NL, D'Aočt K, Richmond B, Gordon A, Aerts P (2010) Comparative in vivo forefoot kinematics of *Homo sapiens* and *Pan paniscus*. *J Hum Evol* 59 (6):608–619.

63. Jashashvili T, Dowdeswell MR, Lebrun R, Carlson KJ (2015) Cortical structure of hallucal metatarsals and locomotor adaptations in hominoids. *PloS One* 10:e0117905.

64. Green DJ, Gordon AD, Richmond BG (2007) Limb-size proportions in *Australopithecus afarensis* and *Australopithecus africanus*. *J*

Hum Evol 52:187–200.

65. DeSilva JM, et al. (2013) The lower limb and mechanics of walking in *Australopithecus sediba*. *Science* 340:1232999.

66. Boyle EK, et al. (2018) A quantification of calcaneal lateral plantar process position with implications for bipedal locomotion in *Australopithecus*. *J Hum Evol* 123:24–34.

67. Wunderlich RE, Ischinger SB (2017) Foot use during vertical climbing in chimpanzees (*Pan troglodytes*). *J Hum Evol* 109:1–10.

68. Venkataraman VV, Kraft TS, Desilva JM, Dominy NJ (2013) Phenotypic plasticity of climbing-related traits in the ankle joint of great apes and rainforest hunter-gatherers. *Hum Biol* 85:309–328.

69. Venkataraman V V, Kraft TS, Dominy NJ (2013) Tree climbing and human evolution. *Proc Natl Acad Sci* 110:1237–1242.

70. Preuschoft H (2004) Mechanisms for the acquisition of habitual bipedality: are there biomechanical reasons for the acquisition of upright bipedal posture? *J Anat* 204: 363–384.

71. Bennett MR, et al. (2009) Early hominin foot morphology based on 1.5-million-year-old footprints from Ileret, Kenya. *Science* 323:1197–1201.

72. Raichlen DA, Gordon AD (2017) Interpretation of footprints from Site S confirms human-like bipedal biomechanics in Laetoli hominins. *J Hum Evol* 107:134–138.

73. Day MH, Wickens E (1980) Laetoli Pliocene hominid footprints and bipedalism. *Nature* 286:385–387.

74. Crompton RH, et al. (2012) Human-like external function of the foot, and fully upright gait, confirmed in the 3.66 million year old Laetoli hominin footprints by topographic statistics, experimental footprint-formation and computer simulation. *J R Soc Interface* 9:707–719.

75. Prang TC (2016) Reevaluating the functional implications of *Australopithecus afarensis* navicular morphology. *J Hum Evol* 97:73–85.

76. Belcastro MG, et al. (2017) The history and composition of the identified human skeletal collection of the Certosa cemetery (Bologna, Italy, 19th–20th century). *Int J Osteoarchaeol* 27:912–

925.

77. Slice DE (2006) *Modern morphometrics in physical anthropology* (Springer Science & Business Media).

78. Gunz P, Mitteroecker P (2013) Semilandmarks: A method for quantifying curves and surfaces. *Hystrix* 24:103–109.

79. Benazzi S, Bookstein FL, Strait DS, Weber GW (2011) A new OH5 reconstruction with an assessment of its uncertainty. *J Hum Evol* 61:75–88.

80. Shaw CN, Ryan TM (2012) Does skeletal anatomy reflect adaptation to locomotor patterns? Cortical and trabecular architecture in human and nonhuman anthropoids. *Am J Phys Anthropol* 147:187–200.

81. Bailey SE, Benazzi S, Hublin JJ (2014) Allometry, merism, and tooth shape of the upper deciduous M2 and permanent M1. *Am J Phys Anthropol* 154:104–114.

82. Adams DC, Felice RN (2014) Assessing trait covariation and morphological integration on phylogenies using evolutionary covariance matrices. *PLoS One* 9:e94335.

83. Lordkipanidze D, et al. (2013) A complete skull from Dmanisi, Georgia, and the evolutionary biology of early *Homo*. *Science* 342:326–332.

84. Clarke RJ (2013) "*Australopithecus* from Sterkfontein Caves, South Africa" in *The Paleobiology of Australopithecus. Vertebrate Paleobiology and Paleoanthropology*, Reed K, Fleagle J, Leakey R, Eds. (Springer, Dordrecht), pp 105–123.

85. Team RC (2017) R: A language and environment for statistical computing. Vienna, Austria: R Foundation for Statistical Computing; 2017.

86. Adams DC, Otárola-Castillo E (2013) Geomorph: An r package for the collection and analysis of geometric morphometric shape data. *Methods Ecol Evol* 4:393–399.

87. Schlager S (2017) "Morpho and Rvcg - Shape Analysis in R: R-Packages for Geometric Morphometrics, Shape Analysis and Surface Manipulations" in *Statistical shape and deformation analysi*s, Zheng G, Li S, Székely G, Eds. (Academic Press).

SUPPLEMENTARY INFORMATION

Supplementary text 1. Individual facets.

Medial malleolar facet. Shape variability of the medial malleolar facet (Fig. S1a) shows a certain degree of overlap between African apes and *H. sapiens,* suggesting that the morphology of this facet is not useful when interpreting locomotor behaviour of fossil hominins. The latter falls mainly within *Pan* and, to a lesser extent, into the *H. sapiens* range of variability. Only TM 1517 (*P. robustus*) plots in the *Gorilla* range of variation. PC1 (31.9%) accounts for significant differences among all three extant groups (ANOVA, Df = 2, *F*-test = 94.7, $P < 0.001$, Table S3) and shape changes recorded on it correlate with logged centroid size (CS; r = 0.1673, $P < 0.05$). Morphological dissimilarity expressed along PC2 (23.2%) and PC3 (13.1%) is influenced by body mass, as suggested by the significant correlation with logged CS measured in both (r = -0.2717, $P < 0.001$ and r = -0.4059, $P < 0.001$ respectively). Larger-bodied taxa like *Gorilla* and *H. sapiens* significantly differ from smaller-bodied taxa such as *Pan* along PC2 (ANOVA, Df = 2, *F*-test = 15.1, $P < 0.001$, Table S3) and PC3 (ANOVA, Df = 2, *F*-test = 37.1, $P < 0.001$, Table S3).

Shape change along axes reflects a general pattern shared by all three PCs exhibiting more concave and distally expanded facets in smaller forms, which could allow greater mobility in dorsal and plantar flexion (Fig. S1c).

The first three form space PCs explain 79.7% of overall variability (Fig. S1b), showing the same overlap between extant taxa as is evident in shape space with fossil hominins falling in this overlapping area. Even if the trajectories of extant groups are not parallel in the plot, neither angles nor magnitudes were found to significantly differ between pairs of extant groups.

Anterior-medial calcaneal facet. Similarly, the anterior-medial calcaneal facet of extant samples overlaps in the shape space PCA (Fig. S1d), suggesting that the anterior calcaneal facet is not helpful in discriminating bipedal from quadrupedal forms. Post hoc ANOVA reveals that PC1 (30.5%) accounts for significant differences between more terrestrial (*Gorilla* and *H. sapiens*) and more arboreal forms (*Pan*) (ANOVA, Df = 2, *F*-test = 17.6, $P < 0.001$, Table S3). PC2 (20.1%) differentiates *H. sapiens* from African apes (ANOVA, Df = 2, *F*-test = 66.8, $P < 0.001$, Table S3), while PC3 (15.8%) accounts for differences between *Pan* and *H. sapiens* (ANOVA, Df = 2, *F*-test = 3.9, $P < 0.05$, Table S3).

Shape change ranges from negative (rounded and extended dorsally)

to positive (flatter and relatively expanded antero-posteriorly) values on PC1, and accounts for differences between more arboreal and more terrestrial taxa (Fig. S1f). Positive values on PC2 reflect bipedal features (flat facet), while PC2 negative values are assigned to the shape observed in knuckle-walkers (more convex, with the anterior facet perpendicularly oriented in respect to the medial facet). Extreme positive values on PC3 reflect flatter and larger anterior-medial calcaneal facets (i.e., *H. sapiens*), while an antero-posterior narrowed and spherical surface occupies the negative extreme (i.e., *Pan*) on the same axis. Shape divergence between *Pan* and *H. sapiens* in PC3 is also related to difference in body mass (r = -0.1968, $P < 0.05$).

Form space (Fig. S1e) also shows fossil hominins falling in the area of overlap between extant groups in the first three PCs (77.7%). No significant differences in angle and magnitude of allometric trajectories were found.

Posterior calcaneal facet. The first three shape-space PCs of the posterior calcaneal facet account for 56.6% of overall variability (Fig. S2a). PC1 (30%) tends to separate African apes from *H. sapiens* (ANOVA, Df = 2, *F*-test = 270.9, $P < 0.001$, Table S3). Fossil hominins show high variability and share morphological affinities with both African apes and *H. sapiens*. No relevant differences were recorded between *Australopithecus* and extinct *Homo* (for example some Neandertals fall inside the African ape range together with some australopiths).

Moving from the PC1 positive extreme to the PC1 negative extreme (Fig. S2c), shape changes from a less concave calcaneal facet (reduced subtalar joint motion) to a more concave and rectangular shape (increased exorotation and endorotation). PC2 (15.8%) separates larger-bodied terrestrial taxa (i.e., exhibiting a broad and flatter calcaneal facet in the negative PC2 direction) from *Pan* (i.e., exhibiting a more concave and antero-posterior shorter calcaneal facet in the positive PC2 direction) (ANOVA, Df = 2, *F*-test = 7.9, $P < 0.001$, Table S3). PC3 (10.8%) discriminates a more oval and relatively flatter facet on the positive extreme from a more rectangular and concave form on the negative extreme (ANOVA, Df = 2, *F*-test = 34, $P < 0.001$, Table S3). All three PCs positively correlate with logged CS PC1, r = 0.4416, $P < 0.001$; PC2, r = -0.2715, $P < 0.001$; PC3, r = 0.1990, $P < 0.05$), which hints at an association between body mass and plasticity of the calcaneal facet. This pattern is clearer in PC2, which separates larger-bodied terrestrial taxa (*Gorilla* and *H. sapiens*) from the smaller-bodied *Pan* (Table S3).

In form space, the three PCs explain 80.3% of overall variability (Fig. S2b). All three extant taxa show parallel allometric trajectories without any

significant differences in angles and magnitude. As it was observed in shape space PCA, fossil hominins share posterior calcaneal features with both African apes and *H. sapiens* on PC2 and PC3.

Trochlea. Shape space PC1 (31.9%) accounts for significant differences among the extant groups (ANOVA, Df = 2, *F*-test = 137.1, $P < 0.001$, Table S3) despite their partial overlap (Fig. S2d). Australopiths surround the area of overlap between *Pan* and *H. sapiens*, except for StW 363 (*A. africanus*) and StW 486 (*A. africanus*), which fall in the range of *H. sapiens* variability with fossil *Homo* specimens. Positive PC1 values reflect a flatter, wider, and more squared trochlea, typical of *H. sapiens*, while negative values reflect a grooved, narrowed, and more trapezoidal trochlea with an elevated lateral rim that is typical of African apes (Fig. S2f). The larger trochlear surface in *H. sapiens* positively correlates with logged CS on PC1 ($r = 0.1560$, $P < 0.05$), while the correlation is negative for PC2 ($r = -0.4086$, $P < 0.001$) and PC3 ($r = -0.2008$, $P < 0.01$). PC2 (12.6%) (ANOVA, Df = 2, *F*-test = 45.46, $P < 0.001$) and PC3 (10%) (ANOVA, Df = 2, *F*-test = 11.57, $P < 0.001$) mainly reflect differences between larger-bodied terrestrial forms (i.e., a trapezoidal trochlea in negative PC2 and PC3) and smaller-bodied arboreal forms (i.e., a rectangular trochlea in positive PC2 and PC3).

In the shape space PCA, extinct *Homo* tend to fall within *H. sapiens* variability while australopiths tend to plot around the area of overlap between *Pan* and *H. sapiens*, likely as a consequence of both (locomotor) behavioural-related form and body size. Nevertheless, two of the three *A. africanus* (StW 363 and StW 486) fall securely within the *H. sapiens* range of variability. Considering the variability in shape space exhibited by these three specimens of *A. africanus*, we test the hypothesis that phenetic distance measured across samples of *A. africanus* is larger than that measured in extant taxa (see Methods), suggesting the presence of multiple species among individuals currently attributed to *A. africanus* (1). Phenetic distances (Fig. S3a) between specimens of *A. africanus* are significantly larger than those measured among 1000 re-sampled *H. sapiens* ($P < 0.05$), whereas the phenetic distance exhibited by a group comprised of A.L. 288-1 (*A. afarensis*), U.W. 88-98 (*A. sediba*) and TM1517 (*P. robustus*) does not differ from that of *H. sapiens*. However, no significant difference was observed when comparing *A. africanus* to *Pan* and borderline non-significance was observed when compared to *Gorilla*, suggesting that StW 363, StW 486 and StW 88 may be attributed to the same species or deme based on trochlear morphology.

Form space analysis (Fig. S2e) reveals that PC1 (63.2%) separates larger-bodied forms (*H. sapiens* and *Gorilla*) from the smaller-bodied *Pan*,

while PC2 (11.6%) and PC3 (4.2%) tend to separate both African ape taxa from *H. sapiens*. Allometric trajectories differ between *Pan* and *H. sapiens* (α= 16.9, P< 0.01; magnitude P < 0.01), as well as between *Pan* and *Gorilla* (α = 26.1, P < 0.001; magnitude P < 0.01). Fossil hominins with lower centroid size (which is a proxy for body mass; 2, 3) fall closer to the smaller-bodied *Pan* and both tend to exhibit greater similarities to smaller-bodied *H. sapiens*. On the other hand, larger-bodied fossil hominins fall within the *H. sapiens* range. Overall, trochlear shape is not diagnostic for hominin morphology as there is overlap between *H. sapiens* and African apes.

These results from the talus support an investigation of the morphology of the distal tibia that suggested the form of the distal tibia is not unequivocally linked to obligate bipedal locomotion due to the high range of motion at the talocrural joint (4). However, extreme shapes represented on PC1 (Fig. S2f) reflect the way in which the leg passes over the foot during stance phase in knuckle-walkers (i.e., an arcuate path) and bipeds (i.e., a straight path) (5–7), and likely overall positional behaviour difference in respect to more flexed lower limb joints and dorsiflexed ankle in African apes even during quadrupedalism compared to the more extended limb postures of modern humans (8–10).

Since the trochlea is the articular facet that is mainly involved in the transfer of weight across the ankle joint towards the ground, body size has an effect on its shape.

Supplementary text 2. Combined facets.

Talocrural joint. The talar structures associated with the talocrural joint were assessed combining the trochlea with 1) the lateral malleolar facet, 2) the medial malleolar facet, and 3) both the lateral and medial malleolar facets. These three combinations are the only ones that exhibit slight overlap between the ranges of extant hominids.

Combined trochlea and lateral malleolar facet. In shape space (Fig. S4a), PC1 (27.9%) tends to separate African apes from *H. sapiens* (ANOVA, Df = 2, *F*-test = 220.5, *P* < 0.001, Table S3), with less clear separation between australopiths and early non-*erectus Homo*(11) (between *Pan* and *H. sapiens*) from extinct *Homo* (close to or falling inside the *H. sapiens* range). Interestingly, StW 486 (*A. africanus*) plots close to late extinct *Homo* and falls inside the *H. sapiens* range. PC1 negative values exhibit a trapezoidal trochlea with an elevated lateral rim accompanied by a more laterally extended and curved lateral surface that allows for dorsiflexion in extant apes during climbing. On the other hand,

H. sapiens (PC1 positive values) are characterized by a relatively more flat and large trochlea with a less extended and weakly curved lateral surface, which reduces inversion posture of the foot and keeps the leg in a vertical position during the stance phase (Fig. S4c). PC2 (12.2%) accounts for significant differences among all three extant groups (ANOVA, Df = 2, *F*-test = 70.9, $P < 0.001$, Table S3). More arboreal forms (PC2 positive values) display a relatively deeper trochlear groove, medial extension of the posterior margin and anteriorly oriented lateral facet when compared to more terrestrial forms (PC2 negative). No significant differences were found among taxa in PC3 (ANOVA, Df = 2, *F*-test = 1.7, Table S3), which only accounts for 9% of overall variation. PC3 seems to reflect a change in medial extension of the lateral malleolar facet. The three PCs are correlated with logged CS (PC1, r = 0.3134, $P < 0.001$; PC2, r = -0.4316, $P < 0.001$; PC3, r = 0.2310, $P < 0.01$). The three form space PCs account for 76.9% of overall variability (Fig. S4b). While PC1 segregates *Gorilla* and *H. sapiens* from *Pan*, PC2 and PC3 separate African apes from *H. sapiens*. Australopiths are closer to *Pan* trajectories than are other fossil hominins, which are closer to *H. sapiens* trajectories or fall between African apes and *H. sapiens*. *Pan* shows a different allometric trajectory from *H. sapiens* ($\alpha = 14$, $P < 0.05$) and *Gorilla* ($\alpha = 19.8$, $P < 0.001$; magnitude $P < 0.05$).

Combined trochlea and medial malleolar facet. In shape space (Fig. S5a), PC1 (32.4%) accounts for significant differences between African apes and *H. sapiens* (ANOVA, Df = 2, *F*-test = 191.8, $P < 0.001$, Table S3) with only small overlap between African apes and *H. sapiens*. A trapezoidal and grooved trochlea with a cupped medial facet (PC1 negative values) separates African apes from *H. sapiens*, which exhibit a flat and squared trochlea with a flat medial facet instead (PC1 positive values; Fig. S5c). Most of the australopiths, early non-*erectus Homo*, and *H. naledi* fall inside or just outside the observed range of *Pan* variability, while other fossil *Homo* specimens fall closer to the range of observed *H. sapiens* variability. StW 486 (*A. africanus*) and StW 363 (*A. africanus*) are exceptions, however, since they fall inside the *H. sapiens*, as is StW 88, which falls inside the *Pan* range. As in the case of the trochlea, we compare phenetic distance measured among specimens of *A. africanus* with those of extant taxa. Results (Fig. S3b) show a comparatively larger distance exhibited by *A. africanus* than exhibited by *H. sapiens* ($P < 0.05$), but not as large as the random distances exhibited by *Pan* and to a markedly lesser extent by *Gorilla*.

Shape space PC2 (12%) shows significant differences among all three extant groups (ANOVA, Df = 2, *F*-test = 103.6, $P < 0.001$, Table S3) and is negatively correlated with logged CS (r = -0.5797, $P < 0.001$), while

PC3 (8.9%) discriminates *Pan* from *Gorilla* (ANOVA, Df = 2, *F*-test = 3.4, $P < 0.05$, Table S3). More arboreal forms (PC2 negative and PC3 positive values) display an antero-posterior extension of the trochlea resulting in a rectangular shape compared to the shorter and trapezoidal trochlea of more terrestrial forms. More cupped medial malleolar facets are also assigned negative values on PC2 and positive values on PC3 (Fig. S5c). In form space, the allometric trajectory of *Pan* differs from that of *H. sapiens* ($\alpha = 16.7$, $P < 0.01$; magnitude $P < 0.05$) and *Gorilla* ($\alpha = 24.2$, $P < 0.001$; magnitude $P < 0.01$). Australopiths, *H. habilis*, *H. naledi* and *H. floresiensis* seem follow the trajectory of *Pan*, while other fossil *Homo* specimens are placed around the *H. sapiens* trajectory.

Combined trochlea, lateral and medial malleolar facets. As already documented for the combination of the trochlea with lateral and medial facets, respectively, shape space PCA (Fig. S6a) shows that australopiths (with the exception of StW 486 and StW 363), early non-*erectus Homo,* and *H. naledi* plot next to *Pan*, while other extinct *Homo* plot closer to the *H. sapiens* range. PC1 (29.6%) discriminates between African apes and *H. sapiens* (ANOVA, Df = 2, *F*-test = 262.3, $P < 0.001$, Table S3) based on the difference between a grooved and trapezoidal trochlea coupled with flared medial and lateral facets that characterise more arboreal taxa versus a squared, flat trochlea and lateral facet that characterise *H. sapiens* (Fig. S6c). PC2 (12%) shows differences among all three extant groups (ANOVA, Df = 2, *F*-test = 116, $P < 0.001$, Table S3), while PC3 (8%) does not exhibit any significant difference among groups (ANOVA, Df = 2, *F*-test = 1.9, Table S3). Morphological change along PC2 is the same as described before (Figs. S4 and S5). All three PCs correlate with logged CS (PC1, $r = 0.3013$, $P < 0.001$; PC2, $r = -0.5180$, $P < 0.001$; PC3, $r = 0.2374$, $P < 0.01$). Form space PCA (Fig. S6b) yields similar results to those obtained for the combination of the trochlea and medial malleolar facet. In this case, however, a significant difference was found between the allometric trajectories of *Pan* and *Gorilla* ($\alpha = 17.8$, $P < 0.001$; magnitude $P < 0.05$).

In sum, the same patterns characterising the fossil hominin distribution are recognizable in the combined trochlea and medial malleolar facet (Fig. S5) and in the combined trochlea, lateral and medial malleolar facets (Fig. S6), suggesting a primitive retention in the geometric configuration of these combinations in australopiths and early non-*erectus Homo.*

Talocrural and subtalar joints. The relationship between talocrural and subtalar joints was explored analysing the combination of the posterior calcaneal facet, trochlea, and the medial and lateral malleolar facets (Fig.

S7), and the combination of the posterior calcaneal facet and trochlea (Fig. S8). Both combinations yielded a relatively clean separation between African apes and *H. sapiens*.

Combined posterior calcaneal facet, trochlea, medial and lateral malleolar facets. In shape space (Fig. S7a), PC1 (29%) separates African apes from *H. sapiens* (ANOVA, Df = 2, *F*-test = 576.1, $P < 0.001$, Table S3), with StW 88 (*A. africanus*) and KNM-ER 1476 (*Homo* spp./ *P. boisei*) plotting close to the African ape range, U.W. 88-98 (*A. sediba*) and A.L. 288-1 (*A. afarensis*) plotting between African apes and *H. sapiens*, StW 363 (*A. africanus*) plotting next to *H. sapiens*, and fossil *Homo* specimens plotting close to or inside the range of *H. sapiens* variability. PC2 (9.3%) accounts for significant differences among all three extant groups (ANOVA, Df = 2, *F*-test = 65.6, $P < 0.001$, Table S3), while PC3 (7.1%) discriminates between *Pan, Gorilla* and *H. sapiens* (ANOVA, Df = 2, *F*-test = 8.1, Table S3). Morphological change in the first three PCs correlates with logged CS (PC1, r = 0.4777, $P < 0.001$; PC2, r = 0.4480, $P < 0.001$; PC3, r=-0.1983, $P < 0.05$). In PC1 (Fig. S7c), African apes exhibit a more concave posterior calcaneal facet, a trapezoidal and grooved trochlea, and flared lateral malleolar facets (PC1 negative values) that all enable a higher degree of dorsiflexion and inversion/eversion capabilities that are advantageous in interacting with the more multidirectional substrates of arboreal environments. Prominently terrestrial and larger-bodied taxa plotting along positive PC2 and PC3 are characterised by a relatively flatter trochlea, a flatter posterior calcaneal facet, and a less concave lateral facet. Form space PCA (Fig. S7b) separates *Gorilla* and *H. sapiens* from *Pan* along PC1 (66.6%), and African apes from *H. sapiens* on PC2 (8%). The *Pan* trajectory is significantly different from that of *H. sapiens* ($\alpha = 11.7$, $P < 0.05$; magnitude $P < 0.01$) and *Gorilla* ($\alpha = 12.4$, $P < 0.05$; magnitude $P < 0.05$). Australopiths are closer to *Pan*, while other fossil hominins are closer to the trajectory of *H. sapiens*.

Combined posterior calcaneal facet and trochlea. Results from shape and form space are similar to those of the combined posterior calcaneal facet, trochlea, and the medial and lateral malleolar facets. The distribution of fossil hominins, however, is clearer in the present case. In shape space (Fig. S8a), significant differences are present in the distribution of values along PC1 (29.9%), which distinguishes African apes from *H. sapiens* (ANOVA, Df = 2, *F*-test = 457.5, $P < 0.001$). *A. afarensis* (A.L. 288-1), *A. africanus* (StW 88), *A. sediba* (U.W. 88-98) and KNM-ER 1476 (*Homo* spp./ *P. boisei*), followed by StW 363 (*A. africanus*), and are closer to the range associated with African apes. Fossil *Homo* specimens fall close to or within the range of *H. sapiens* variability. Shape of the talus changes from

a trapezoidal and sloping trochlea with a relatively more concave posterior calcaneal facet - typical of great apes - to essentially a squared and flatter trochlea and a less concave posterior calcaneal facet – typical of *H. sapiens* (Fig. S8c). These morphological differences are consistent with higher mobility of the ankle in African apes compared to *H. sapiens* (7, 12), particularly related to greater flexion-extension (e.g., a sagittally-oriented posterior calcaneal facet) (13). In *H. sapiens*, the trochlea appears dorsally elevated with respect to the posterior calcaneus, resulting in taller talar corpora that have been considered as reflective of the longitudinal arch (12). PC3 (8.1%) accounts for differences among all extant taxa (ANOVA, Df = 2, *F*-test = 64.2, $P < 0.001$, Table S3), while no significant values have been found for PC2 (ANOVA, Df = 2, *F*-test = 0.4, Table S3), which explains 9% of overall variation. Both PC1 ($r = 0.4823$, $P < 0.001$) and PC3 ($r = -0.4389$, $P < 0.001$) correlate with logged CS.

The three form space PCs explain 78% of overall variability. *Gorillas* and *H. sapiens* differ from *Pan* in PC1 (66.6%), while African apes are separated from *H. sapiens* in PC2 (8%). *Gorilla* and *Pan* trajectories differ in angle and magnitude ($\alpha = 11.7$, $P < 0.05$; magnitude $P < 0.05$), while *H. sapiens* are different from *Pan* in magnitude only ($P < 0.01$). Smaller specimens (australopiths, *H. habilis*, *H. naledi*, *H. floresiensis*) and KNM-ER 1476 (*H. erectus*) plot next to *Pan*, while larger (bodied) specimens are closer to *H. sapiens*.

Transverse, talocrural and subtalar joints. Being a component of the transverse tarsal joint, the navicular facet was associated in turn with the posterior calcaneal facet and trochlea.

Combined navicular and posterior calcaneus facets. The combined navicular and posterior calcaneus facets (Fig. S9a) distinguish African apes from *H. sapiens* in shape space (ANOVA, Df = 2, *F*-test = 371.4, $P < 0.001$, Table S3) along PC1 (35.6% of total variation). The flatter, larger head found in *H. sapiens* is characterised by a reduced distance from the posterior calcaneus. This reflects a reduction in the length of the talar neck that opposes increased stress caused by weight transfer along the medial side during push-off (5). The posterior calcaneal facet is more sagittally-oriented in African apes, suggesting a higher possibility of flexion-extension (13). From this perspective, fossil hominins are intermediate between extant taxa, with the exception of *A. sediba* (U.W. 88-98), which falls inside the range of *Pan*, and a few Neandertals and one *H. naledi* talus that all fall within the range of *H. sapiens* variability. *A. afarensis* (A.L. 288-1), *A. africanus* (StW 88) and Dmanisi (D4110) exhibit more ape-like relationships between the navicular and posterior calcaneal facets. This suggests variability exists among hominins in this combination

of features, likely due to the mosaic nature of human-like and ape-like features characterising the posterior calcaneal facet (Fig. S2a-c). PC2 (8.9%) represents differences between *Pan* and both *H. sapiens* and *Gorillas* (i.e., from rounded navicular facets with a more concave posterior calcaneal facet plotting close to negative values on PC2 to a fatter, more rectangular navicular facet with a less concave posterior facet plotting close to positive values (ANOVA, Df = 2, *F*-test = 7.6, $P < 0.001$, Table S3). Both PC1 and PC2 correlate with logged CS (PC1, r = -0.3188, $P < 0.001$; PC2, r = -0.2829, $P < 0.001$). PC3 (7.8%) shows no significant differences among extant taxa (ANOVA, Df = 2, *F*-test = 0.8). The three form space PCs account for 81.9% of overall variability. While PC1 accounts for differences in overall body size, PC2 tends to separate African apes from *H. sapiens*. Modern humans are different from *Pan* in magnitudes of their allometric trajectory ($P < 0.05$), but not in the angle. Fossil hominins plot between *Pan* and *H. sapiens*, except for Neandertals, which plot inside the range of *H. sapiens* variability.

Combined navicular facet and trochlea. With the combined navicular facet and trochlea (Fig. S10), we obtained a clearer separation among fossils than the one obtained through the previous combination of features (Fig. S9). **S**hape space PC1 (40.6%) discriminates *H. sapiens* from African apes (ANOVA, Df = 2, *F*-test = 574.4, $P < 0.001$, Table S3).

A. africanus (StW 88) and *A. sediba* (U.W. 88-98) are the hominins that plot closest to the ranges of African apes, but *H. habilis* (OH8) and D4110 are also quite close. *A. afarensis* (A.L. 288-1) is the only *Australopithecus* talus plotting close to the *H. sapiens* range, while more recent hominin species (one *H. naledi*, *H. floresiensis* and Neandertals; Fig. S10a) also do. In *H. sapiens*, the navicular facet is more centrally displaced and downward oriented with respect to the trochlea (Fig. S10c). This may likely be an indicator of an efficient weight transfer along the first ray (5) rather than an indicator of an adducted hallux (6, 14, 15). Furthermore, a large angle of torsion of the talar head provides increased stability at the transverse tarsal joint (13, 16, 17). This could indicate that *A. afarensis* had a more stable midtarsal region compared to more recent australopiths. PC2 (8.7%) shows differences between *Pan* and *Gorilla* (ANOVA, Df = 2, *F*-test = 4.3, $P < 0.001$, Table S3). The latter exhibit larger surfaces compared to those of *Pan* and a less dorsally extended navicular facet as consequence of less intense arboreal activities. For PC3 (6.4%), no significant differences were found (ANOVA, Df = 2, *F*-test = 0.8). PC1 and PC2 are correlated with logged CS (PC1, r = 0.4584, $P < 0.001$; PC2, r = 0.1851, $P < 0.05$), suggesting that larger-bodied taxa (i.e., *Gorilla* and *H. sapiens*) may require larger articular surfaces. Form space (Fig. S10b) reveals that, beside the differences in body size along PC1 (67.7%), combined navicular facet and

trochlea are affected by locomotor behaviour as African apes are separated from *H. sapiens* along PC2 (11.2%). Small-bodied *A. afarensis* seem to follow the *H. sapiens* trajectory, while small-bodied *A. africanus*, *A. sediba*, *H. habilis* are closer to the trajectory of *Pan*. No differences in angles and magnitudes of allometric trajectories are present among extant taxa.

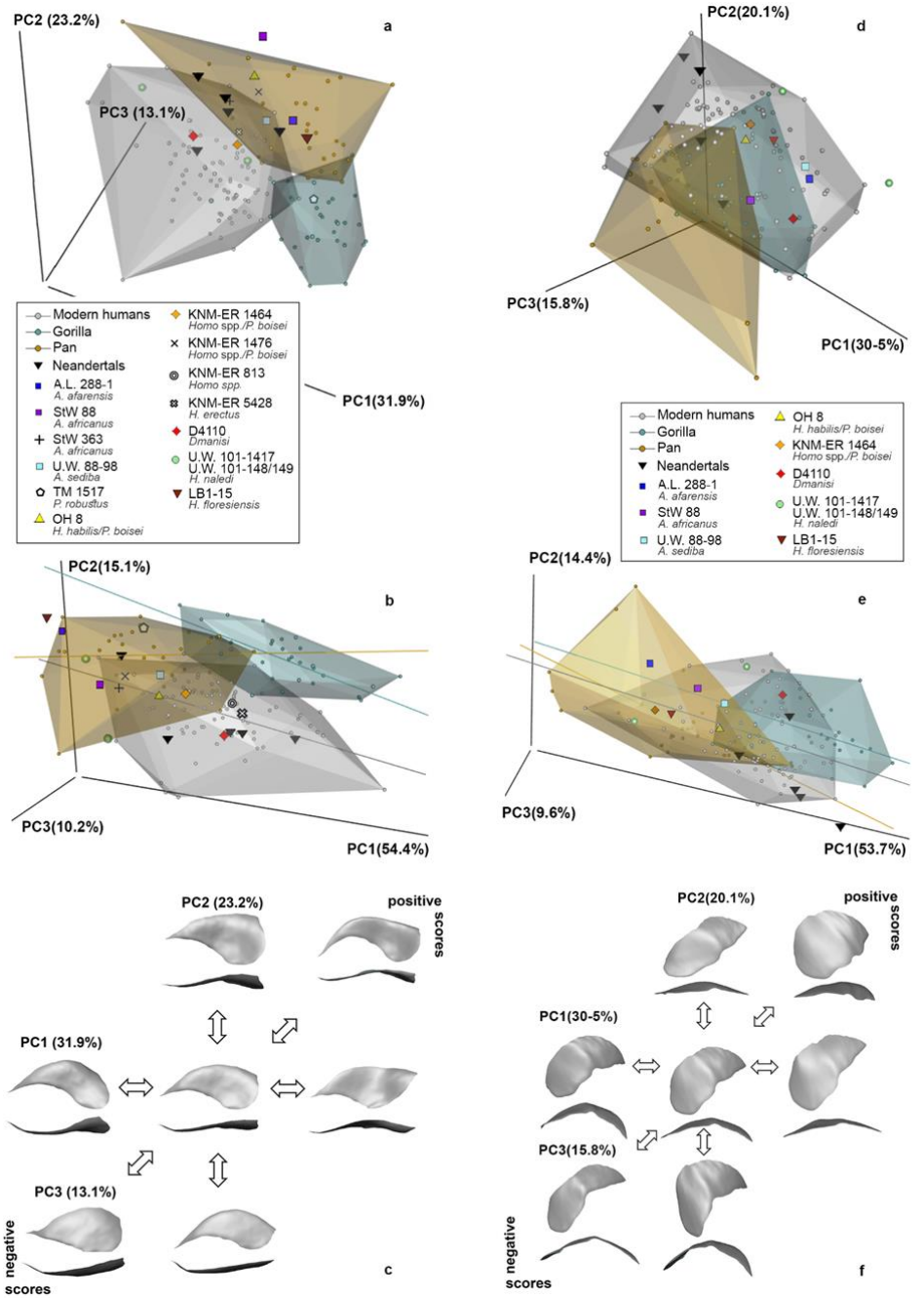

Fig. S1. Medial malleolar facet and anterior-medial calcaneal facet. 3D PCA plot in shape space (**a**), form space (**b**) and shape changes of the medial malleolar facet along the first three shape PCs (**c**) in medial (above) and dorsal (down) views. 3D PCA plot in shape space (**d**), form space (**e**) and shape changes of the anterior-medial calcaneal facet along the first three shape PCs (**f**) in plantar (above) and posterior (below) views.

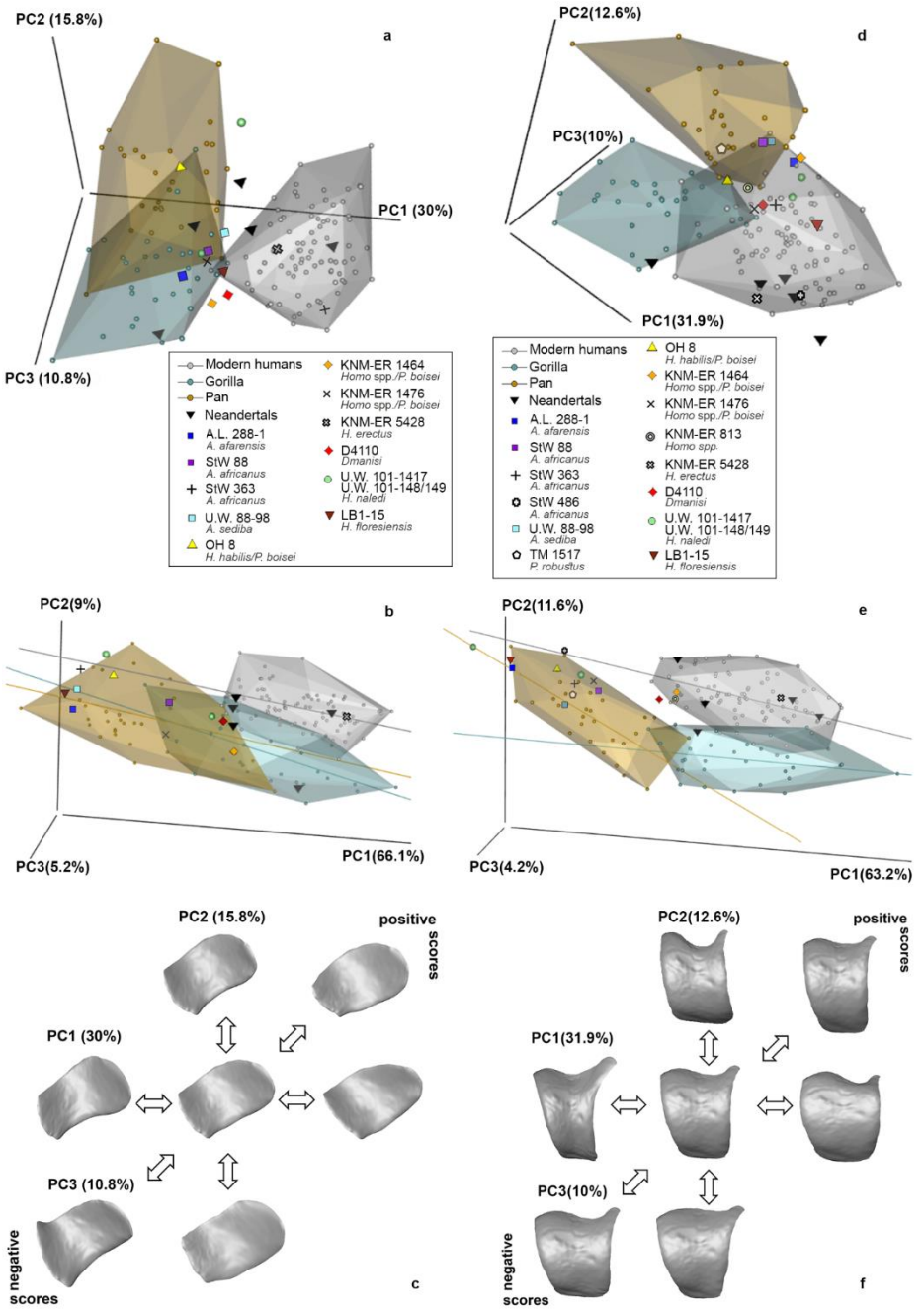

Fig. S2. Posterior calcaneal facet and trochlea. 3D PCA plot in shape space (**a**), form space (**b**) and shape changes of the posterior calcaneal facet along the first three shape PCs (**c**) in plantar view. 3D PCA plot in shape space (**d**), form space (**e**) and shape changes of the trochlea along the first three shape PCs (**f**) in dorsal view.

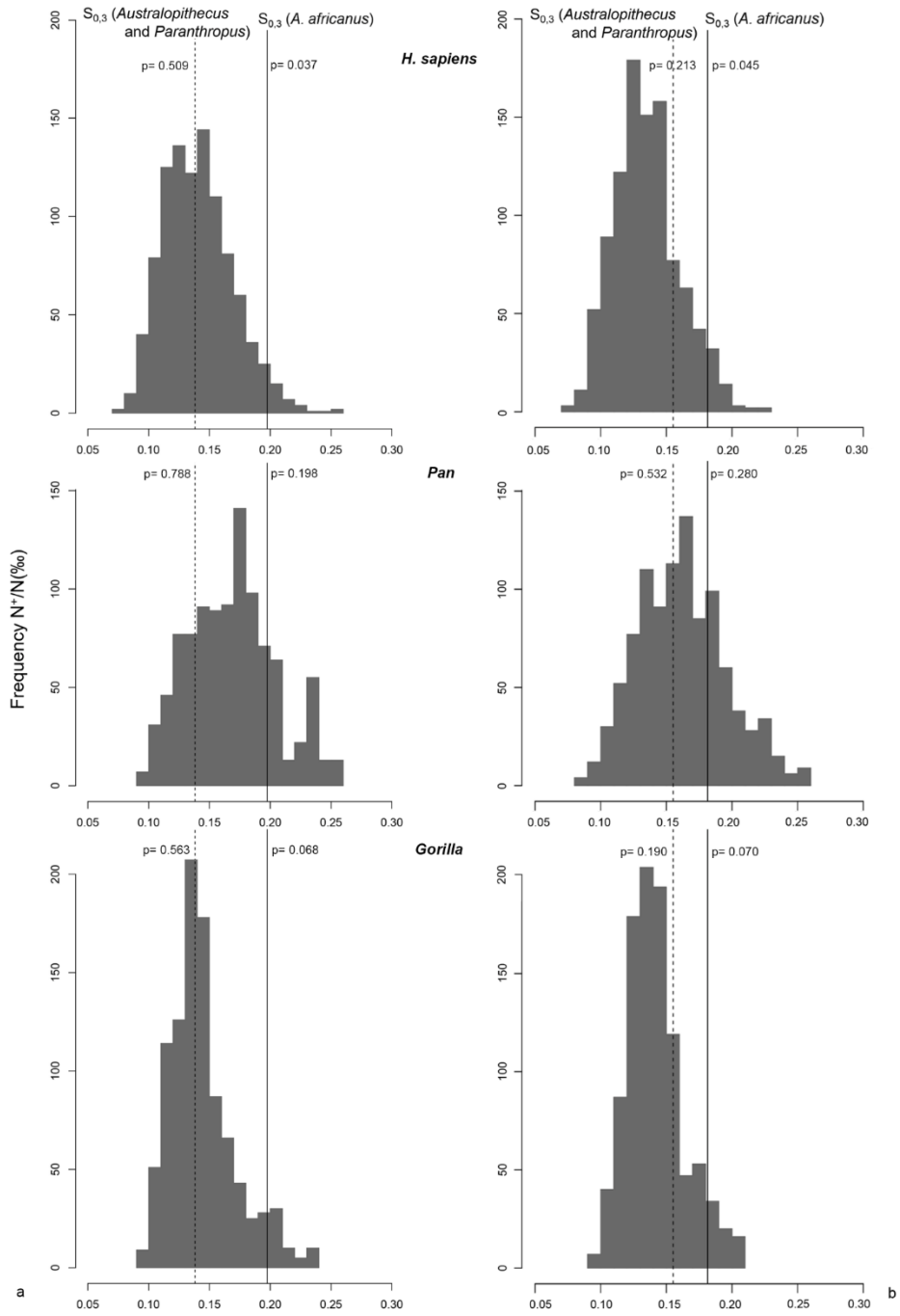

Fig. S3. Histograms of phenetic distances of *A. africanus* (black line) and combined A.L. 288-1, U.W. 88-98 and TM1517 (dashed line) with *H. sapiens*, *Pan* and *Gorilla* for both trochlea (a) and combined trochlea and medial malleolar (b).

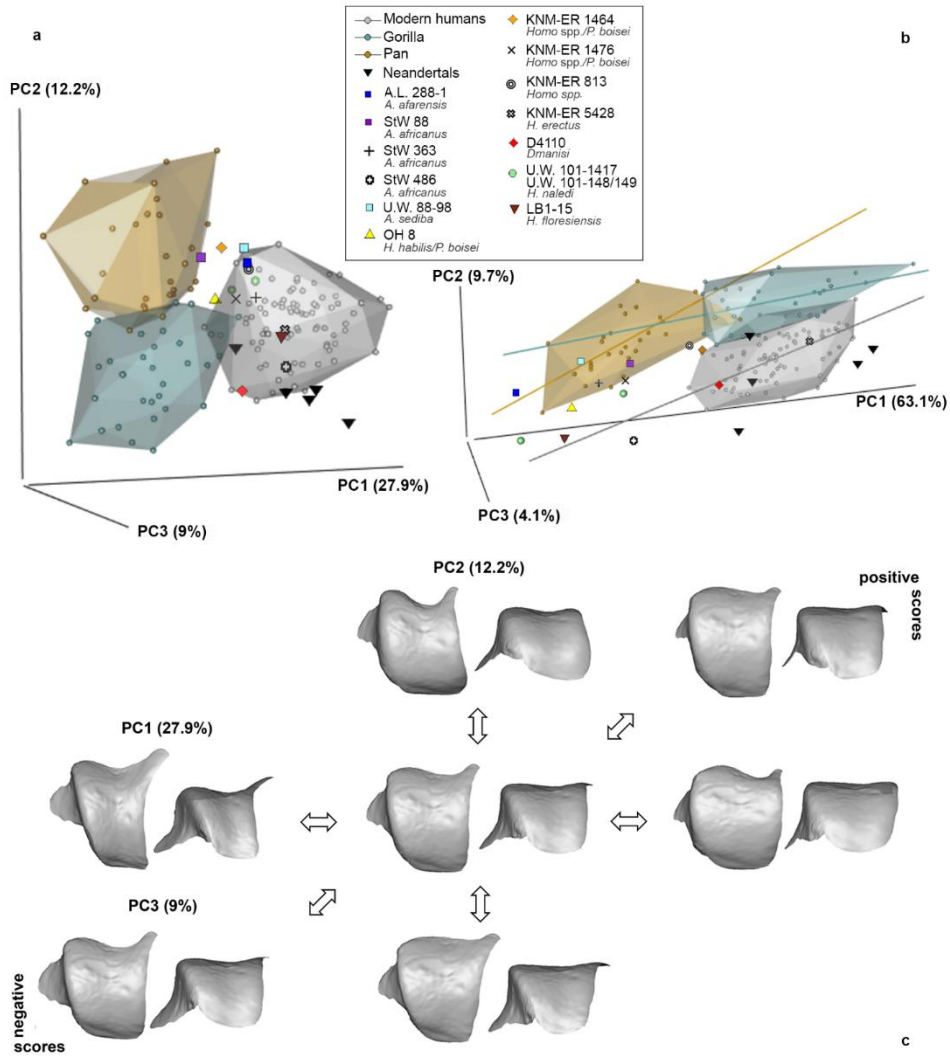

Fig. S4. Combined trochlea and lateral malleolar facet. PCA plot of the trochlea and lateral malleolar facet in shape space (a) and in form space (b). Below shape changes along the first three PC axes (c) in dorsal (left) and posterior (right) views.

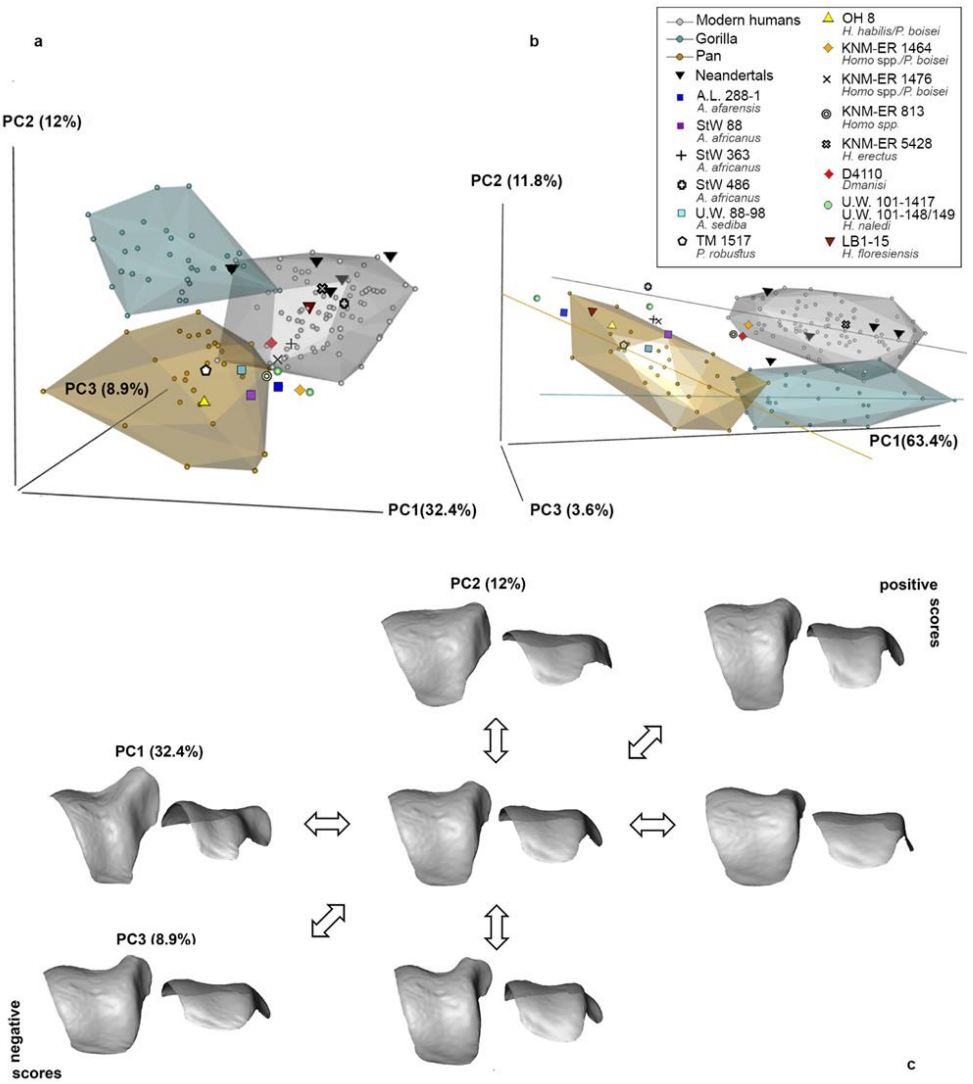

Fig. S5. Combined trochlea and medial malleolar facet. PCA plot of the trochlea and medial malleolar facet in shape space (a) and in form space (b). Below shape changes along the first three PC axes (c) in dorsal (left) and posterior (right) views.

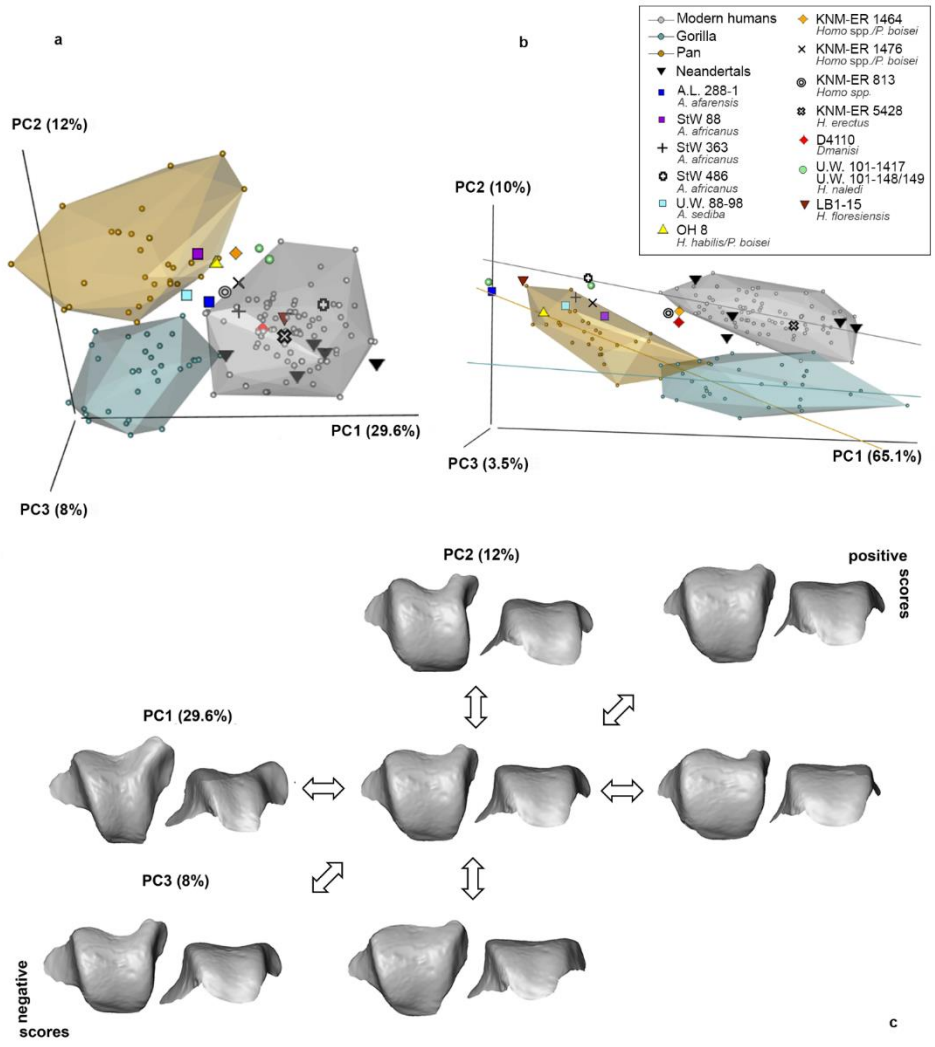

Fig. S6. Combined trochlea, medial and lateral malleolar facets. PCA plot of the trochlea, medial and lateral malleolar facets in shape space (a) and in form space (b). Below shape changes along the first three PC axes (c) in dorsal (left) and posterior (right) views.

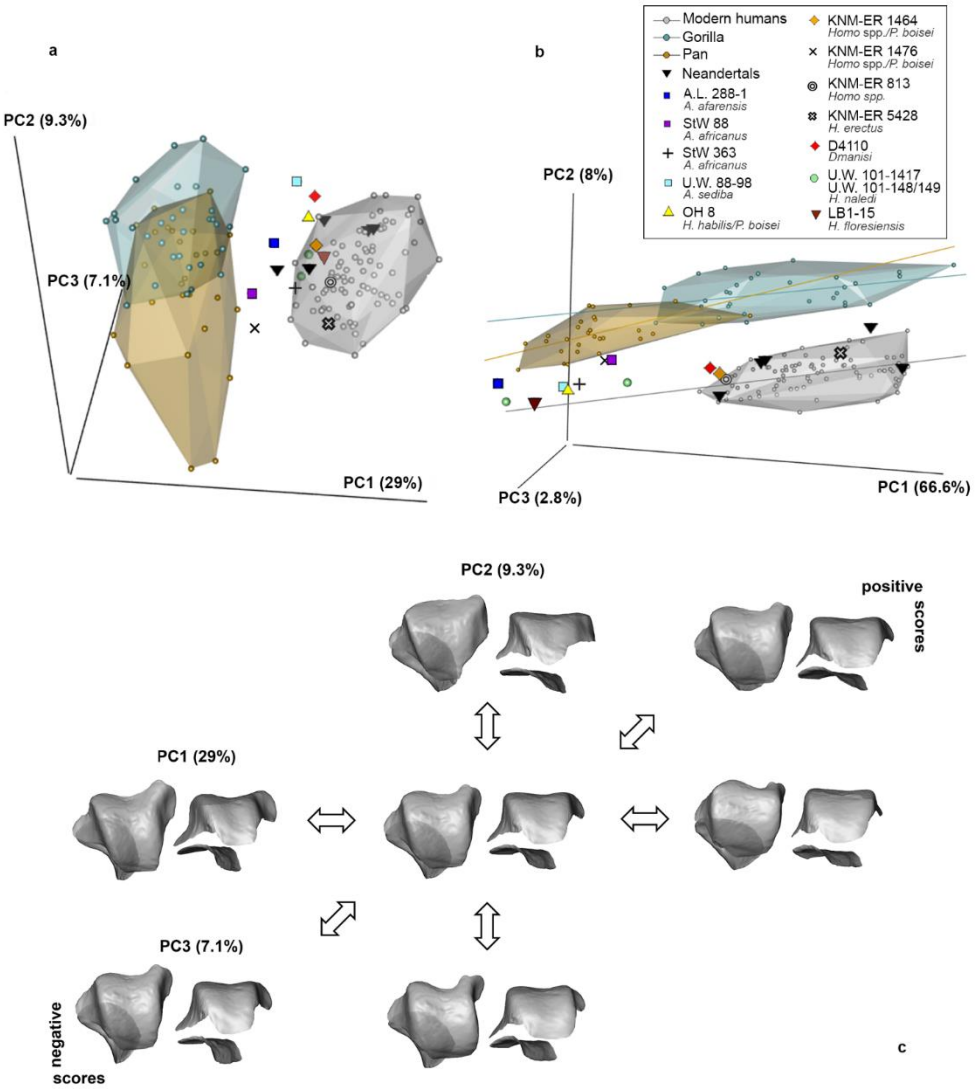

Fig. S7. Combined posterior calcaneal facet, trochlea, medial and lateral malleolar facets. PCA plot of the combined posterior calcaneal facet, trochlea, medial and lateral malleolar facets in shape space (a) and in form space (b). Below shape changes along the first three PC axes (c) in dorsal (left) and posterior (right) views.

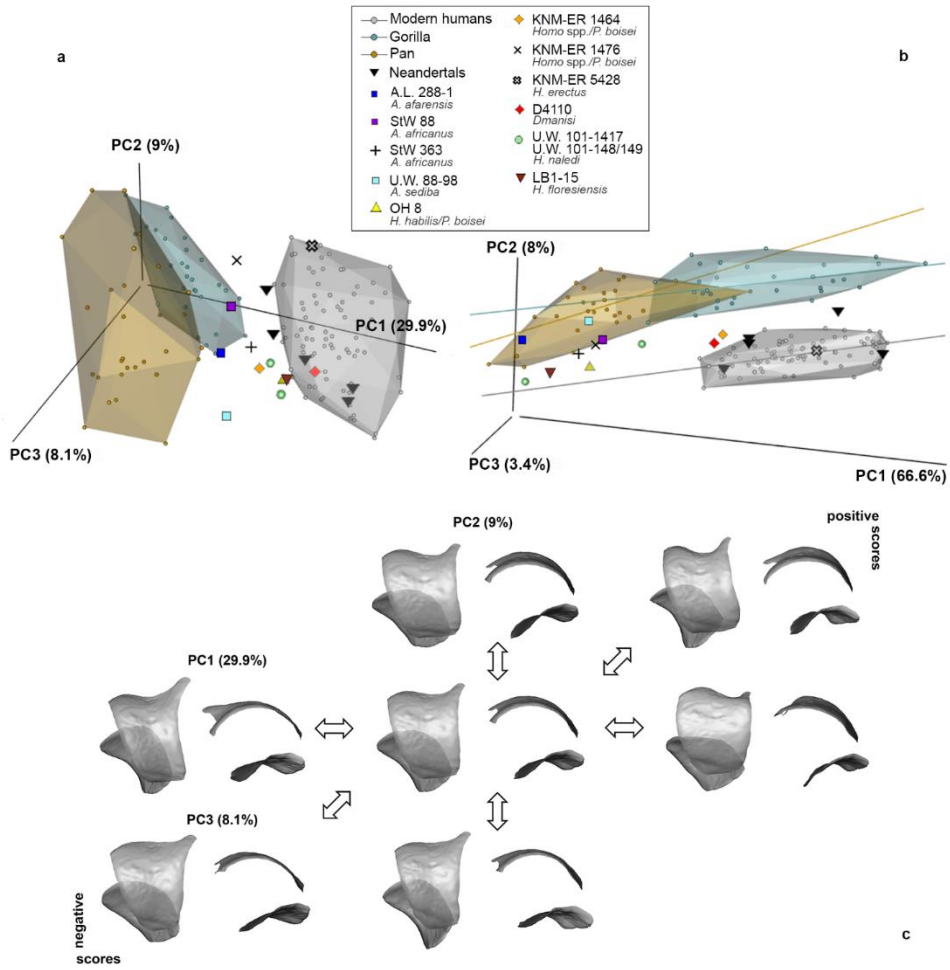

Fig. S8. Combined posterior calcaneal facet and trochlea. PCA plot of the combined posterior calcaneal facet and trochlea in shape space (a) and in form space (b). Below shape changes along the first three PC axes (c) in dorsal (left) and lateral (right) views.

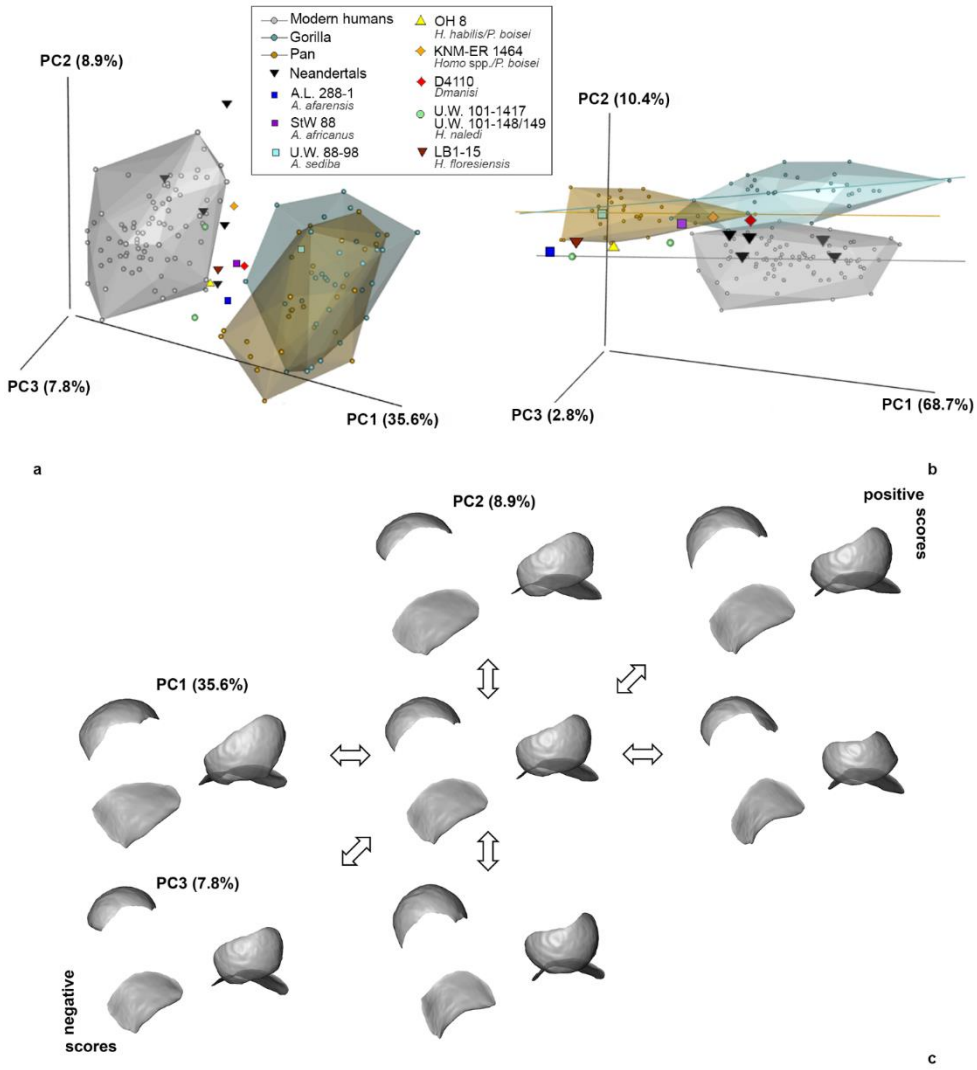

Fig. S9. Combined navicular and posterior calcaneus facets. PCA plot of the combined navicular and posterior calcaneus facets in shape space (a) and in form space (b). Below shape changes along the first three PC axes (c) in plantar (left) and frontal (right) views.

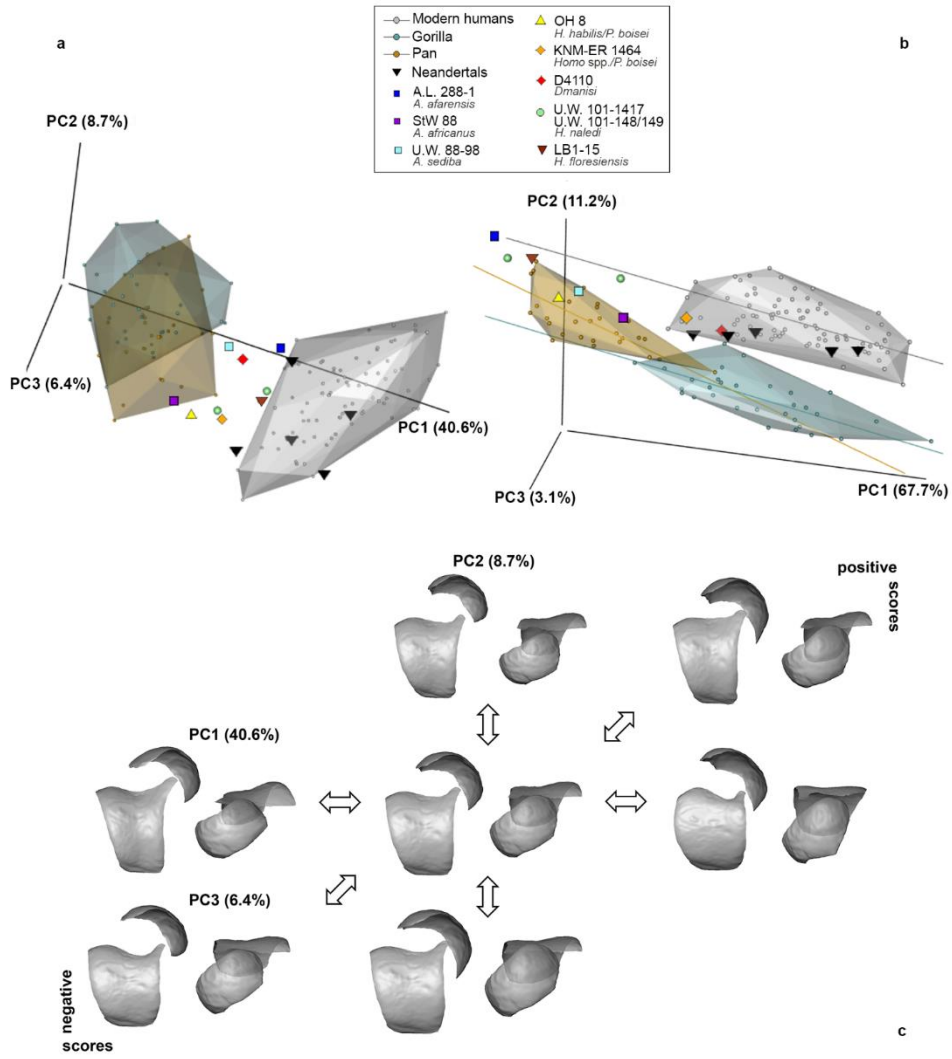

Fig. S10. Combined navicular facet and trochlea. PCA plot of the combined navicular facet and trochlea in shape space (a) and in form space (b). Below shape changes along the first three PC axes (c) in dorsal (left) and frontal (right) views.

Table S1. Extant sample.

Sample	Sample size	Collections[a]
H. sapiens		
UP-LSA[b]	5	DBP, NHMP
Medieval	3	DBC
Roccapelago	15	SAPAB
Norris Farms	5	ISM
Native Americans	8	PAHM
Bologna	39	BiGeA
Nguni	6	BiGeA
Gorilla		
Gorilla gorilla	31	NHM, PCM, UCL, NMNH, CMNH
Pan		
Pan troglodytes	29	NHM, PCM, UCL, NMNH, CMNH

[a]DBP, Department of Biology, University of Pisa, Pisa; NHMP, The Natural History Museum, Department of Earth Sciences, London; DBC, Department of Cultural Heritage, University of Bologna, Ravenna; SAPAB, Soprintendenza Archeologia, Belle Arti e Paesaggio per la città metropolitana di Bologna e le province di Modena, Ferrara e Reggio Emilia; ISM, Illinois State Museum, Springfield; PAHM, P. A. Hearst Museum Collections, University of California, Berkeley; BiGeA, Department of Biological, Geological and Environmental Sciences, University of Bologna, Bologna; NHM, Natural History Museum London, Mammals collection, London; PCM, Powell Cotton Museum, Birchington, Kent; UCL, Anthropology Department Napier Collection, University College London; NMNH, National Museum of Natural History, Smithsonian, Washington; CMNH, Cleveland Museum of Natural History, Cleveland.

[b]UP, Upper Paleolithic (Romito 7, Romito 8, Romito 9 and Veneri 2); LSA, Late Stone Age (Clark Howell Omo, Ethiopia).

Supplementary Table 2 | Fossil hominin sample.

Specimens	Taxon designation	Date	Main references for fossils listed
A.L. 288-1	*A. afarensis*	3.18 Ma	Prang, 2016(13); Boyer et al., 2015(18); Boyle & DeSilva, 2015(19); Harcourt-Smith, 2015(20); Prang, 2015(12); Parr et al., 2011(2); Zipfel et al., 2011(21); Pontzer et al., 2010(22); Jungers et al., 2009(23); DeSilva, 2008(24); Gebo & Schwartz, 2006(25); Harcourt-Smith, 2002(5); Latimer et al.,1987(26); Lamy, 1986(27), Stern & Susman, 1983(28).
StW 363	*A. africanus*	2.0-2.6 Ma	Harcourt-Smith, 2015(20); Boyle & DeSilva, 2015(19); Prang, 2015(12); Zipfel et al., 2011(21); DeSilva, 2008(24); Harcourt-Smith, 2002(5).
StW 486	*A. africanus*	2.0-2.6 Ma	Boyle & DeSilva, 2015(19); Zipfel et al., 2011(21); DeSilva, 2008(24).
StW 88	*A. africanus*	2.0-2.6 Ma	Prang, 2016(13); Boyle & DeSilva, 2015(19); Prang, 2015(12); Harcourt-Smith, 2015(20); Zipfel et al., 2011(21); Jungers et al., 2009(23); DeSilva, 2008(24); Harcourt-Smith, 2002(5).
U.W. 88-98	*A. sediba*	1.97 Ma	Prang, 2016(13); Boyle & DeSilva, 2015(19); Harcourt-Smith, 2015(20); Prang, 2015(12); DeSilva et al., 2013(29); Zipfel et al., 2011(21).
TM 1517	*P. robustus*	1.9 - 2.0 Ma	Prang, 2016(13); Boyle & DeSilva, 2015(19); Harcourt-Smith, 2015(20); Zipfel et al., 2011(21); DeSilva, 2008(24); Gebo & Schwartz, 2006(25); Harcourt-Smith, 2002(5).
OH 8	*H. habilis*/ *P. boisei?*	1.8 Ma	Prang, 2016(13); Boyer et al., 2015(18); Boyle & DeSilva, 2015(19); Harcourt-Smith, 2015(20); Prang, 2015(12); Parr et al., 2011(2); Zipfel et al., 2011(21); Pontzer et al., 2010(22); Jungers et al., 2009(23); DeSilva, 2008(24); Gebo & Schwartz, 2006(25); Harcourt-Smith, 2002(5); Lamy, 1986(27); Oxnard & Lisowski, 1980(30); Day & Wood, 1968(14); Day & Napier, 1964(31).
KNM-ER 1464	*Homo* spp./ *P. boisei?*	1.7 Ma	Prang, 2016(13); Boyer et al., 2015(18); Boyle & DeSilva, 2015(19); Harcourt-Smith, 2015(20); Prang, 2015(12); Su et al., 2013(32); Parr et al., 2011(2); Zipfel et al., 2011(21); Pontzer et al., 2010(22); Jungers et al., 2009(23); DeSilva, 2008(24); Gebo & Schwartz, 2006(25); Harcourt-Smith, 2002(5); Lamy, 1986(27).
KNM-ER 1476	*Homo* spp./ *P. boisei?*	1.88 Ma	Prang, 2016(13); Boyle & DeSilva, 2015(19); Harcourt-Smith, 2015(20); Parr et al., 2011(2); Zipfel et al., 2011(21); Pontzer et al., 2010(22); Jungers et al., 2009(23); DeSilva, 2008(24); Gebo & Schwartz, 2006(25); Harcourt-Smith, 2002(5); Lamy, 1986(27).
KNM-ER 813	*Homo* spp.	1.85 Ma	Prang, 2016(13); Boyer et al., 2015(18); Boyle & DeSilva, 2015(19); Prang, 2015(12); Harcourt-Smith, 2015(20); Zipfel et al., 2011(21); Pontzer et al., 2010(22); Jungers et al., 2009(23); DeSilva, 2008(24); Gebo & Schwartz, 2006(25); Harcourt-Smith, 2002(5); Lamy, 1986(27).
KNM-ER 5428	*H. erectus*	1.6 Ma	Prang, 2016(13); Boyle & DeSilva, 2015(19); Harcourt-Smith, 2015(20); Prang, 2015(12); Zipfel et al., 2011(21); DeSilva, 2008(24).
D4110 (Dmanisi)	*H. erectus*	1.77 Ma	Pontzer et al., 2010(22).
U.W. 101-148/149	*H. naledi*	236 - 335 Ka	Harcourt-Smith, 2015(20).
U.W. 101-1417	*H. naledi*	236 - 335 Ka	Harcourt-Smith, 2015(20).
LB1-15	*H. floresiensis*	60-100 Ka	Prang, 2016(13); Harcourt-Smith, 2015(20); Prang, 2015(12); Jungers et al., 2009(23),Sutikna et al., 2016(33).
Ferrassie 1	*H. neanderthalensis*	43 - 45 Ka	Boyle & DeSilva, 2015(19); Jungers et al., 2009(23); Trinkaus, 1983(34); Rhoads & Trinkaus, 1977(35).
Ferrassie 2	*H. neanderthalensis*	43 - 45 Ka	Boyle & DeSilva, 2015(19); Trinkaus, 1983(34); Rhoads & Trinkaus, 1977(35).
SP4B (Spy 2)	*H. neanderthalensis*	ca. 36 Ka	Parr et al., 2011(2); Trinkaus, 1983(34); Rhoads & Trinkaus, 1977(35).
EM 3519 (Tabun C1)	*H. neanderthalensis*	122±16 Ka	Boyle & DeSilva, 2015(19); Parr et al., 2011(2); Trinkaus, 1983(34). Rhoads & Trinkaus, 1977(35).
Krapina 235	*H. neanderthalensis*	130 Ka	Rhoads & Trinkaus, 1977(35).

Table S3. P-values for post hoc (ANOVA) comparisons of shape space scores of PCs (1-3) among extant taxa.

	PC1			PC2			PC3		
Variable	*H. sapiens*	*Pan*	*Gorilla*	*H. sapiens*	*Pan*	*Gorilla*	*H. sapiens*	*Pan*	*Gorilla*
Talus									
Homo sapiens	x	0.000*	0.000*	x	0.000*	0.000*	x	0.02*	0.937
Pan		x	0.162		x	0.000*		x	0.117
Gorilla			x			x			x
Navicular facet									
Homo sapiens	x	0.000*	0.000*	x	0.089	0.828	x	0.000*	0.621
Pan		x	0.982		x	0.065		x	0.000*
Gorilla			x			x			x
Trochlea									
Homo sapiens	x	0.000*	0.000*	x	0.000*	0.000*	x	0.003*	0.034*
Pan		x	0.590		x	0.000*		x	0.000*
Gorilla			x			x			x
Posterior calcaneal facet									
Homo sapiens	x	0.000*	0.000*	x	0.004*	0.996	x	0.000*	0.000*
Pan		x	0.901		x	0.000*		x	0.000*
Gorilla			x			x			x
Anterior-medial calcaneal facet									
Homo sapiens	x	0.000*	0.197	x	0.000*	0.000*	x	0.018*	0.984
Pan		x	0.001*		x	0.664		x	0.080
Gorilla			x			x			x
Medial malleolar facet									
Homo sapiens	x	0.000*	0.000*	x	0.000*	0.983	x	0.000*	0.225
Pan		x	0.000*		x	0.000*		x	0.000*
Gorilla			x			x			x
Lateral malleolar facet									
Homo sapiens	x	0.000*	0.000*	x	0.000*	0.000*	x	0.347	0.050
Pan		x	0.573		x	0.992		x	0.006*
Gorilla			x			x			x
Trochlea and navicular facet									
Homo sapiens	x	0.000*	0.000*	x	0.340	0.087	x	0.570	0.520
Pan		x	0.199		x	0.011*		x	0.998
Gorilla			x			x			x
Posterior calcaneal and navicular facets									
Homo sapiens	x	0.000*	0.000*	x	0.000*	0.791	x	0.386	0.962
Pan		x	0.026*		x	0.019*		x	0.648
Gorilla			x			x			x
Trochlea and posterior calcaneal facet									
Homo sapiens	x	0.000*	0.000*	x	0.707	0.748	x	0.000*	0.000*
Pan		x	0.161		x	0.997		x	0.000*
Gorilla			x			x			x
Trochlea, posterior calcaneal and navicular facets									
Homo sapiens	x	0.000*	0.000*	x	0.008*	0.025*	x	0.000*	0.432
Pan		x	79,000		x	0.000*		x	0.000*
Gorilla			x			x			x
Trochlea and medial malleolar facet									
Homo sapiens	x	0.000*	0.000*	x	0.000*	0.000*	x	0.516	0.111
Pan		x	0.227		x	0.000*		x	0.029*
Gorilla			x			x			x
Trochlea and lateral malleolar facet									
Homo sapiens	x	0.000*	0.000*	x	0.000*	0.000*	x	0.188	0.533
Pan		x	0.929		x	0.000*		x	0.823
Gorilla			x			x			x
Trochlea, medial and lateral malleolar facets									
Homo sapiens	x	0.000*	0.000*	x	0.000*	0.000*	x	0.118	0.788
Pan		x	0.180		x	0.000*		x	0.497
Gorilla			x			x			x
Trochlea, posterior calcaneal, medial and lateral malleolar facets									
Homo sapiens	x	0.000*	0.000*	x	0.000*	0.000*	x	0.032*	0.169
Pan		x	0.686		x	0.000*		x	0.045*
Gorilla			x			x			x

*Significant P-value ($P < 0.05$).

Table S4. Number and percentages of estimated (semi)landmarks for singular and combined facets[a].

Specimens	Shape[b]	NF	AMCF	TF	PCF	MMF	LMF	TF-NF	PCF-NF	PCF-TF	TF-PCF-NF	TF-LMF	TF-MMF	TF-LMF-MMF	TF-PCF-LMF-MMF
A.L. 288-1	0	0	0	0	0	0	0	0	0	0	0	0	0	0	0
StW 363	-	-	-	5 (10.4%)	11 (26.2%)	0	8 (24.2%)	-	-	16 (17.8%)	-	13 (18.1%)	5 (8.3%)	13 (15.5%)	24 (19%)
StW 486	-	-	-	15 (31.3%)	-	4 (19%)	0	-	-	-	-	13 (18.1%)	17 (28.3%)	17 (28.3%)	-
StW 88	22 (8.8%)	13 (31.7%)	3 (13%)	0	0	0	0	13 (14.6%)	13 (15.7%)	0	13 (9.9%)	0	0	0	0
U.W. 88-98	0	0	0	0	0	0	0	0	0	0	0	0	0	0	0
TM 1517	-	-	-	14 (29.2%)	-	0	-	-	-	-	-	-	14 (23.3%)	-	-
OH 8	29 (11.6%)	0	0	0	14 (33.3%)	0	2 (6.1%)	0	14 (16.9%)	14 (15.6%)	14 (10.7%)	2 (2.8%)	0	2 (2.4%)	16 (12.7%)
KNM-ER 813	-	-	-	7 (14.6%)	14 (33.3)	0	7 (21.2%)	-	-	21 (23.3%)	-	14 (9.4%)	7 (11.7%)	14 (16.7%)	28 (22.2%)
KNM-ER 1464	0	0	0	0	0	0	0	0	0	0	0	0	0	0	0
KNM-ER 1476	-	-	-	0	0	0	0	-	-	0	-	0	0	0	0
D4110	13 (5.2%)	4 (9.8)	3 (13%)	0	2 (4.8%)	0	0	4 (4.5%)	4 (4.9%)	0	4 (3.1%)	0	0	0	0
KNM-ER 5428	-	-	-	10 (20.8%)	15 (35.7%)	1 (4.8%)	3 (9.1%)	-	-	10 (11.1%)	-	13 (18.1%)	11 (18.3%)	14 (16.7%)	14 (11.1%)
U.W. 101-148/149	26 (10.4%)	7 (17.1%)	0	1 (2.1%)	4 (9.5%)	0	0	8 (9%)	11 (13.3%)	5 (5.6%)	12 (9.2%)	1 (1.4%)	1 (1.7%)	1 (1.2%)	5 (4%)
U.W. 101-1417	18 (7.2%)	6 (14.6%)	3 (13%)	1 (2.1%)	0	0	0	7 (7.9%)	6 (7.2%)	1 (1.1%)	7 (5.3%)	1 (1.4%)	1 (1.7%)	1 (1.2%)	1 (0.8%)
LB1-15	8 (3.2)	7 (17.1%)	1 (4.3%)	0	0	0	0	7 (7.9%)	7 (8.4%)	0	7 (5.3%)	0	0	0	0
Ferrassie 1	0	0	0	0	0	0	0	0	0	0	0	0	0	0	0
Ferrassie 2	0	0	0	0	0	0	0	0	0	0	0	0	0	0	0
SP4B	0	0	0	0	0	0	0	0	0	0	0	0	0	0	0
EM 3519	0	0	0	0	0	0	0	0	0	0	0	0	0	0	0
Krapina 235	21 (8.4)	1 (2.4%)	0	4 (8.3%)	0	0	4 (12.1%)	5 (%.6%)	1 (1.2%)	4 (4.4%)	5 (3.8%)	8 (11.1%)	4 (6.7%)	8 (9.5%)	8 (6.4%)

[a]List of acronyms used: NF, navicular facet; AMCF, anterior and medial calcaneal facets; TF, trochlea facet; PCF, posterior calcaneal facet; MML, medial malleolar facet; LMF, lateral malleolar facet; TF-NF, combined trochlea and navicular facets; PCF-NF, combined posterior calcaneal facet and navicular facets; PCF-TF, combined posterior calcaneal facet and trochlea facets; TF-PCF-NF, combined trochlea, posterior calcaneal and navicular facets; TF-LMF, combined trochlea and lateral malleolar facets; TF-MMF, combined trochlea and medial malleolar facets; TF-LMF-MMF, combined trochlea, lateral and medial malleolar facets; TF-PCF-LMF-MMF, combined trochlea, posterior calcaneal, lateral and medial malleolar facets.

Supplementary references

1. Clarke RJ (2013) "*Australopithecus* from Sterkfontein Caves, South Africa" in *The Paleobiology of Australopithecus. Vertebrate Paleobiology and Paleoanthropology*, Reed K, Fleagle J, Leakey R, Eds. (Springer, Dordrecht), pp 105–123.

2. Parr WCH, Chatterjee HJ, Soligo C (2011) Inter- and intra-specific scaling of articular surface areas in the hominoid talus. *J Anat* 218:386–401.

3. Parr WCH, et al. (2014) Three-dimensional shape variation of talar surface morphology in hominoid primates. *J Anat* 225:42–59.

4. Frelat MA, et al. (2017) Evolution of the hominin knee and ankle. *J Hum Evol* 108:147–160.

5. Harcourt-Smith WEH (2002) Form and function in the hominoid tarsal skeleton. Dissertation (University of London).

6. Harcourt-Smith WEH, Aiello LC (2004) Fossils, feet and the evolution of human bipedal locomotion. *J Anat* 204:403–416.

7. Turley K, Frost SR (2013) The shape and presentation of the Catarrhine talus: a geometric morphometric analysis. *Anat Rec* 296:877–890.

8. Finestone EM, Brown MH, Ross SR, Pontzer H (2018) Great ape walking kinematics: Implications for hominoid evolution. *Am J Phys Anthropol* 166:43–55.

9. O'Neill MC, et al. (2015) Three-dimensional kinematics of the pelvis and hind limbs in chimpanzee (*Pan troglodytes*) and human bipedal walking. *J Hum Evol* 86:32–42.

10. Aiello LC, Dean C (1990) *An introduction to human evolutionary anatomy* (Academic Press).

11. Antón SC, Potts R, Aiello LC (2014) Evolution of early *Homo*: An integrated biological perspective. *Science* 345: 1236828-1–1236828-13.

12. Prang TC (2015) Rearfoot posture of *Australopithecus sediba* and the evolution of the hominin longitudinal arch. *Sci Rep* 5: 17677.

13. Prang TC (2016) The subtalar joint complex of *Australopithecus sediba*. *J Hum Evol* 90:105–119

14. Day MH, Wood BA (1968) Functional affinities of the Olduvai hominid 8 talus. *Man* 3:440–455.

15. Kidd R (1999) Evolution of the rearfoot. A model of adaptation with evidence from the fossil record. *J Am Podiatr Med Assoc* 89:1–17.

16. DeSilva JM (2010) Revisiting the "midtarsal break". *Am J Phys Anthropol* 141:245–258.

17. Kidd RS, O'Higgins P, Oxnard CE (1996) The OH8 foot: a reappraisal of the functional morphology of the hindfoot utilizing a multivariate analysis. *J Hum Evol* 31: 269-291.

18. Boyer DM, Yapuncich GS, Butler JE, Dunn RH, Seiffert ER (2015) Evolution of postural diversity in primates as reflected by the size and shape of the medial tibial facet of the talus. *Am J Phys Anthropol* 157:134-177.

19. Boyle EK, DeSilva JM (2015) A large *Homo erectus* talus from Koobi Fora, Kenya (KNM-ER 5428), and Pleistocene hominin talar evolution. *PaleoAnthropology* 2015:1–13.

20. Harcourt-Smith WHE, et al. (2015) The foot of *Homo naledi*. *Nat Commun* 6:1–8.

21. Zipfel B, et al. (2011) The foot and ankle of *Australopithecus sediba*. *Science* 333:1417–1420.

22. Pontzer H, et al. (2010) Locomotor anatomy and biomechanics of the Dmanisi hominins. *J Hum Evol* 58:492–504.

23. Jungers WL, et al. (2009) The foot of *Homo floresiensis*. *Nature* 459:81–84.

24. DeSilva JM (2008) Vertical climbing adaptations in the Anthropoid ankle and midfoot: implications for locomotion in Miocene Catarrhines and Plio-Pleistocene hominins. Dissertation (The University of Michigan).

25. Gebo DL, Schwartz GT (2006) Foot bones from Omo: implications for hominid evolution. *Am J Phys Anthropol* 129:499–511.

26. Latimer B, Ohman JC, Lovejoy CO (1987) Talocrural joint in African hominoids: Implications for *Australopithecus afarensis*. *Am*

J Phys Anthropol 74:155–175.

27. Lamy P (1986) The settlement of the longitudinal plantar arch of some African Plio-Pleistocene hominids: a morphological study. *J Hum Evol* 15:31–46.

28. Stern JT, Susman RL (1983) The locomotor anatomy of *Australopithecus afarensis*. *Am J Phys Anthropol* 60:279–317.

29. DeSilva JM, et al. (2013) The lower limb and mechanics of walking in A*ustralopithecus sediba*. *Science* 340:1232999.

30. Oxnard CE, Lisowski FP (1980) Functional articulation of some hominoid foot bones: implications for the Olduvai (Hominid 8) foot. *Am J Phys Anthropol* 117:107–117.

31. Day MH, Napier JR (1964) Hominid fossils from Bed I, Olduvai Gorge, Tanganyika: Fossil foot bones. *Nature* 201:970.

32. Su A, Wallace IJ, Nakatsukasa M (2013) Trabecular bone anisotropy and orientation in an Early Pleistocene hominin talus from East Turkana, Kenya. *J Hum Evol* 64:667–677.

33. Sutikna T, et al. (2016) Revised stratigraphy and chronology for *Homo floresiensis* at Liang Bua in Indonesia. *Nature* 532:366–369.

34. Trinkaus E (1983) Functional aspects of Neandertal pedal remains. *Foot Ankle* 3:377–390.

35. Rhoads JG, Trinkaus E (1977) Morphometrics of the Neandertal talus. *Am J Phys Anthropol* 46:29–43.

Chapter 3

3.1 Conclusions

In this thesis, talar shape and form variation of extinct and extant hominids has been investigated by means of geometric morphometric (GM) methods. The goals were three-folds: first, to explore sexual dimorphism in modern human tali; second, to assess morphological differences between groups of modern humans with different subsistence, mobility, and footwear use; third, to compare fossil hominins with extant hominid taxa (*Pan*, *Gorilla*, *Homo sapiens*).

In the Paper I, we investigate the role of shape, form and size in discriminating biological sex based on geometric morphometric analysis of the talus. Three modern human populations from the early 20th century (Sassari, Bologna, New York) and from different geographical locations (Italy and USA) were analyzed. We followed two different approaches, i.e., 1) considering the populations as a unique sample and exploring sex-related interpopulation trajectories and 2) focusing on each individual population to assess the discriminatory power of the talus for sex determination. Furthermore, a talus from the Bologna sample was selected to run a virtual resection, followed by two digital reconstructions based on the mean shape of both the pooled sample and the Bologna sample, respectively. The virtual reconstruction allows to use the damaged talus for sex determination.

When considering the pooled early 20th century sample, the amount of sexual dimorphism differs significantly among populations. Indeed, permutation test returns significant different sexual trajectories ($P<0.05$) between Sassari and Bologna, as well as between New York and Bologna in both shape and form space, while this is not the case between Sassari and New York. This result suggests to favor a specific population approach to evaluate sexual dimorphism in modern human tali.

Using specific population approach for sex assessment, our results show that there are no significant differences in shape related to sexual dimorphism, while form space variables and centroid size (CS) account for significant differences ($P<0.001$) between the sexes. Correct individual assignment to their gender is more accurate using form variables (78.2%-97.2%) and CS (73.9% - 94.42%), contra shape variables (82.6% - 83.3%) for each population. New York sample gives the lowest accuracy.

Finally, in this contribution we emphasize the opportunity offered by (semi)landmark-based methods when dealing with fragmentary tali, which are usually discarded from traditional analysis. We digitally simulated a trivial condition that hampers the collection of fundamental linear

measurement (e.g., length and width of the talus, length and breadth of the trochlea, length and breadth of the posterior articular surface for the calcaneus), and we carried out two digital reconstructions based on the mean of both the pooled sample and the Bologna sample. Both virtual reconstructions are very similar and allow to correctly classify the sex of the individual with a P_{post} between 99.9% and 100% using form space PCs and CS.

Overall, our extensive morphometric study of the talus aims to assess the most accurate approach for sex discrimination of isolated tali, ultimately providing useful tools for forensic and bioarchaeological investigations.

In the Paper II, we apply (semi)landmark-based methods and whole-bone trabecular analysis to the tali of modern human populations with different subsistence economies, lifestyles and footwear use to explore how cultural and environmental factors influence the external shape and internal trabecular structure.

Our results show distinct differences in shape and structure between highly mobile hunter-gatherers and more sedentary groups belonging to a mixed post-agricultural/industrial background. Hunter-gatherers have a more "flexible" talar shape with high bone volume fraction, which we interpret as long-distance walking strictly barefoot along uneven ground. The talus of post-industrial population exhibits a "rigid" profile with low bone volume fraction, as consequence of sedentary lifestyle and stiff shoes use.

This results are in line with the observed progressive gracilization of lower limb in recent Holocene modern humans as consequence of decrease daily activities (e.g., Parr et al., 2011; Chirchir et al., 2015). In addition to distance travelled, talar robusticity in hunter-gatherers may also reflect adaptation to uneven terrain which increases mediolateral movement of the ankle to reach the stability (Carlson et al., 2007). Individuals walking in modern substrate, such as asphalt, reduce the search for stability of the foot to adhere to the ground. Furthermore, wearing shoes may lead a loss of mobility in the talar articulations of sedentary group. The use of heavy leather shoes and boots may reduce dorsal and plantar flexion, as well as eversion and inversion excursion, by blocking the region around the ankle and decreasing the space in which the foot can move (remaining constricted by the shoe).

Ultimately, these results highlight the critical functional role that talus plays in facilitating mobility, with variation in external shape and internal trabecular structure showing how it adapts to variation in locomotion. Here

we show evidence that human talar shape and internal bone structure varies as a result of the loading differences that exist in relation to footwear use and terrain (i.e., highly mobile barefoot/minimal covering vs. sedentary stiff footwear). These results are relevant to interpretations of the fossil record and may be useful in inferring the ranges of joint movements (arthrokinematics), mobility patterns, and the behavior of extinct hominin taxa.

In the Paper III, we analyze the talar configuration from an evolutionary point of view. Morphological variability of extinct and extant hominid tali has been investigated using a 3D geometric morphometric approach. Beside the whole talus, individual and combined talar facets are analyzed to determine the evolutionary timing and emergence of human-like features associated with bipedal locomotion.

Results obtained for the whole talus are consistent with those of previous studies (Harcourt-Smith, 2002; Jungers et al., 2009; Turley and Frost, 2013; Parr et al., 2014; Harcourt-Smith et al., 2015) showing that differences in talar shape among hominids are due to different locomotor behaviors (bipedalism *versus* knuckle-walking and climbing). No fossil hominins fall within the ape range, suggesting that all extinct hominins, to some degree, were bipedal. However, we cannot assume that fossil hominins are like humans. They fall in their own area in shape space likely reflects their own unique combination of locomotor modes than either humans or apes (e.g. more terrestrial than apes), particularly habitual ones, or specifically their morphological solutions to their unique behavioral repertoires.

The analysis of individual facets reveals different levels in distinguishing bipeds *versus* knuckle-walkers. The navicular facet best discriminates between humans and African apes. This facet is a key element for enhancing stability of the midtarsal region (Aiello and Dean, 1990; Harcourt-Smith, 2002; Turley and Frost, 2013; Parr et al., 2014; Harcourt-Smith et al., 2015) as decreasing curvature of the navicular facet represents a derived feature of human toe-off (Lamy, 1986; Aiello and Dean, 1990; DeSilva, 2010; Prang, 2016). Most fossil hominins show modern human-like navicular morphology, including *A. afarensis*. This suggests that *A. afarensis* could have achieved a stable midtarsal region, while *Australopithecus africanus* and *A. sediba* retain a navicular facet morphology closer to great apes (DeSilva and Throckmorton, 2010; Raichlen et al., 2010; Ward et al., 2011; Parr et al., 2014; Prang, 2015, 2016).

The lateral malleolar facet also seems to effectively discriminate hominins from African apes (Desilva, 2009; Turley and Frost, 2013). High

concavity and greater lateral projection of the lateral malleolar facet in apes is usually interpreted as facilitating greater dorsiflexion and inversion of the ankle joint in arboreal environments (Harcourt-Smith, 2002). Hominins lack these morphological characteristics as consequence of decreasing arboreality.

When combining articular surfaces, the combined trochlea, navicular and posterior calcaneal facets perform the best, with a net separation between australopiths (close to ape range) and *Homo* (close to human range). In humans, the trochlea is dorsally elevated with respect to the posterior calcaneal facet, resulting in a taller talar corpus, while the talar head is plantarly oriented. Following Prang (2015), the relative configuration of these talar facets might be a proxy for inferring the presence of a medial longitudinal arch, which is absent in great apes while it is a derived feature of the human foot (Aiello and Dean, 1990). Since australopiths are more similar to apes in this regard, our results suggest that the medial longitudinal arch could be absent or extremely reduced in all australopith taxa (contra Stern and Susman, 1983; Lamy, 1986; Raichlen et al., 2010; Ward et al., 2011; Prang, 2015), implying it is a derived feature that only characterizes the genus *Homo* (Harcourt-Smith, 2002; Gebo and Schwartz, 2006; DeSilva and Throckmorton, 2010; Pontzer et al., 2010; Harcourt-Smith et al., 2015; Prang, 2015) and completely reaches its modern human-like state only in *H. sapiens* and Neandertals (Day and Wood, 1968)

This study provides a more comprehensive understanding of bipedal locomotor adaptations in the hominin foot, as evident in the talus, and thus sheds light on one of the evolutionary steps that strictly defined modern humans. Joints, such as those implicated by the lateral malleolar and navicular facets, seem to evolve towards a modern human-like form (i.e., structured for bipedal efficiency) earlier than others. The combined trochlea, navicular and posterior calcaneal facets, instead, reflect a gradual expression of the longitudinal arch from australopiths to *Homo*, marking the transition from facultative to obligate bipedalism.

Overall, our results offer an evolutionary model for the insurgence of bipedalism and the transition from facultative to obligate bipedalism.

In conclusion, this thesis shows the effectiveness of (semi)landmark-based methods which applied to the hominid talus aims to address broad questions about variation related to human evolution, physiology, behavior and culture.

References

Adams DC, Rohlf FJ, Slice DE. 2004. Geometric morphometrics: Ten years of progress following the 'revolution'. Ital J Zool 71:5–16.

Aiello LC, Dean C. 1990. An introduction to human evolutionary anatomy. Academic Press.

Anselmi S. 1995. Contadini marchigiani del primo Ottocento: Un'inchiesta del Regno Italico (Sapere Nuovo Senigallia).

Antón SC, Potts R, Aiello LC. 2014. Evolution of early Homo: An integrated biological perspective. Science 345:1236828.

Baab KL, Mcnulty KP, Rohlf FJ. 2012. The shape of human evolution: A geometric morphometrics perspective. Evol Anthropol 21:151–165.

Belcastro MG, Bonfiglioli B, Pedrosi ME, Zuppello M, Tanganelli V, Mariotti V. 2017. The History and Composition of the Identified Human Skeletal Collection of the Certosa Cemetery (Bologna, Italy, 19th–20th Century). Int J Osteoarchaeol 27:912–925.

Benazzi S, Bookstein FL, Strait DS, Weber GW. 2011. A new OH5 reconstruction with an assessment of its uncertainty. J Hum Evol 61: 75-88.

Bonnefoy-Mazure A, Armand S. 2015. Normal gait. In: Canavese F, Deslandes J, editors. Orthopedic Management of Children with Cerebral Palsy, Nova Science Publishers, p 199–214.

Bookstein FL. 1991. Morphometric tools for landmark data: geometry and biology, Cambridge University Press.

Bramble DM, Lieberman DE. 2004. Endurance running and the evolution of Homo. Nature 432:345–352.

Brunet M. 2002. Reply to Wolpoff, Senut, Pickford and Hawks. Nature 419:582.

Carlson KJ, Grine FE, Pearson OM. 2007. Robusticity and sexual dimorphism in the postcranium of modern hunter-gatherers from Australia. Am J Phys Anthropol 134:9–23.

Chirchir H, Kivell TL, Ruff CB, Hublin J, Carlson KJ, Zipfel B. 2015. Recent origin of low trabecular bone density in modern humans. Proc Natl Acad Sci USA 112:366-371.

Christie PW, Ridley JN. 1989. Mathematical analysis of articular surfaces: application to the anatomy of early Hominid ankle joint. In: Giacobini G, editor. Hominidae: Actes Du 2ème Congrès International de Paléontologie Humaine, Turin, 28 Septembre-3 Octobre 1987. Editoriale Jaca Book, p 61-65

Crompton RH. 2016. The hominins: A very conservative tribe? Last

common ancestors, plasticity and ecomorphology in Hominidae. Or, What's in a name? J Anat 228:686–699.
Day MH, Wood BA. 1968. Functional Affinities of the Olduvai Hominid 8 Talus. Man 3:440–455.
DeSilva JM. 2009. Functional morphology of the ankle and the likelihood of climbing in early hominins. Proc Natl Acad Sci USA 106:6567-6572.
DeSilva JM. 2010. Revisiting the "Midtarsal Break ". Am J Phys Anthropol 141:245–258.
DeSilva JM, Throckmorton ZJ. 2010. Lucy' s Flat Feet : The Relationship between the ankle and rearfoot arching in early hominins. PLoS One, 5:e14432.
Drapeau MSM, Harmon EH. 2013. Metatarsal torsion in monkeys, apes, humans and australopiths. J Hum Evol 64:93–108.
Dumond DE. 2011. Archaeology on the Alaska Peninsula: The Northern Section: Fifty Years Onward. Museum of Natural and Cultural History and Department of Anthropology, University of Oregon.
Gebo DL, Schwartz GT. 2006. Foot bones from Omo: Implications for hominid evolution. Am J Phys Anthropol 129:499–511.
Geib PR. 2000. Sandal types and Archaic prehistory on the Colorado Plateau. Am Antiq 65:509–524.
Gentili AM. 1995. Il leone e il cacciatore. Storia dell'Africa sub-sahariana. Roma: Carocci.
Griffin NL, Miller CE, Schmitt D, Ao KD. 2015. Understanding the evolution of the windlass mechanism of the human foot from comparative anatomy: Insights, obstacles, and future directions. Am J Phys Anthropol 156:1–10.
Gunz P, Mitteroecker P. 2013. Semilandmarks: A method for quantifying curves and surfaces. Hystrix 24:103–109.
Gunz P, Mitteroecker P, Bookstein FL. 2005. Semilandmarks in three dimensions. In: Modern morphometrics in physical anthropology. Springer. p 73–98.
Haeusler M, McHenry HM. 2004. Body proportions of Homo habilis reviewed. J Hum Evol 46:433–465.
Haile-Selassie Y. 2001. Late Miocene hominids from the Midle Awash, Ethiopia. Nature 412:178-181.
Haile-Selassie Y, Saylor BZ, Deino A, Levin NE, Alene M, Latimer BM. 2012. A new hominin foot from Ethiopia shows multiple Pliocene bipedal adaptations. Nature 483:565–569.
Harcourt-Smith WEH. 2002. Form and function in the hominoid tarsal skeleton. PhD Thesis. University of London.
Harcourt-Smith WEH. 2016. Early hominin diversity and the emergence of

the genus Homo. J Anthropol Sci 94:19–27.

Harcourt-Smith WEH, Aiello LC. 2004. Fossils, feet and the evolution of human bipedal locomotion. J Anat 204:403–416.

Harcourt-Smith WHE. 2010. The First Hominins and the Origins of Bipedalism. Evol Educ Outreach 3:333–340.

Harcourt-Smith WHE, Throckmorton Z, Congdon KA, Zipfel B, Deane AS, Drapeau MSM, Churchill SE, Berger LR, Desilva JM. 2015. The foot of Homo naledi. Nat Commun 6:1–8.

Harmand S, Lewis JE, Feibel CS, Lepre CJ, Prat S, Lenoble A, Boës X, Quinn RL, Brenet M, Arroyo A, Taylor N, Clément S, Daver G, Brugal JP, Leakey L, Mortlock RA, Wright JD, Lokorodi S, Kirwa C, Kent D V., Roche H. 2015. 3.3-million-year-old stone tools from Lomekwi 3, West Turkana, Kenya. Nature 521:310–315.

Hens SM, Rastelli E, Belcastro G. 2008. Age estimation from the human os coxa: A test on a documented Italian collection. J Forensic Sci 53:1040–1043.

O'Higgins P. 2000. The study of morphological variation in the hominid fossil record : biology , landmarks and geometry. 197:103–120.

Huson A. 1991. Functional anatomy of the foot. Disord foot ankle 1:409–431.

Ingold T. 2004. Culture on the ground: The world perceived through the feet. J Mater Cult 9:315–340.

Jefferies RW. 2013. The archaeology of Carrier Mills: 10,000 years in the Saline Valley of Illinois. SIU Press.

Jungers WL, Harcourt-Smith WEH, Wunderlich RE, Tocheri MW, Larson SG, Sutikna T, Due RA, Morwood MJ. 2009. The foot of Homo floresiensis. Nature 459:81–84.

Kankainen K, Casjens L. 1995. Treading in the Past: Sandals of the Anasazi. Univ of Utah Pr.

Kidd R. 1999. Evolution of the rearfoot. A model of adaptation with evidence from the fossil record. J Am Podiatr Med Assoc 89:2–17.

Kidd RS, O'Higgins P, Oxnard CE. 1996. The OH8 foot: a reappraisal of the functional morphology of the hindfoot utilizing a multivariate analysis. J Hum Evol 31:269-291.

Kidd RS, Oxnard CE. 2002. Patterns of Morphological Discrimination in Selected Human Tarsal Elements. Am J Phys Anthropol 117:169–181.

Kivell TL, Schmitt D. 2009. Independent evolution of knuckle-walking in African apes shows that humans did not evolve from a knuckle-walking ancestor. Proc Natl Acad Sci 106:14241–14246.

Klingenberg CP. 2016. Size, shape, and form: concepts of allometry in geometric morphometrics. Dev Genes Evol 226:113–137.

Knigge RP, Tocheri MW, Orr CM. 2015. Three-dimensional geometric morphometric analysis of talar morphology in extant gorilla taxa from highland and lowland habitats. Anat Rec 298:277–290.

Lamy P. 1986. The settlement of the longitudinal plantar arch of some African Plio-Pleistocene Hominids: A morphological study. J Hum Evol 15:31–46.

Latimer B, Ohman JC, Lovejoy CO. 1987. Talocrural joint in African hominoids: Implications for Australopithecus afarensis. Am J Phys Anthropol 74:155–175.

Lovejoy CO, Latimer B, Suwa G, Asfaw B, White TD. 2009. Combining prehension and propulsion: The foot of Ardipithecus ramidus. Science 326:72-72e8.

Lovejoy OC. 1988. Evolution of human walking. Sci Am 259:118–125.

Lugli F, Brunelli D, Cipriani A, Bosi G, Traversari M, Gruppioni G. 2017. C4-Plant Foraging in Northern Italy: Stable Isotopes, Sr/Ca and Ba/Ca Data of Human Osteological Samples from Roccapelago (16th–18th Centuries AD). Archaeometry 59:1119–1134.

Parr WCH, Chatterjee HJ, Soligo C. 2011. Inter- and intra-specific scaling of articular surface areas in the hominoid talus. J Anat 218:386–401.

Parr WCH, Soligo C, Smaers J, Chatterjee HJ, Ruto A, Cornish L, Wroe S. 2014. Three-dimensional shape variation of talar surface morphology in hominoid primates. J Anat 225:42–59.

Pontzer H. 2012. Ecological Energetics in Early *Homo*. Curr Anthropol 53:S346–S358.

Pontzer H, Rolian C, Rightmire GP, Jashashvili T, Ponce de León MS, Lordkipanidze D, Zollikofer CPE. 2010. Locomotor anatomy and biomechanics of the Dmanisi hominins. J Hum Evol 58:492–504.

Prang TC. 2015. Rearfoot posture of Australopithecus sediba and the evolution of the hominin longitudinal arch. Sci Rep. 5: 17677.

Prang TC. 2016. The subtalar joint complex of Australopithecus sediba. J Hum Evol 90:105–119.

Preuschoft H. 2004. Mechanisms for the acquisition of habitual bipedality : are there biomechanical reasons for the acquisition of upright bipedal posture? J Anat 204:363–384.

Raichlen DA, Gordon AD, Harcourt-smith WEH, Foster AD, Randall W. 2010. Laetoli footprints preserve earliest direct evidence of human-like bipedal biomechanics. PLoS One 5: e9769.

Rhoads, John G., Trinkaus E. 1977. Morphometrics of the Neandertal Talus. Am J Phys Anthropol 46:29–43.

Richmond BG, Jungers WL. 2008. Orrorin tugenensis femoral morphology and the evolution of hominin bipedalism. Science 319:1662–1665.

Rohlf FJ, Slice D. 1990. Extensions of the Procrustes method for the

optimal superimposition of landmarks. Syst Biol 39:40–59.

Saers JPP, Cazorla-Bak Y, Shaw CN, Stock JT, Ryan TM. 2016. Trabecular bone structural variation throughout the human lower limb. J Hum Evol 97:97–108.

Santure SK, Harn AD, Esarey D. 1990. Archaeological investigations at the Morton Village and Norris Farms 36 cemetery. Illinois State Museum.

Sarrafian SK. 1987. Functional characteristics of the foot and plantar aponeurosis under tibiotalar loading. Foot Ankle 8:4–18.

Schlager S. 2017. Morpho and Rvcg - Shape Analysis in R: R-Packages for Geometric Morphometrics, Shape Analysis and Surface Manipulations. In: Guoyan Z, Shuo L, Gabor S. Statistical shape and deformation analysis. Academic Press. p 217-256.

Shaw CN, Ryan TM. 2012. Does skeletal anatomy reflect adaptation to locomotor patterns? cortical and trabecular architecture in human and nonhuman anthropoids. Am J Phys Anthropol 147:187–200.

Slice DE. 2005. Modern morphometrics in physical anthropology. Springer Science & Business Media.

Steele DG, Bramblett CA. 1988. The anatomy and biology of the human skeleton. Texas A&M University Press.

Stern JT, Susman RL. 1983. The locomotor anatomy of Australopithecus afarensis. Am J Phys Anthropol 60:279–317.

Su A, Carlson KJ. 2017. Comparative analysis of trabecular bone structure and orientation in South African hominin tali. J Hum Evol 106:1–18.

Su A, Wallace IJ, Nakatsukasa M. 2013. Trabecular bone anisotropy and orientation in an Early Pleistocene hominin talus from East Turkana , Kenya. J Hum Evol 64:667–677.

Team RC. 2017. R: A language and environment for statistical computing. Vienna, Austria. R Foundation for Statistical Computing.

Traversari M. 2017. Ricostruzione del profilo bioculturale e biodemografico di una piccola comunita'montana del XVI-XVIII secolo attraverso i dati archeoantropologici e documentari: il caso degli inumati di Roccapelago (Modena). Dissertation (alma).

Trinkaus E. 2005. Anatomical evidence for the antiquity of human footwear use. J Archaeol Sci 32:1515–1526.

Turley K, White FJ, Frost SR. 2015. Phenotypic plasticity: The impact of habitat and behavior (substrate use) on adult talo-crural appositional articular joint shape both between and within closely related Hominoid species . *Hum Evol* 30:49–67.

Turley K, Frost SR. 2013. The shape and presentation of the Catarrhine talus: A geometric morphometric analysis. Anat Rec 296:877–890.

Turley K, Frost SR. 2014. The appositional articular morphology of the

talo-crural joint: the influence of substrate use on joint shape. Anat Rec 297:618–629.

Ward CV, Kimbel WH, Johanson DC. 2011. Complete fourth metatarsal and arches in the foot of Australopithecus afarensis. Science 331:750–753.

Ward CV. 2002. Interpreting the posture and locomotion ofAustralopithecus afarensis: Where do we stand? Am J Phys Anthropol 119:185–215.

White TD, Asfaw B, Beyene Y, Haile-Selassie Y, Lovejoy O, Suwa G, Woldegabriel G, Lovejoy CO, Suwa G, Woldegabriel G. 2009. Ardipithecus ramidus and the paleobiology of early hominids. Science 326:64–86.

Wolpoff MH, Senut B, Pickford M, Hawks J. 2002. Palaeoanthropology: Sahelanthropus or 'Sahelpithecus'? Nature 419:581–582.

Wood B, Richmond BG. 2000. Human evolution: taxonomy and paleobiology. J Anat 197:19–60.

Zipfel B, DeSilva JM, Kidd RS, Carlson KJ, Churchill SE, Berger LR. 2011. The foot and ankle of Australopithecus sediba. Science 333:1417–1420.

Zollikofer CPE, Ponce De León MS, Lieberman DE, Guy F, Pilbeam D, Likius A, Mackaye HT, Vignaud P, Brunet M. 2005. Virtual cranial reconstruction of Sahelanthropus tchadensis. Nature 434:755–759.

Acknowledgements

At the end of this thesis, I would like to thank the people who supported me during my PhD period.

Firstly, I would like to thank my two supervisors Prof. Maria Giovanna Belcastro and Prof. Stefano Benazzi for the guidance and the precious suggestions provided in this project. Thank you so much for giving excellent advices when it was most needed. I am also very grateful for the possibilities you gave me to extend my research experiences beside the PhD project. Yet, many thanks for your patience and friendly support.

My thanks also go to Prof. Timothy M. Ryan who supervised me during my period abroad in his laboratory at Pennsylvania State University. Thank you so much for your teachings and for making me part of your team during those months.

Thank so much Nicholas Stephens for your considerable willingness to help me whenever I text you.

I would also like to thank all the co-authors, who contributed to these papers that made this thesis, and from whom I learned a lot.

Many thanks to my colleagues for all the time spent talking of scientific arguments and exchanging ideas, and mostly for all those coffee breaks spent in supporting each others when we needed.

My private thanks, grazie di cuore alla mia famiglia e a Giuseppe per aver trovato sempre le giuste parole nei momenti più difficili, per aver sopportato tutti i miei discorsi sul talus e per il loro amorevole indispensabile sostegno nel corso di questo cammino.